EXPERIMENTAL INVESTIGATION OF PLASTIC HEAT EXCHANGER FOR SINGLE PHASE AND CONDENSATION HEAT TRANSFER

A Thesis

by

ZAKI MOHSIN

Submitted to the Office of Graduate and Professional Studies of
Texas A&M University
in partial fulfillment of the requirements for the degree of

MASTER OF SCIENCE

Chair of Committee,	Jorge L. Alvarado
Committee Members,	David Claridge
	Karen Vierow Kirkland
Head of Department,	Andreas Polycarpou

May 2020

Major Subject: Mechanical Engineering

ABSTRACT

A comprehensive experimental investigation of plastic shell and tube heat exchangers (PHX) was performed under single phase and condensation modes. The performance tests were conducted for four prototypes consisting of 61 tubes arranged in a triangular layout. The PHX considered in the study consisted of different baffle configurations including continuous helical, trisection, quadrant and a conventional segmental baffle. The experimental results show that both the heat transfer rate, effectiveness and pressure drop increases with the shell side volume flow rate for all schemes. Furthermore, the segmental baffle heat exchanger was found to perform better than the continuous helical, trisection and quadrant baffle heat exchanger configurations. However, the continuous helical, trisection and quadrant baffle heat exchanger configurations were more energy efficient than the segmental baffle when taking into account heat transfer rate and pumping power simultaneously.

The PHX with segmental baffle and continuous helical baffle configurations depicted highly effective heat transfer performance under condensation conditions. Moreover, the PHX showed good agreement with the Braun model for condensers. In summary, PHX have a great potential as condensing units.

ACKNOWLEDGEMENTS

I would like to thank my advisor, Dr. Jorge Alvarado, for his constant guidance, mentorship, and encouragement during the course of this research. It has been a pleasure working with him and learning everything he has taught me. I would also like to extend my thanks to my committee members, Dr. David Claridge and Dr. Karen Kirkland, for their guidance and suggestions to improve the quality of this work.

I would also like to express my gratitude to Mr. Dean Calton of E Poly Tech for his expertise and help with material selection for the plastic heat exchangers/condensers.

In addition, I would also like to thank my parents for their support and trust they had placed in me. Their belief in me is a big part of my accomplishment.

Last but not the least, I would like to thank my friends who believed in me and supported me throughout my work with this project.

TABLE OF CONTENTS

Page

LIST OF FIGURES

Page

LIST OF TABLES

Page

CHAPTER I

INTRODUCTION

1.1 Background and motivation

Heat exchangers are devices that are used for efficient heat transfer between two fluids. Heat exchangers are broadly categorized based on the flow configuration, heat transfer mode, construction types and number of fluids. Among the different types of heat exchangers, shell and tube heat exchangers (STHXs) are widely used in industries. Moreover, most of the heat exchangers used in industries are made of metal. According to Master et al.[1], more than 35-40% of the heat exchangers are of shell and tube type and this primarily is due to their simple manufacturing, robust construction, geometry and ease of maintenance. In a shell-and-tube heat exchangers one fluid flows through the tube while the other flows through the shell across the tube bundle.

However, the conventional metallic shell and tube heat exchangers (STHX) are used for a variety of applications. However, metallic shell and tube exchangers are heavy, expensive, and can experience corrosion degradation [2]. Keeping these in view, polymer heat exchangers (PHX) can therefore be used for certain heat transfer applications, in which the attributes of polymers such as flexibility, low weight, corrosion resistance, and ease of manufacturing, have proven to be attractive characteristics. However, plastic heat exchangers need to be designed carefully to compensate for the inferior thermal properties of polymers including low thermal conductivity.

In most STHXs, baffles are used to distribute the flow evenly or in a zig zag pattern between the tube bundle and the flowing fluid. Baffles also enhance turbulence intensity and local mixing, thereby increasing the overall heat transfer coefficient. This is particularly important in the design and characterization of plastic STHX, in which fine plastic tubing with high surface-to-volume ratio is used to enable adequate level of heat transfer. Furthermore, configurable baffles in plastic STHX need to provide structural support and enhance the fluid interaction on the shell side to increase the overall heat transfer process.

In this thesis, four different baffle arrangements used in plastic STHXs are presented and discussed. Experimental heat transfer efficiency and pressure drop of four plastic STHXs with different baffle configurations are also presented.

1.2 Research Questions

The goal of this work was to perform single phase and dehumidification heat transfer tests on all the four prototypes to determine the flow and heat transfer characteristics of each of them. The specific research objectives, are as follows:

- Identify optimal baffle arrangement that allows maximum heat transfer performance under the single phase and dehumidification conditions.
- Investigate the effect of varying flowrate mass flowrate on the overall heat transfer coefficient for different baffle arrangements, under dry and moist air conditions.
- Determine the effect of flowrate and STHX configuration type on pressure drop under different mass flowrate.

- Determine the effectiveness of each plastic heat exchanger prototype under single phase and dehumidification (condensation) heat transfer conditions.

With the proposed research activities, the effects of different baffle configuration of plastic heat exchanger on the overall heat transfer performance will be elucidated

CHAPTER II

LITERATURE REVIEW

Shell and tube heat exchangers are robust in handling high temperature and high-pressure media fluids and are flexible in meeting almost any process requirement. In shell and tube heat exchangers, the shape and arrangement of baffles are important to achieve optimal thermal performance. This review covers the different configurations of baffles that have been used in SHTX for single phase and condensation heat transfer in the past.

2.1 Single Phase Heat Transfer

2.1.1 Segmental Baffle Heat Exchanger

The STHX with segmental baffles are typical in conventional shell and tube heat exchangers and has been the standard in many industrial applications. This type of baffle has a cut that allows the fluid to pass through the shell in a parallel or counter flow direction. The baffle cut (B_c) is measured as a percent of the shell diameter. These baffles are arranged along the shell in an alternating orientation[3]. This configuration is shown in Fig. 1.

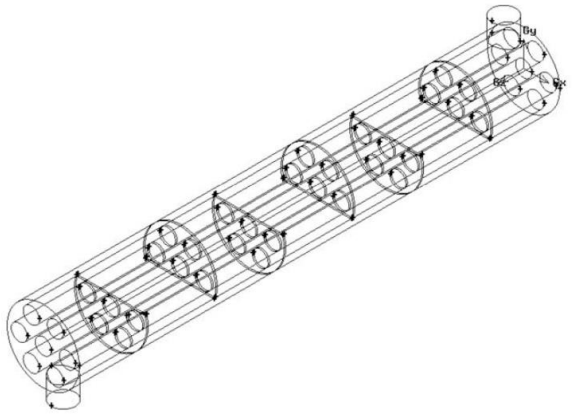

Figure 1. Segmental Baffle Heat Exchanger[3]

The baffles shown in Fig.1, direct the fluid in a zig-zag manner through the shell. However, these types of baffles have many drawbacks, which includes a high pressure drop on the shell side due to the sudden contraction and expansion of the flow; low heat transfer efficiency due to the flow stagnation in the so-called “dead zones”, which are located at the corners between baffles and shell wall; low shell-side mass velocity across the tubes due to the leakage between baffles and shell wall; and vibration caused by the shell-side flow normal to tube banks[4].

When the traditional segmental baffles are used in STHX, higher pumping power is often needed to offset the higher pressure drop under the same heat load. Hence, to overcome the above-mentioned drawbacks of the conventional segmental baffle, a number of improvements have been proposed to enhance the heat transfer coefficient and also to reduce the tube vibration and fouling factor.

2.1.2 Helical Baffle Heat Exchanger

Helical baffles offer a feasible alternative to segmental baffles by circumventing many of the aforementioned problems common to segmental baffles. Some of the advantages offered by the helical baffles includes improved heat transfer, lower pressure drop for a given shell side mass flow rate, reduced shell side fouling and reduced vibration[5]. Helical baffles can be classified into two categories: continuous and discontinuous. The continuous helical baffles are preferred due to the induced spiral flow within the shell side of STHX; however, they are difficult to manufacture, especially in large heat exchangers. Hence, the discontinuous helical baffles are more commonly used, due to their manufacturability and ease of installation.

2.1.2.1 Non-continuous helical baffle

Generally, non-continuous helical baffles consist of four elliptical sector shaped plates that are joined end-to-end. Each baffle occupies one quarter of the cross section of the heat exchanger and is angled along the axis of the heat exchanger. The helical baffles in STHXs are shaped approximately as helicoids, which direct the fluid flow on the shell side. The resulting flow approached continuous helical flow conditions, which is characterized by a uniform and homogenous velocity distribution. This in turn causes a decrease in pressure drop with an increase in the heat transfer on the shell side of the heat exchanger. [6] Fig. 2 shows the arrangement of the discontinuous helical baffles inside the STHXs.

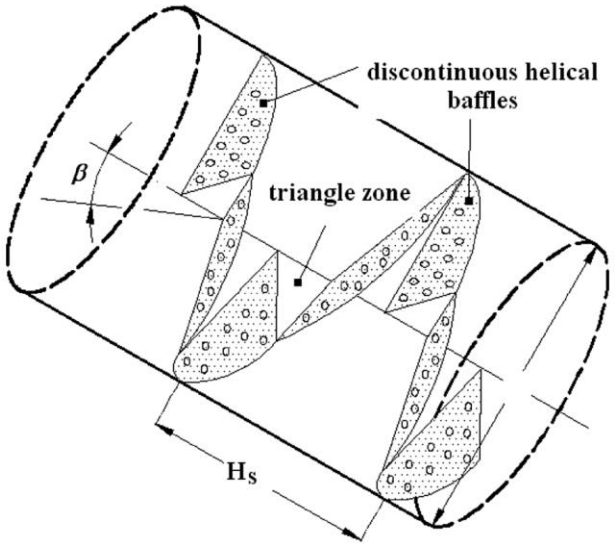

Figure 2. Schematic of discontinuous helical baffles[6]

However, there are two factors, which need to be considered when determining the performance of discontinuous helical baffle heat exchanger. One is the baffle inclination angle and the other is the baffle arrangement inside the shell[7].

In the following review all the various designs of helical baffle heat exchangers will be discussed along with the baffle inclination angle and the configuration of the helical baffles.

Quadrant Baffle Heat Exchanger

Lutcha and Nemcansky [8] firstly invented the helical baffle heat exchanger with quadrant helical baffles. They investigated the flow pattern produced by such helical baffle geometry at different helix angles. They found that for all helical inclination angles under identical pressure drop, the helical baffles produced a higher heat transfer rate than a tubular heat exchanger with segmental baffles. They found an optimum helical inclination angle of 40 degree at which the flow patterns inside the shell were much closer to plug flow conditions. They indicated that plug flow conditions have significant advantage in heat transfer versus the mixing flow seen in segmental STHX, since the latter decreases the local driving force for heat transfer. They also performed a comparison between helical and segmental baffle arrangement and found that the helical baffles induce a flow pattern closer to the plug flow pattern. Fig. 3 shows how helical baffles led to greater heat transfer effectiveness.

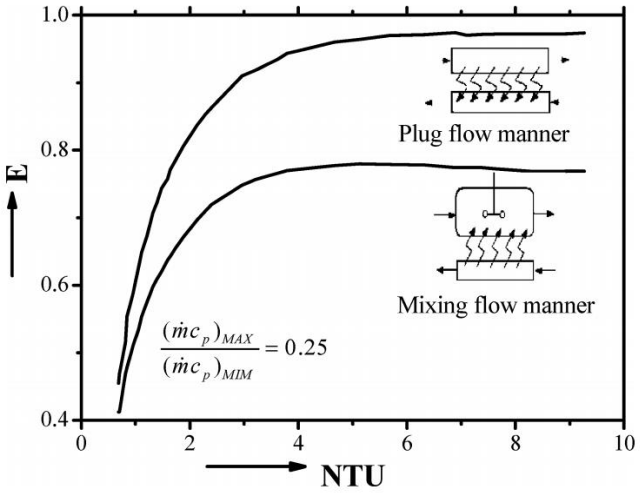

Figure 3. Comparison of heat exchanger effectiveness for perfect mixing flow and plug flow [8]

Kral *et al.* [9] discussed the performance of heat exchangers with helical baffles (STHXsHB) based on test results of various baffle geometries. A comparison between the test data of a shell side heat transfer coefficient versus shell side pressure drop were provided for five helical baffles and one with a segmental baffle. The tests were performed with water on both sides of the heat exchanger. They concluded that a helix angle of 40 degrees is the optimum angle at which the heat transfer per unit of pressure drop on the shell side is maximized. Fig. 4 shows the variation of heat transfer coefficient versus pressure drop for different helix angle and confirms their finding that 40-degree helix angle was the best among all.

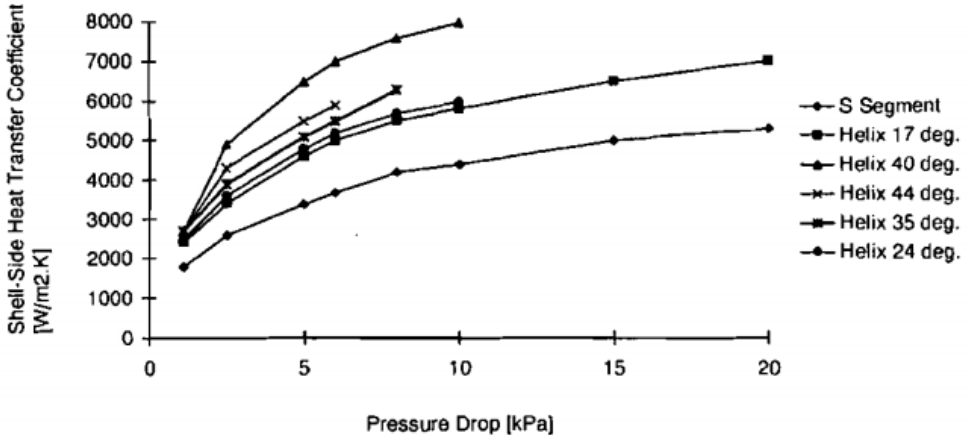

Figure 4. Heat transfer coefficients versus pressure drop for various helix angles [9]

Zhang *et al.* [10] experimentally measured the shell side flow and heat transfer characteristics of a series of middle overlapped quadrant helical baffle heat exchangers. They found that for the same shell side flow rate, the shell side heat transfer coefficient of the STHXs with helical baffle was lower than that of the STHXs with the segmental baffle, although shell side pressure drop of the former was lower than that of the latter one. Accordingly, for the same shell side volume flow rate, the heat transfer coefficient per unit of pressure drop or per unit pumping power was greater for STHXs with helical baffles when compared to the segmental ones. Also, they concluded that the 40^{o} inclination angle was the optimum angle, which resulted in the best performance of all the heat exchangers considered in the study. Fig 5. shows the relationship between shell side average heat transfer coefficient and the shell side volume flowrate as an independent variable. It can be seen that under the same volume flowrate the shell side heat transfer coefficient of the

helical baffle STHXs is lower than that of the segmental baffle STHXs. However, among all the helical baffles the 40° helical baffle has the highest heat transfer coefficient.

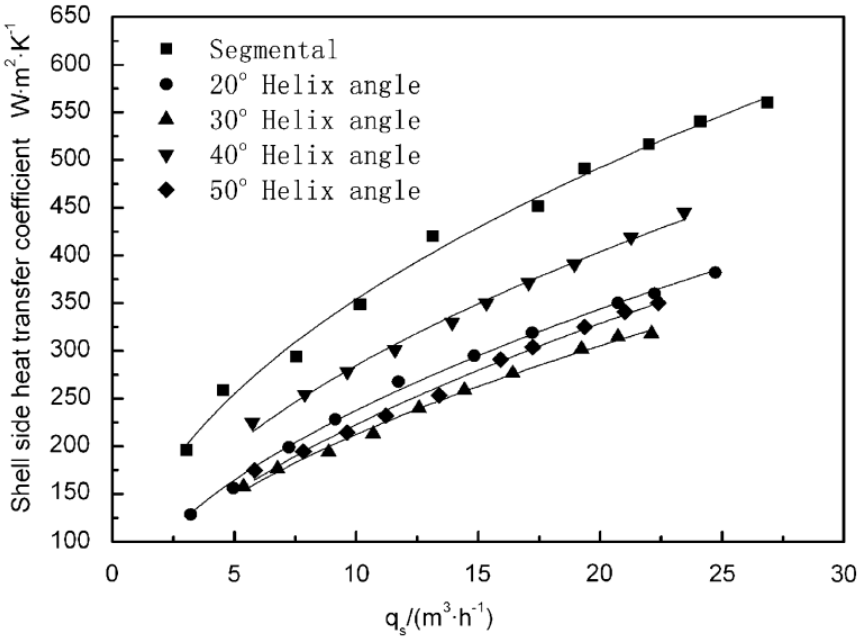

Figure 5. Shell side heat transfer coefficient as function of flowrate [10]

Similarly, Fig 6 shows the relationship between the comprehensive performance index and the shell side volume flowrate. It can be seen that the 30° and 40° helical baffles perform the best among the five heat exchangers tested.

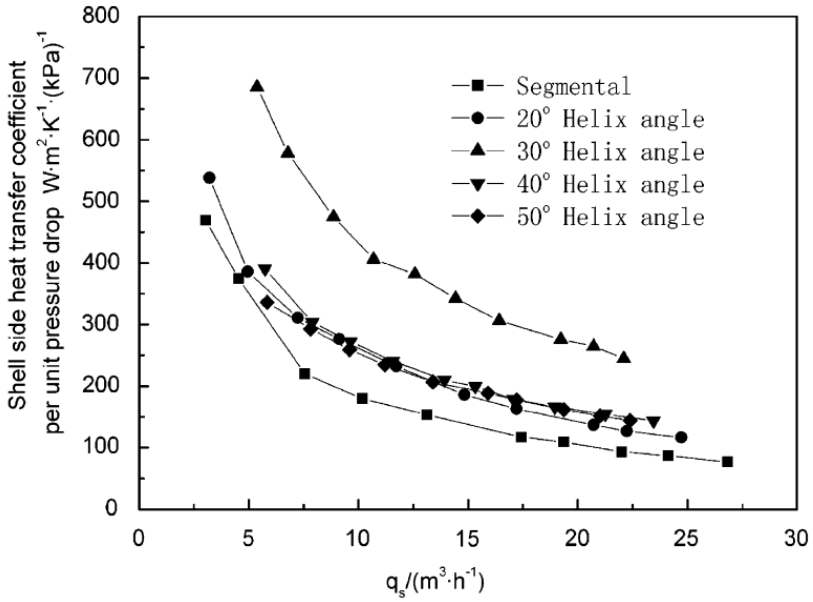

Figure 6. Shell side heat transfer coefficient per unit pressure drop a function of flowrate in the shell side[10]

Xiao *et al*.[11] performed numerical simulations for a quadrant helical baffle heat exchanger but with different Prandtl number (ratio of momentum to thermal diffusivities) fluids. They also considered different helical tilt angles of 10°, 20°, 30°, 40° and 50°. Five test fluids, which were water, gasoil, ethylene glycol, glycerin and engine oil were used in the study to determine the effect of Prandtl number on heat transfer characteristics. When fluids with a low Prandtl number were used, they found that the helical baffle enhanced the heat transfer performance and led to reduced pressure drop. For fluids with a high Prandtl number, a small helical tilt angle increased the level of turbulence, which led to enhanced heat transfer performance. They also found that a 40° tilt angle was the best selection for the same heat transfer capacity; however, the effect of tilt angle on heat transfer diminished as Prandtl number increased. Fig. 7 depicts the heat transfer coefficient

per unit pressure drop against the helical tilt angle for different fluids. It can be seen from the figure that water has the highest value of the performance evaluation coefficient ($K/\Delta P$) over the tested helical tilt angles. The reason for this is because water has a low Prandtl number when compared to the other fluids considered in the study. In general, a fluid with low Prandtl number exhibits a thinner momentum boundary layer on the tube surface, which leads to greater heat transfer. Hence, it was concluded that heat exchanger design should consider helical tilt angle (β) when different Prandtl number fluids are taken account.

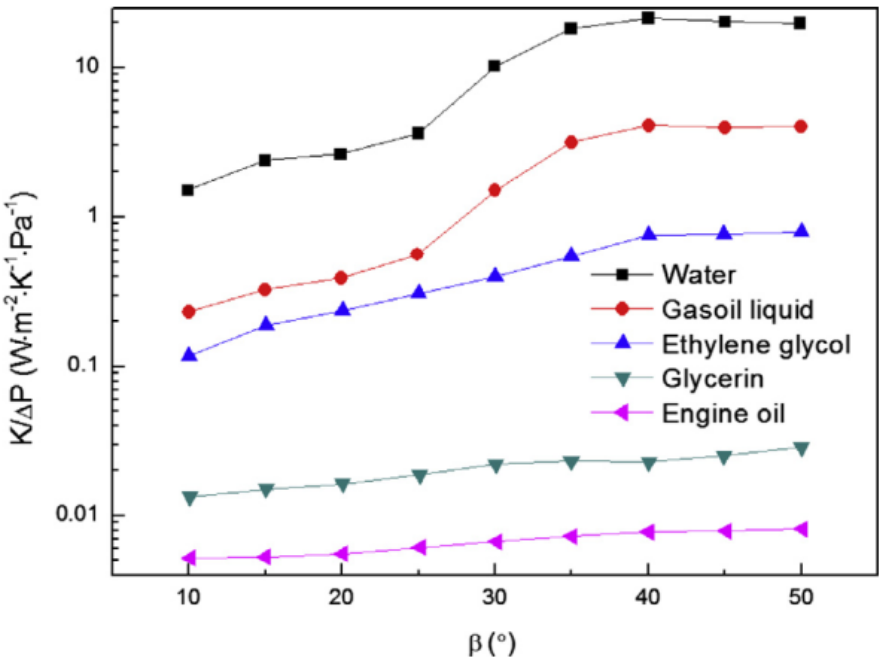

Figure 7. Total heat transfer coefficient per unit pressure drop as a function of baffles tilt angle for fluids with different Prandtl number[11]

Lei et *al.*[12] conducted a numerical and experimental investigation to determine the heat transfer and pressure drop characteristics of heat exchangers with three different

baffle configurations. The three configurations included single segmental baffles, single helical baffles and two-layer helical baffles. The single-segmental baffles were perpendicular to the tubes with a baffle cut of 25%, including eight baffles positioned on the shell side. The helical baffles were quadrant-elliptical shaped baffles at an angle of 20° to the tube axis, which occupied one quadrant of the cross section of the shell, and in the case of a single helical baffle, six periods or turns were included in the shell. They found that the heat exchangers with helical baffles had higher heat transfer per unit pressure drop than that of the heat exchanger with segmental baffles (HX1). Fig. 8 confirms their findings and shows that the ratios of the heat transfer coefficient to pressure drop in heat exchangers with two-layer helical baffles (HX3) was 10% higher than that in heat exchangers with one-layer helical baffles (HX2). It was concluded that the two-layer baffles reduced the bypass leakage stream and increased the turbulence in the central region of the shell side of the heat exchanger.

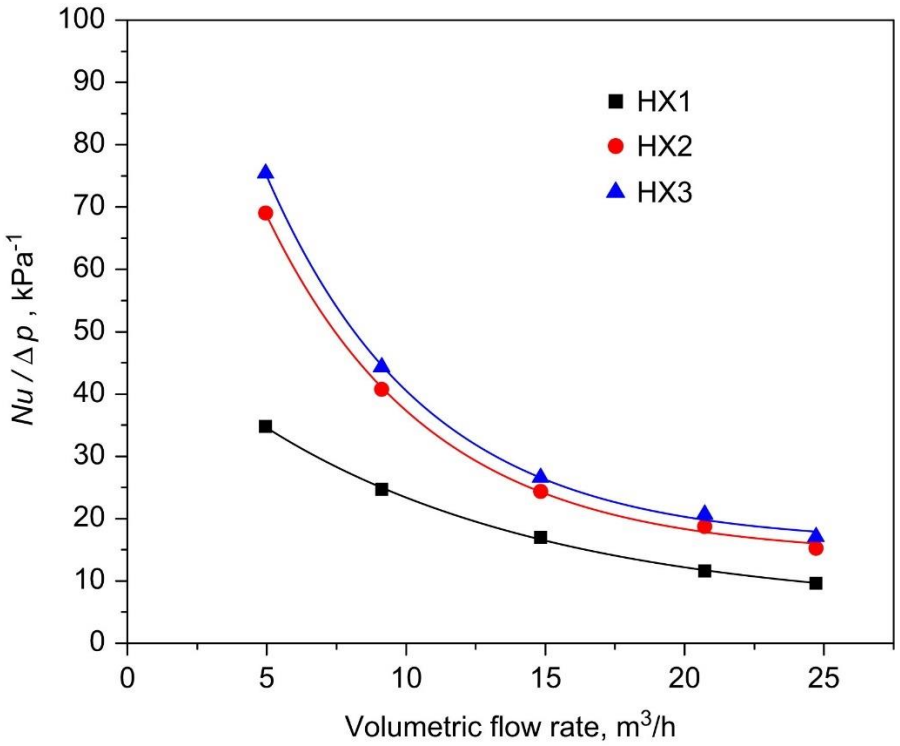

Figure 8. Ratio of heat transfer to pressure drop for three heat exchangers[12]

Trisection Baffle Heat Exchanger

Dong *et al*. [13] numerically examined four heat exchanger schemes with approximately identical spiral pitch and tube geometry but different baffle shapes and connections. These included a circumferential overlap (CO) scheme, an end-to-end (EE) scheme, a blocked V-notch (BV) scheme, and a middle axial overlap (MO) scheme. Fig. 9 shows the geometric model of the four helical baffle heat exchangers.

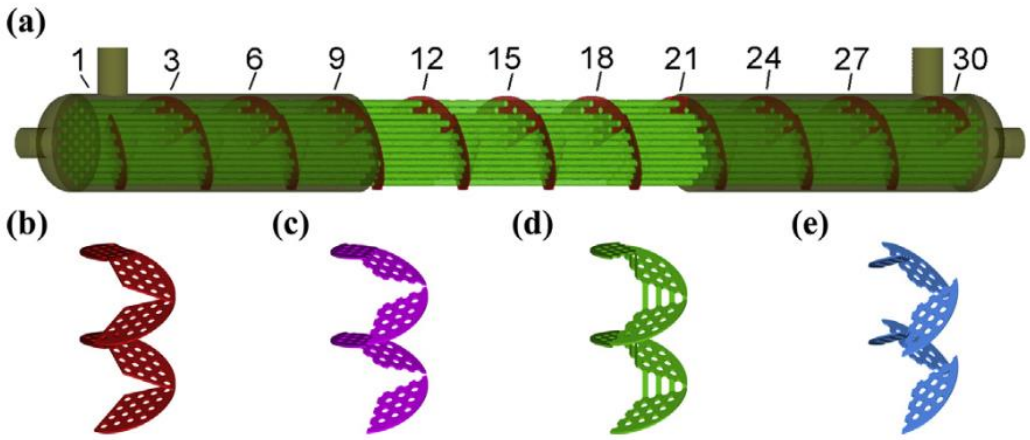

Figure 9. Models of four trisection helical baffle HXs: (a) assembly model of trisection helical baffle heat exchanger; (b) circumferential overlap baffle (CO); (c) end-to-end baffle (EE); (d) blocked V-notches baffle (BV); (e) middle axial overlap baffle (MO)[13]

Based on the numerical simulation, the authors found that for a given mass flow rate, the CO scheme has the highest shell side heat transfer coefficient and has the best comprehensive index denoted as $h_o/\Delta p_o$. They concluded that the circumferential overlap trisection helical baffle scheme with an incline angle of 20^o performed the best. It not only reduced the shortcut leakage stream between adjacent baffles, but also resulted in the elimination of the stagnant flow regions, while inhibiting tube bundle vibration and fouling and reduced the shell side pressure drop.

Chen *et al*. [14] experimentally investigated five circumferential overlap trisection helical baffle heat exchangers and compared their performance with a segmental baffle. They used different inclinations of 20°, 24°, 28° and 32° (both single thread and dual thread). Each helical baffle was angled to the axis of the heat exchanger and occupied more than one third of the cross section of the heat exchanger shell. The results showed

that the scheme with an inclined angle of 20° performed the best, followed by the scheme with an inclined angle of 24°, and the segmental baffle. They concluded that the circumferential overlap reduced the reverse leakage flow in the triangular zones of the adjacent baffles, and only a small optimal inclined angle could enhance the overall heat transfer performance. Hence, the difficulty of manufacturing helical baffles with large inclined angles was also diminished. Fig. 10 shows the comprehensive performance index denoted as Nu/Eu (shell side Nusselt number, Nu, and the shell side axial Euler number, Eu) for comparison of heat transfer properties of different schemes. It can be seen from the figure that a 20^{o} circumferential overlap trisection baffle was the best among all cases. The circumferential overlapping of baffles reduced the reverse leakage flows in the triangular zones of the adjacent baffles and produced a flow pattern closer to a plug flow type in the shell side of the heat exchanger.

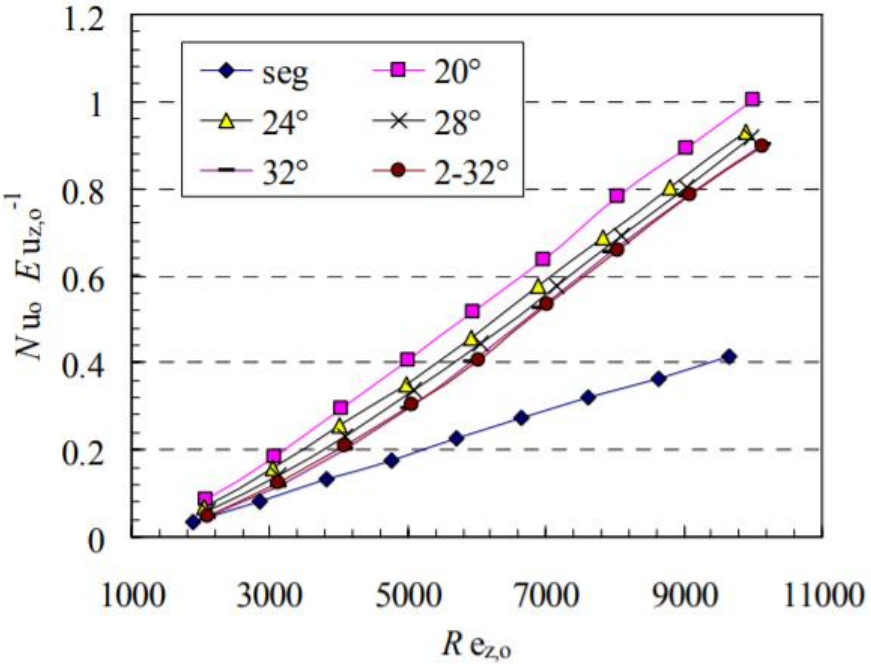

Figure 10. Shell side comprehensive index Nu/Eu versus shell[14]

Dong *et al.*[15] experimented with the flow and thermal performance of four trisection helical baffle heat exchangers with the same angle of inclination. However, the amount of circumferential overlap in each of the four prototypes was different. The four schemes included one end-to-end and three circumferential overlap configurations. The three circumferential overlap schemes were different in terms of the overlap in the triangular area in between adjacent baffles. They included one row overlap (20°-TCO), two row overlap(20°-T2CO), and three row overlap (20°-T3CO). Fig. 11 shows the geometric model of the four helical baffle heat exchangers.

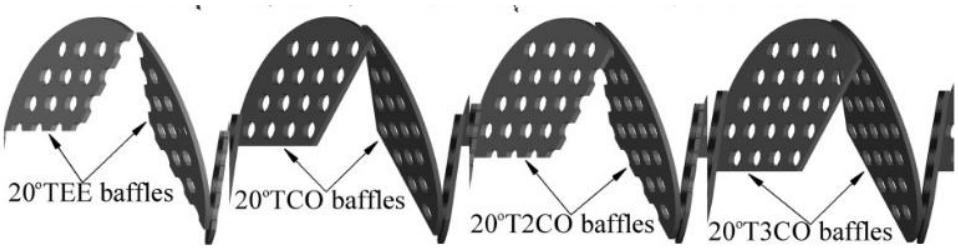

Figure 11. Geometric structures of different circumferential overlap for trisection helical baffle heat exchangers[15]

They found that the trisection baffle produced a spiral flow and eliminated the stagnant zones. Moreover, the circumferential overlap also prevented a considerable amount of leakage fluid through the triangular area into the downstream chamber. They concluded that the 20°-TCO scheme exhibited the strongest secondary flow and also minimized the leakage stream.

Continuous Helical baffle Heat Exchanger

Peng *et al.* [16] designed and tested three shell and tube heat exchangers consisting of helical and segmented baffles. Two of the STHXs consisted of continuous helical baffles one consisted of segmental baffles. The STHX with helical baffles consisted of side-in-side-out and middle-in-middle-out configuration while STHX with segmental baffles consisted of middle-in-middle-out shell arrangement. They found that the continuous helical baffle (both side-in-side-out and middle-in-middle-out) resulted in higher heat transfer coefficient than the segmental baffles. Among the two helical baffle shell configurations, the one with a side-in-side-out arrangement produced 10% higher heat transfer coefficient than the conventional segmental baffle. They concluded that the flow in the shell side of the continuous helical baffle heat exchanger was smooth and

rotational, which caused a significant increase in the heat transfer coefficient per unit pressure drop. Fig. 12. shows the heat transfer coefficient on the shell side of the heat exchanger as a function of pressure drop. It can be seen from the figure that for the same overall pressure drop, the shell side heat transfer coefficient is greater in helical baffle case than in the segmental baffle case.

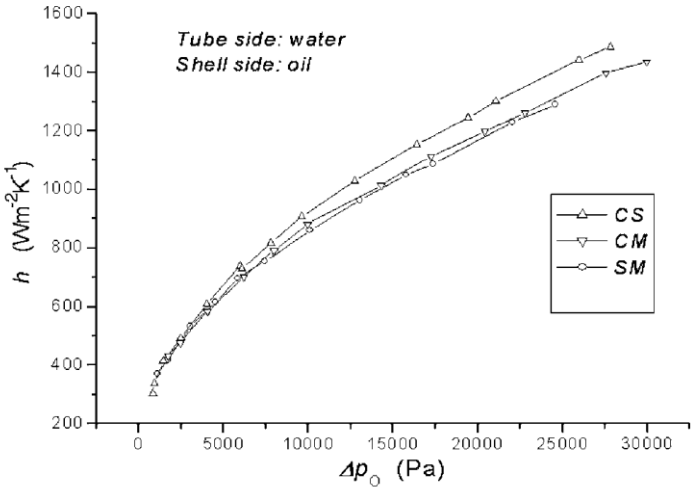

Figure 12. Heat transfer coefficient versus overall pressure drop[16]

Lei et al. [17] numerically studied a continuous helical baffle heat exchanger composed of 9 tubes for different shell-side Reynolds number and inclination angles. The Reynolds number varied from 500 to 3500 and the helical inclination angles varied from 15^o to 50^o. They found that the flow pattern in the shell side for all the cases was near plug flow with no dead regions. They observed that increasing the Reynolds number on the shell side of a HX with helical baffles, pressure drop also increased but at a lower rate than in a HX with segmental baffles. Also, the results showed that pressure drop decreased with baffle inclination angle. Finally, they concluded that the heat transfer coefficient per unit

pressure drop was much higher for HX with helical baffles than for the segmental ones, and it reached a maximum at an optimum angle of 45^{o}. Fig. 13 shows the flow pattern on the shell side for different baffle inclination angle at a shell side Reynolds number of 1000. It can be seen from the figure that the inclination angle of the stream lines increases with baffle inclination angles.

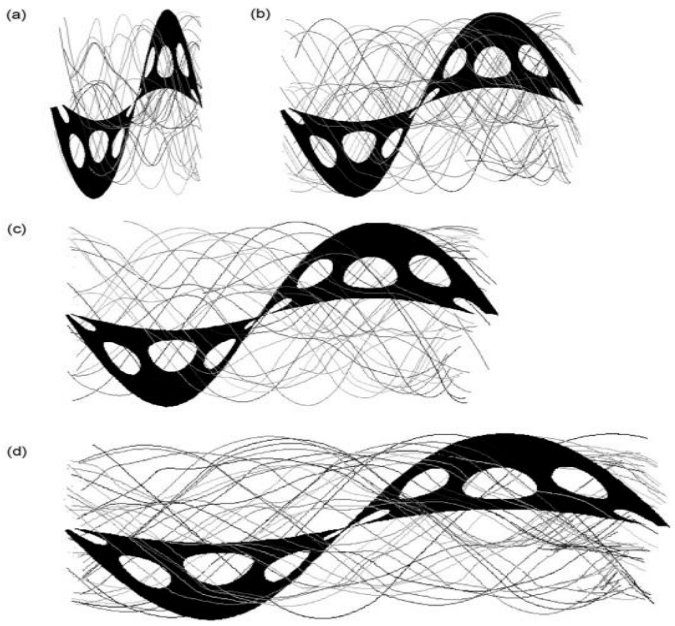

Figure 13. Stream lines for different baffle inclination angles (a) α = 15◦; (b) α = 30◦; (c) α = 40◦; and (d) α = 50◦ [17]

Similarly, Fig. 14 shows the variation of the heat transfer coefficient and pressure drop for different baffle inclination angles. A higher position in this plot indicates a reduced pumping power required for the same heat transfer rate. As it can be seen from the figure, the heat transfer efficiency of all of the helical baffles is greater than the heat exchanger with segmental baffles, and the performance of the helical baffles increases with baffle inclination angle until β approaches 45^{o}.

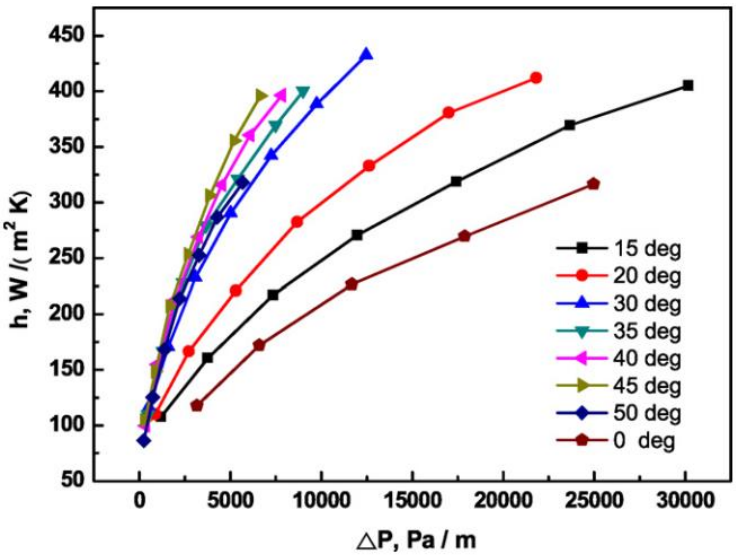

Figure 14. Heat transfer coefficient versus pressure drop for different baffle inclination angles[17]

Wang *et al.* [6] provided a general review of the improvements and developments of helical heat exchangers, which included discontinuous, continuous and combined helical baffles. He concluded that the continuous helical baffle heat exchangers were better in performance followed by HX with combined helical baffles due to their higher heat transfer coefficient per unit pressure drop.

2.2 Condensation Heat Transfer

Shell and tube condensers are widely used in many applications, including power generation and refrigeration. Many condensers consist of horizontal tubes in which dropwise and filmwise condensation modes take place. Most conventional condensers used in refrigeration have the refrigerant (i.e. two-phase fluid) flowing on the outside of the tubes, and the coolant flowing inside the tubes [18]. In such configurations, the condensed liquid accumulates at the bottom of the shell below the tubes. Fig. 15 shows

that phenomenon. In Fig. 15 it can be seen that, the condensing vapor enters the top of the heat exchanger as saturated or superheated vapor and is condensed on a bank of horizontal tubes, where it reaches the saturated or subcooled liquid state.

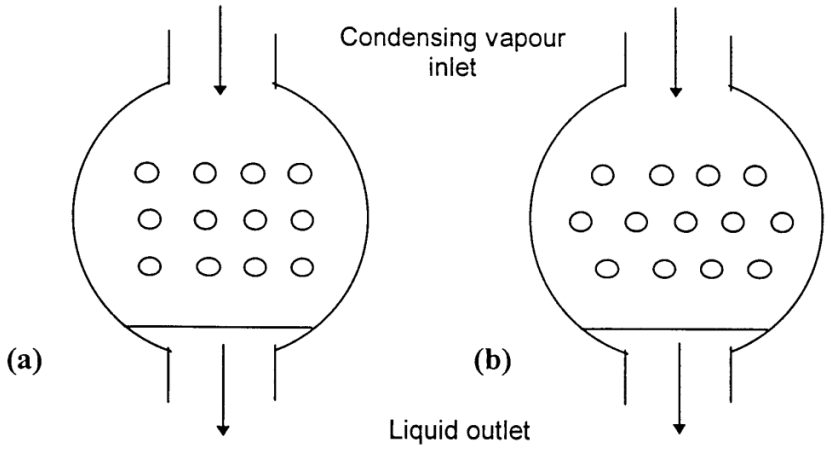

Figure 15. Schematic of shell-and-tube condensing heat exchanger (a) an in-line tube bundle (b) a staggered tube bundle configuration[18]

2.2.1 Segmental Baffle Heat Exchanger - Condenser

Grant *et al*.[19] experimentally studied the pressure drop flow patterns and phase distribution on the shell side of segmented-baffles shell and tube heat exchanger. They tested a condenser consisting of rectangular cross sections, which contained 40 tubes arranged in an equilateral triangular layout with 1.25 pitch/tube diameter ratio. They used three segmental baffles with four passes on the shell side. A schematic of their model is shown in Fig. 16.

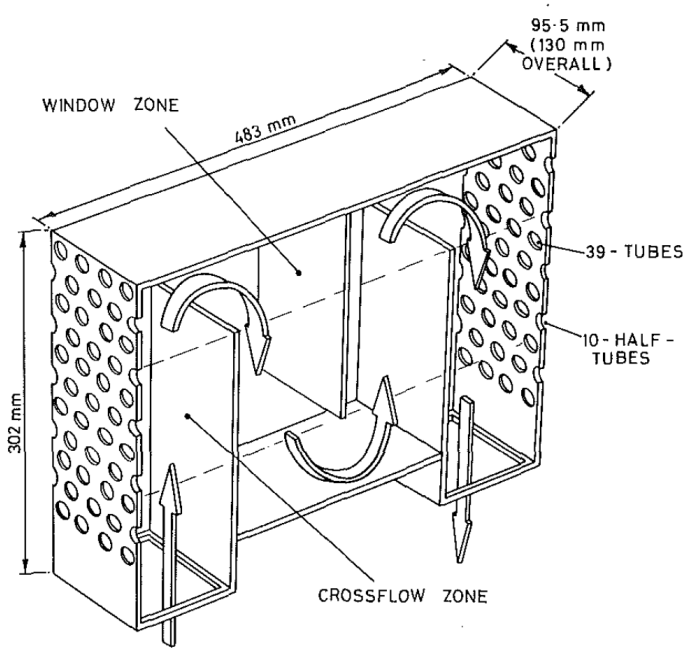

Figure 16. Experimental segmental shell and tube condenser[19]

They developed different flow patterns maps based on visual observations obtained through transparent end tube plates. Spray and bubbly flow occurred for either vertical up-and-down flow or horizontal side-to-side flow cases. Intermittent flow only occurred with vertical up-and-down flow and stratified-spray and stratified flow with horizontal side-to-side flow. The different flow patterns are shown in Fig. 17.

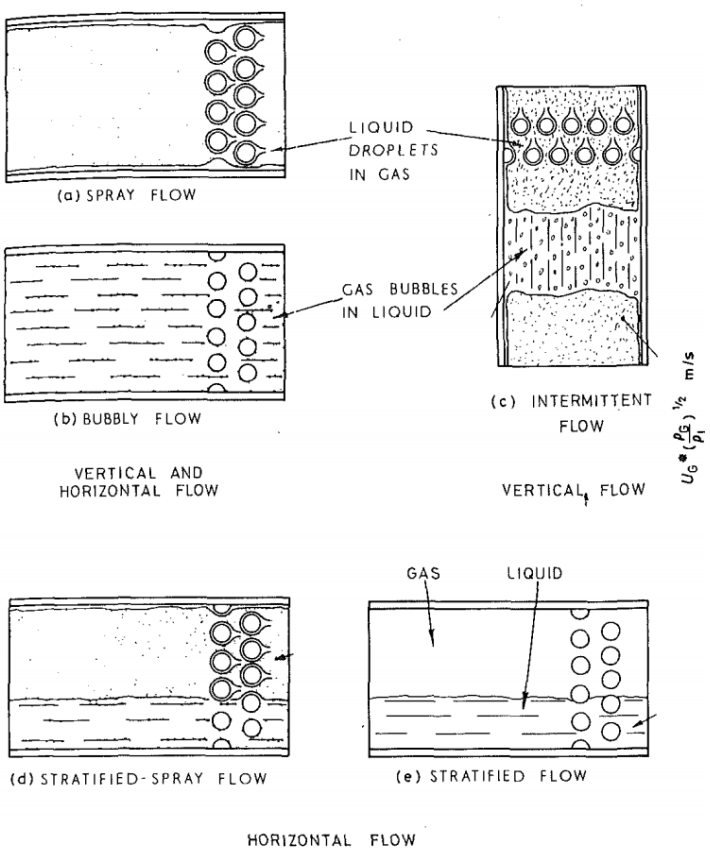

Figure 17. Shell side two phase flow pattern [19, 20]

Most condensation studies have focused primarily on condensers with segmental baffles [21, 22]. However, few studies have considered the flow and heat transfer characteristics of shell and tube condensers with helical baffles [23].

2.2.2 Helical Baffle Heat Exchanger - Condenser

2.2.2.1 Non-continuous helical baffles in condensers

Lin *et al*. [24] numerically and experimentally investigated a trisection helical baffle vertical condenser. They tested three vertical condensers, with two having helical baffles and one with segmental baffles. Each condenser consisted of 16 tubes, which were

arranged in an equilateral triangular layout. The shell had inlets and outlets for steam/condensate and cooling water. Fig. 18 shows the geometric model of the segmental and helical baffle heat exchangers.

They concluded that condenser with inclined baffles with liquid dam were more effective in draining the condensate from tube bundle surfaces. In general, condensers with horizontal surfaces and segmental baffles need to account for the possibility of poor drainage. In many applications, vertical condensers are preferred even though it could change the mode of condensation from dropwise to filmwise. Moreover, most condensers are made of hydrophilic materials such as aluminum and copper. Furthermore, metallic condenser can be expensive to manufacture and heavy to transport.

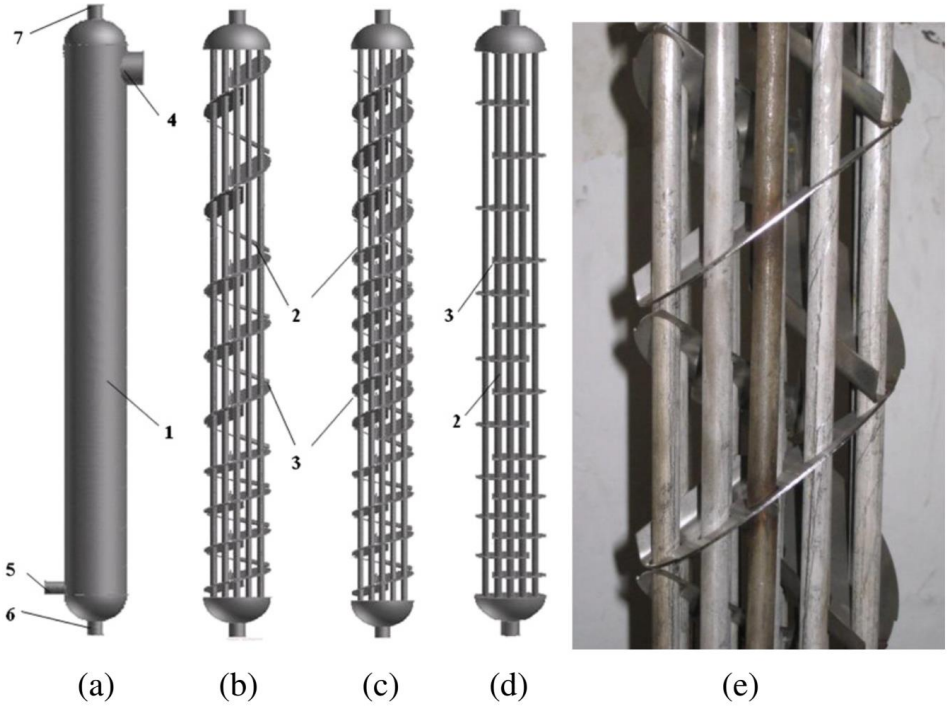

Figure 18. Schematic diagram of vertical helical baffle condensers and segmental baffle condenser: (a) Condenser shell (b)/(c) tube bundle with single/dual thread trisection baffle (d) Tube bundle with segmental baffles [24]

2.3 Plastic Heat Exchanger

As mentioned earlier, plastic as a heat exchanger material has many advantages over metallic materials since they are flexible, light weight and have long life, which could lead to cost savings and increased reliability. However, very few studies have been conducted in which plastics were used as heat exchange material.

Marco and Shafey [20] experimentally investigated the performance of a plastic heat exchanger assembled using commercial grade PVC. It consisted of plastic turbulators, which were placed inside the exchanger tubes to enhance the overall heat transfer process. The units consisted of six tubes, which were distributed uniformly in two passes inside the shell in a staggered arrangement.

A generalized performance evaluation of the plastic heat exchanger from [21] is shown in Fig. 19, which shows the relationship between two dimensionless parameters including effectiveness and number of transfer units (NTU). As it can be seen from the figure, an effectiveness of 0.6 can be achieved in a plastic heat exchanger. Marco and Shafey [20] also found that inserting turbulators could enhance the heat transfer performance to up to 3.5 times without any considerable amount of pressure drop.

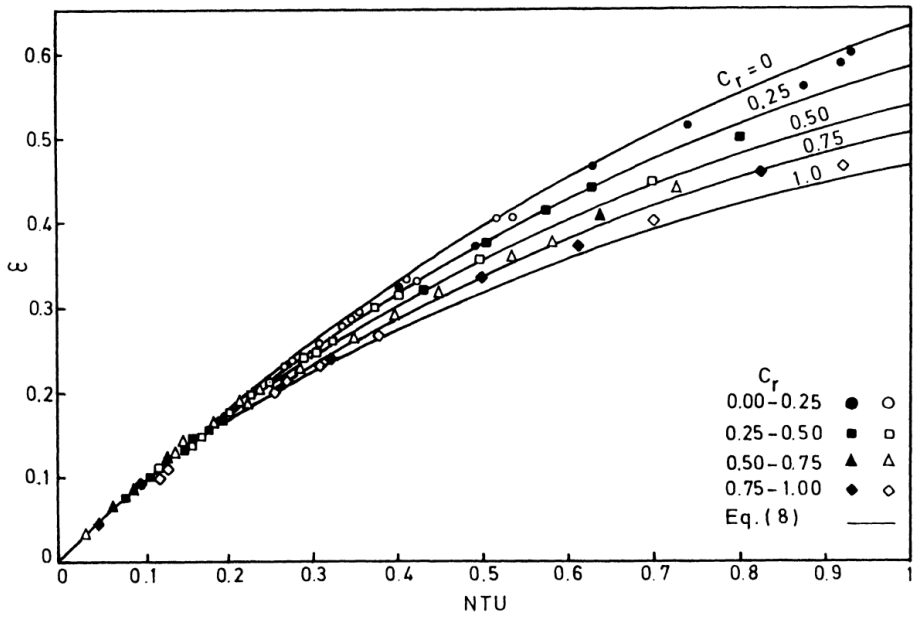

Figure 19. Heat exchanger effectiveness as a function of NTU[20]

Amer *et al*. [25] performed experimental investigation to determine the condensation heat transfer in three novel plastic heat exchangers. The experimental setup consisted of three plastic heat exchangers, which consisted of a conventional plate heat exchanger, a bare tube plastic heat exchanger with asymmetrical tube arrangement (BTHX) and a round tube plastic heat exchanger (RTHX) with uniform tube layout. They found that both the BTHX and RTHX showed superior heat transfer performance than the PHX. Based on this finding, they concluded that the BTHX and RTHX offered an additional condensate splashing mode, which helped remove the condensate from the condensation surfaces. This resulted in an increase of heat transfer coefficient on the condensation side of the heat exchanger. Fig. 20 shows the heat transfer coefficient for the hot side (condensation side) as a function of the hot side flow rate. It can be seen from the

figure that heat transfer coefficient of BTHX is comparable to RTHX and is about two times higher than PHX. The reason for this considerable difference between the performance of BTHX and PHX has been explained earlier. However, the difference between the heat transfer coefficient in the case of BTHX over RTHX is due to the asymmetrical tube design of BTHX. In BTHX the larger tubes were located at the bottom part of the tube bundle, which helped in the shedding of the condensate to fall to the bottom surface. In summary, the work by Amer *et al*. [25] is one of the very few in the area of plastic condensers.

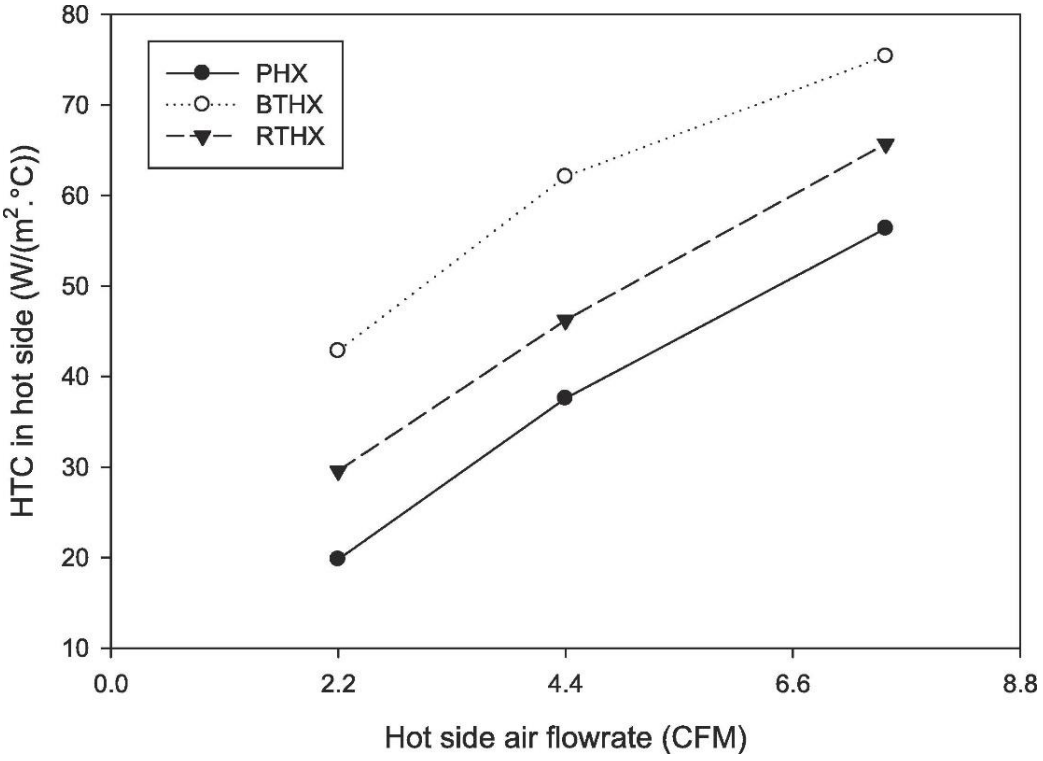

Figure 20. Comparison of heat transfer coefficients as a function of hot side (condensation side) flow rate [25]

2.4 Summary of Literature Review

Although multiple structure modifications of helical baffle heat exchangers have been proposed and discussed based on experimental or numerical results, the optimal baffle assembly in terms of the heat transfer performance is still unknown. The bypass streams through the triangular area between adjacent baffles are deemed to be one of the main adverse factors to the heat transfer performance of discontinuous helical baffle heat exchangers. The baffle incline angle is also a key parameter for heat transfer and flow performances of helical baffle heat exchangers.

Moreover, little to nothing experimental characterization has been done using plastics as the heat exchanger material to investigate the flow and heat transfer performance for different baffle configurations. Furthermore, little is known about the condensation heat transfer characteristics of PHXs with continuous and non-continuous baffles. This study is a first comprehensive attempt to understand how plastic heat exchangers perform under single phase and condensation conditions with different baffle configurations.

CHAPTER III

EXPERIMENTAL SETUP AND PROCEDURE

3.1 Description of experimental system

In an effort to understand the effect of different baffle configurations in plastic heat exchangers (PHX), an experimental setup consisting of PHXs was designed for that purpose. The experimental setup consists of a submersible pump for the tube side, a tube side flowmeter, a centrifugal blower and coiled heater for the shell side, a data acquisition unit, and other experimental instruments including thermocouples, pressure manometer and hand-held anemometer.

Fig. 21 shows the schematic drawing of the experimental system for single-phase heat transfer. It consists of a water loop, a hot air loop and a data acquisition system. In the water loop, water is pumped from the water tank to the flowmeter. A bypass connection has been installed in between the discharge of the pump and flowmeter to regulate the flow of water into the test section. The water then flows through the tube side of the heat exchanger where it is heated by the hot air flowing through the shell side before it returns back to the tank. On the hot air side, the air is drawn in by the centrifugal blower and is heated by a heating element before it enters the shell of the PHX. The air is then cooled using cold water, which flows through the tube. The cooled air is then exhausted to the atmosphere. The arrangement of the physical experimental system is shown in Fig. 22.

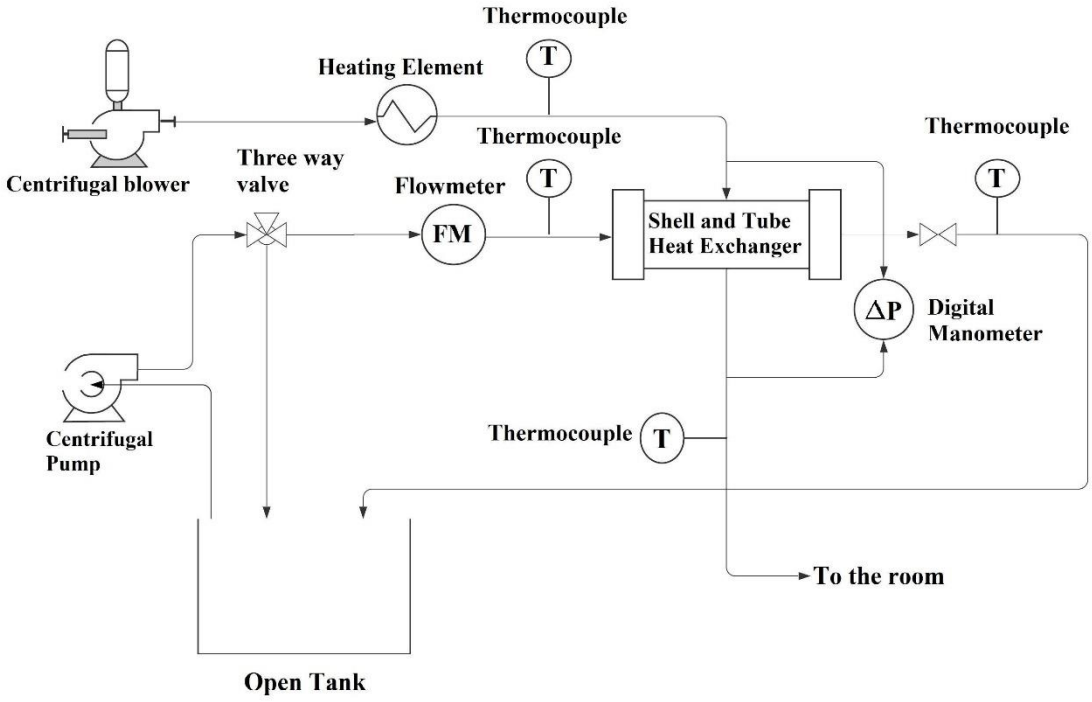

Figure 21. Schematic of the experimental system for single phase heat transfer tests

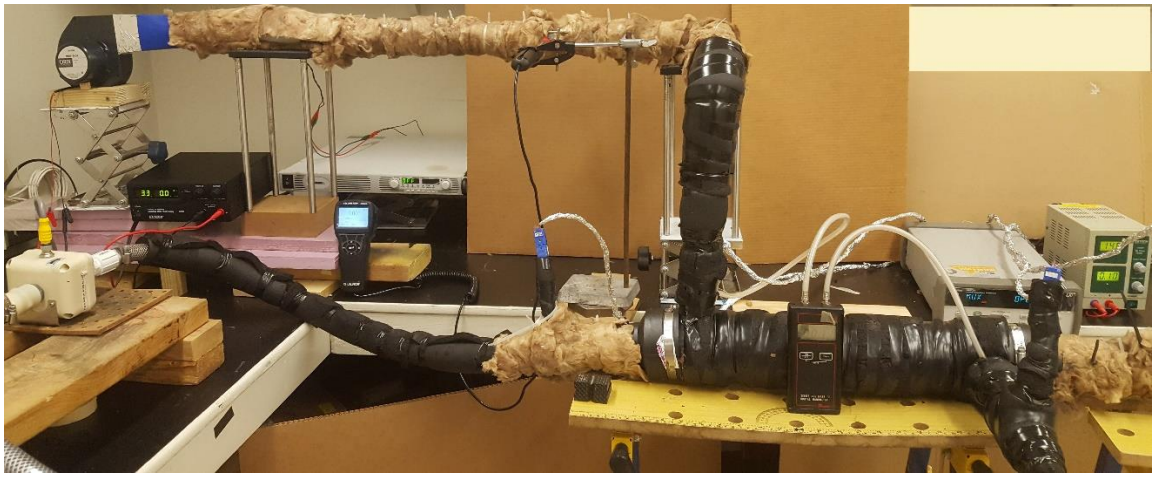

Figure 22. Arrangement of physical experimental set up for single phase heat transfer tests

Fig. 23 shows the schematic drawing of the experimental system for the condensation heat transfer tests. It consists of a water loop, a hot air loop and a data acquisition system. In the water loop, water is pumped from the water tank to the flowmeter. The water loop is the same as the one used for single phase heat transfer. On the air side, a humidifier has been installed along with an axial fan that directs the humid air into the test section. In order to warm the incoming air, a heat gun has been installed just before the humid air enters the test section. The hot and humid air then enters the test section where it cools and gives off both the sensible and latent heat to the coolant flowing on the tube side. The dehumidified air then leaves the shell side of the heat exchanger and is exhausted into the atmosphere. The condensate produced during the process is drained through 12.5 mm (0.5 inch) hole drilled at the bottom of the shell side. The arrangement of the experimental setup is shown in Fig. 24.

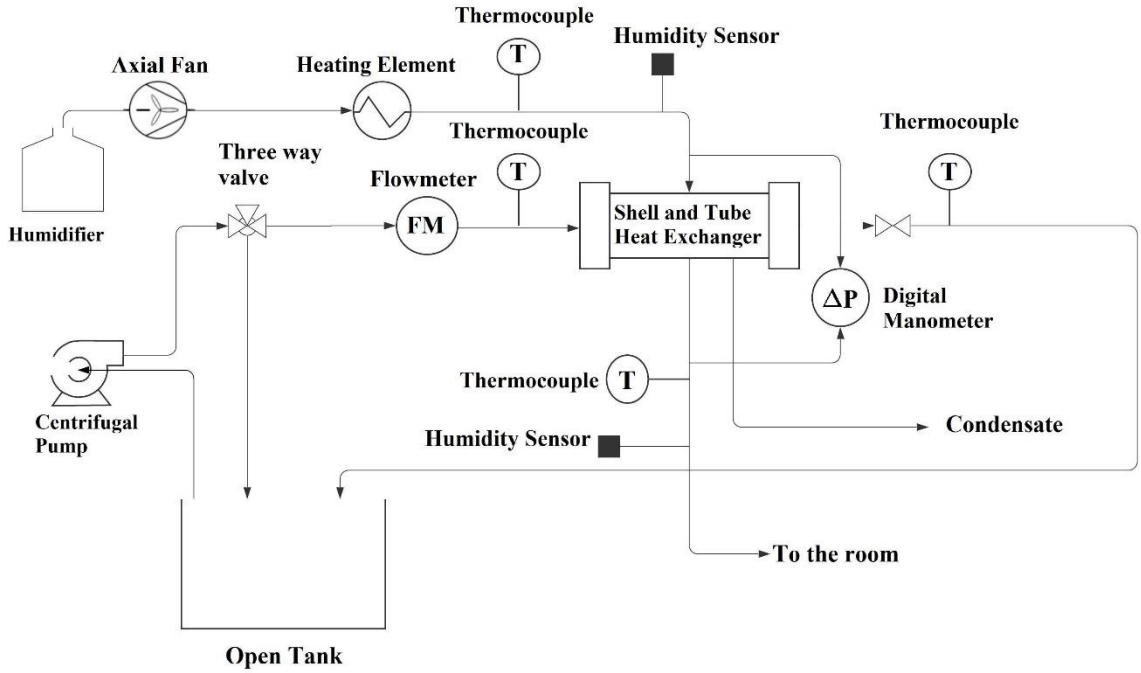

Figure 23. Experimental setup for condensation heat transfer tests

Figure 24. Arrangement of physical experimental set up for condensation heat transfer tests

All the main components of the experimental set up shown in Fig. 22 and 24 are described in detail below.

3.1.1 Plastic Shell-and-Tube Heat Exchangers

Four plastic shell and tube heat exchangers were designed and fabricated for the study. For the tube side, low density Polyethylene tubing 4.7 mm in diameter was used. The tubing was provided by E Poly Tech. The tubing was arranged using different plastic baffle configurations. The shell of the heat exchanger was made of PVC. The exchangers were classified in a group of two, each of which exhibits approximately the same baffle pitch but different baffle configurations. The first group consisted of segmental baffle and continuous helical baffle heat exchanger. The second group consisted of circumferential overlapped quadrant baffle and end-to-end trisection baffle with and incline angle of 40^{o}.

The shell side of all the prototypes was made from 76 mm (3-inch) schedule 40 PVC pipe, which was purchased from McMaster Carr. Each shell was 457.2 mm (18 inch) long. There were three holes drilled on the shell side, two of which were 25.4 mm (1 inch) diameter and the third one was 6.35 mm (0.25 inch) diameter. The 25.4 mm (1 inch) hole was used as the inlet and outlet from the shell and the smaller hole of 6.35 mm (0.25 inch) was used for condensate drainage.

The end manifolds contain a modified baffle as shown in Fig. 25. The manifold had a gap of 3.175 mm (0.125 inch) between the sheets that allowed 3M 8010 epoxy to be injected into the manifold and to create a watertight seal between the tube and the manifold holes. The manifolds have an outside diameter of 89 mm (3.5 inch) to match the outer

diameter of the schedule 40 PVC shell. This allowed the epoxy to be placed between the manifold and PVC to create a watertight seal as shown in Fig 26.

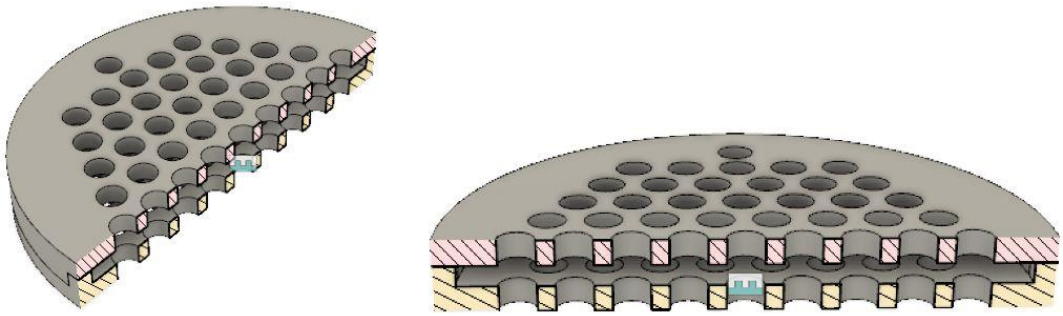

Figure 25. Sectioned view of the manifold

Figure 26. Sealed manifold with tubing

The segmental baffle was manufactured via 3D printing from a polyjet printer using a Full-Cure 720 material. The baffle was 76.7 mm (3.02 inch) in diameter with a 10% baffle cut. Each baffle has 61 holes that are 5.58 mm (0.22 inch) in diameter allowing the 4.76 mm (0.1875 inch) diameter tubing to be smoothly inserted. Fig. 27 and 28 shows the segmental baffle and the prototype containing the segmental baffles.

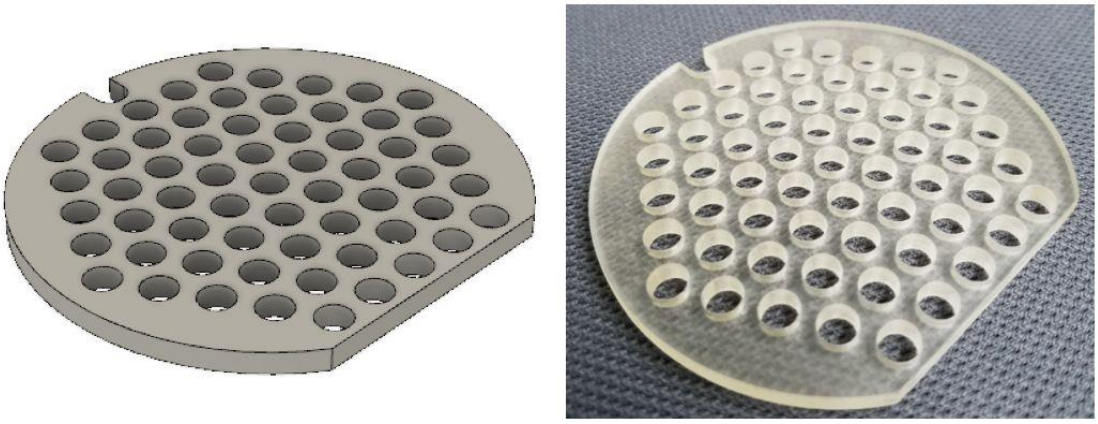

Figure 27. Segmental baffle

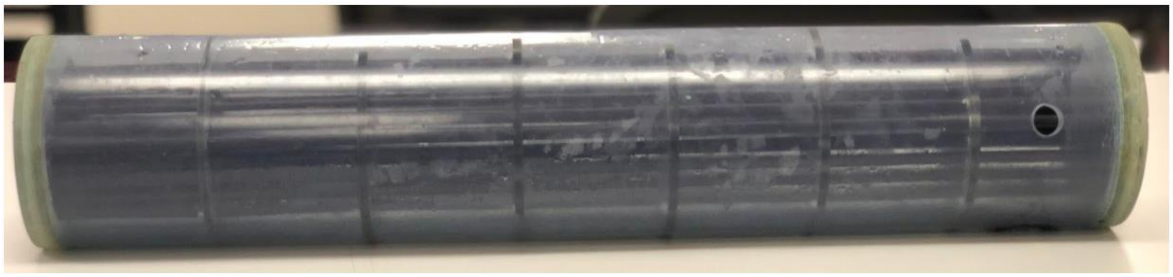

Figure 28. Heat Exchanger with segmental baffles

The continuous helical baffle was printed via 3D printing from a polyjet printer using Full-Cure 720 material. Using a large amount of solvent soluble support structures,

the continuous helix was printed horizontally with one baffle at the end to provide structural support. Once the printing process was completed, a solvent was added to remove all of the support structures. A manifold could not be printed on both sides of the baffle because this would have prevented assembling the baffle inside the shell. The continuous helix assembly was printed to a length of 457.2 mm (18 inch) with an outer diameter of 75.69 mm (2.98 inch). A clearance of 0.254 mm (0.01 inch) between the baffle and shell was taken into account to allow the condensed water to flow to the collection point downwards. A 20° angle was used to make the part easy to fabricate, which gave the continuous helical baffle 6 full rotations. Fig. 29 and 30 shows the continuous helical baffle and the prototypes in which they have been installed.

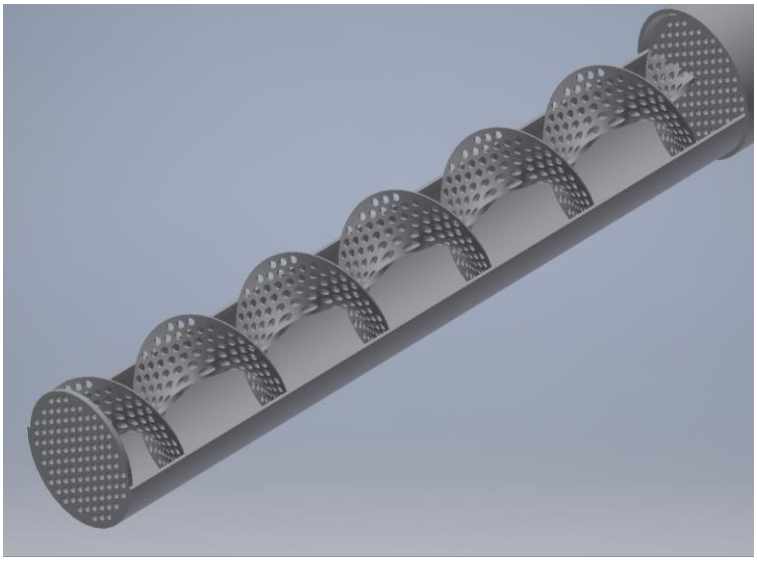

Figure 29. Continuous Helical baffles

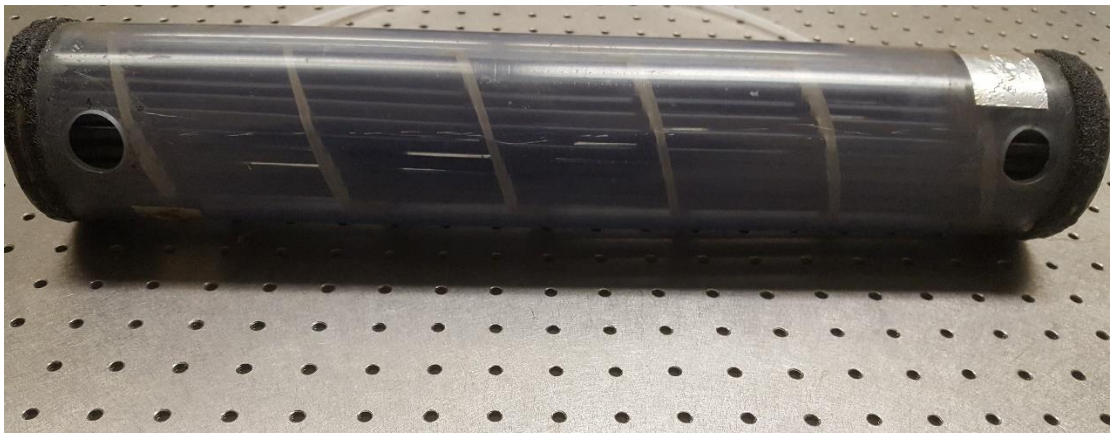

Figure 30. Continuous Helical Baffle Heat Exchanger

The trisection baffles were also 3D printed. The baffles were easier to manufacture with no secondary processing required. They consist of three pieces which are equal in size, with a cut angle of 120°, which when assembled together make a complete circle. The trisection baffles were arranged at an angle relative to the tube axis. Furthermore, they were placed in such a way that they formed a helical flow path through the shell side of the heat exchanger. This kind of baffle arrangement is a non-continuous helical baffle arrangement, where the interspace between the two consecutive segment baffles is the so-called triangle region. They were arranged end to end with no circumferential or middle overlap. Eight printed baffles were used, which were spaced uniformly at a helix angle of 40^{o}. To accommodate the tubing, the baffle has holes of 5.58 mm (0.22 inch). Fig. 31 and 32 show the trisection helical baffle and the prototype in which they have been installed.

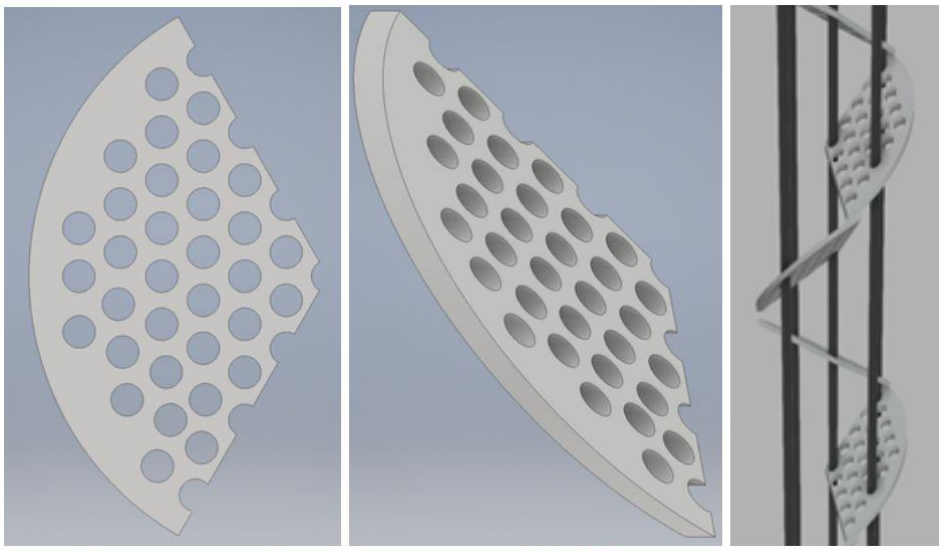

Figure 31. Trisection Baffle

Figure 32. Tri-section Helical Baffle Heat Exchanger

The quadrant baffle has been designed in a similar manner as the trisection baffle. A major difference is that now the baffle is segmented into four equally sized portions and cut at 90° angle. The baffle holes have a diameter of 5.58 mm (0.22 inch) that allows the 4.76

mm (0.1875-inch) diameter LLDPE tubing to pass through them. These baffles were arranged in the shell with end to end overlap. This prototype contains twelve baffles. These baffles are also oriented at a helix angle of 40°. Fig. 33 and 34 show the trisection helical baffle and the prototype in which they have been installed. Table 1 shows all the physical dimension of the four prototypes used in the study.

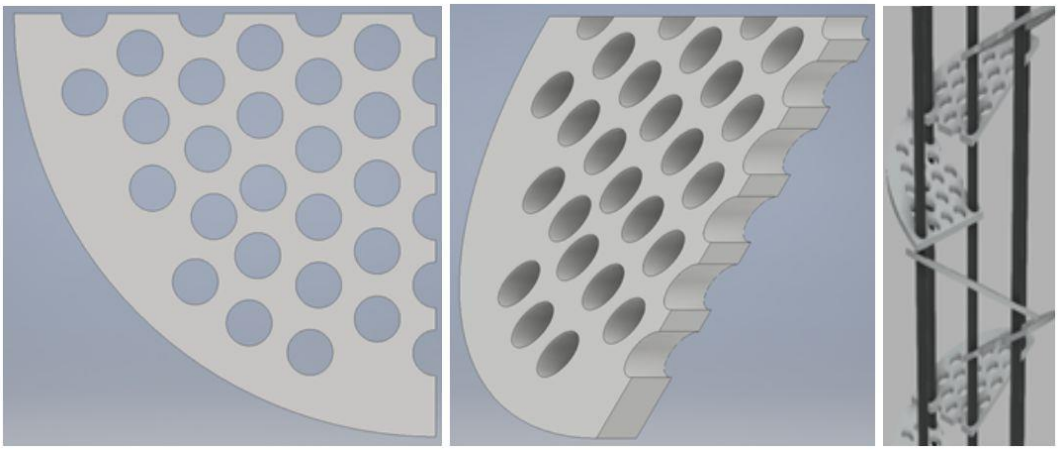

Figure 33. Quadrant baffle

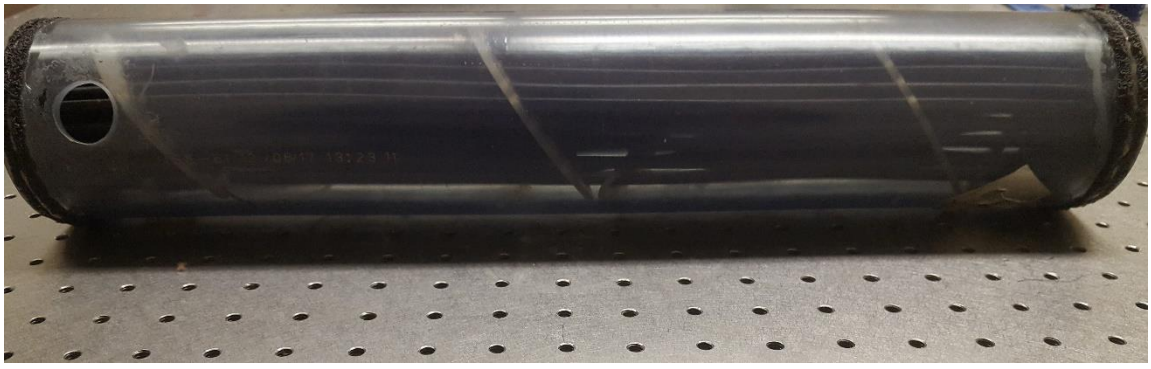

Figure 34. Quadrant Helical Baffle Heat Exchanger

Table 1. Geometric Characteristics of PHXs

Shell Side Parameters		Material of shell	PVC
		Shell Inside Diameter (ID, mm)	76.2
		Diameter of shell inlet and outlet nozzle(mm)	25.4
Tube Side Parameters		Material of tubes	LLDPE
		Outer diameter of tubes (mm)	4.76
		Inside diameter of tube(mm)	4.41
		Tube Pitch (mm)	7.62
		Clearance between adjacent tubes (mm)	10.23
		Effective Length of the tube (mm)	457
		Number of tubes (n)	61
		Thermal Conductivity of tubes(W/m-°C)	0.33
Baffle Parameters	Segmental baffle	Incline angle of baffle (°)	0
		Baffle configuration	Segmental
		Thickness of baffle (mm)	3
		Baffle Pitch (mm)	51
	Continuous helical baffle	Incline angle of baffle	20
		Baffle configuration	Continuous
		Thickness of baffle	3
		Baffle Pitch (mm)	70
	Trisection baffle	Incline angle of baffle (°)	40
		Baffle configuration	End to End
		Thickness of baffle (mm)	3
		Baffle Pitch (mm)	140
	Quadrant baffle	Incline angle of baffle (°)	40
		Baffle configuration	Circumferential overlap
		Thickness of baffle (mm)	3
		Baffle Pitch (mm)	140

3.1.2 Submersible Pump

A submersible pump manufactured by Superior Pump circulated the chilled water through the tube side of the shell and tube heat exchanger. This pump came with its own motor and was rated at 150 W and delivered 6 m^3/h (1560 GPM) to 7.6 m (25 feet) of vertical height. The pump is shown in Fig. 35.

Figure 35. Submersible Pump

3.2.2 Flowmeter

The flowrate on the tube side of the heat exchanger was controlled using a gate valve and it was measured by using an electromagnetic flowmeter model PE-202 with an accuracy of $\pm$ 0.1% manufactured by Seametrics. The full scale of the flowmeter is from

0-0.68 m^3/h (0 to 3 GPM) with an output 4 to 20 milliamps (mA). It can operate up to temperature of 93 °C and pressure of 1000 kPa (150 Psi).

3.2.3 Centrifugal Blower

A centrifugal blower model MBD10-24 manufactured by Oriental Motors was used to direct the air on the shell side of the heat exchanger. The fan uses a 24 VDC to deliver a maximum air flow of 116 m^3/h (68.8 CFM) under maximum static pressure of 0.29 kPa (1.18 inH_2O).

3.3.4 Heating Element:

A Master Appliance HAS-043K heating element was used to heat the air coming from the blower. The heater has a power rating of 1740 W and operates in a temperature range of 400 to 540 °C. The heater was operated by a separate power supply. Fig. 36 shows the heater that was used in the experiments.

Figure 36. Heating Element

3.3.5 Digital Manometer

The Dwyer Series 475-FM Mark III handheld digital manometer was used to measure the pressure drop on the shell side of the heat exchanger. This device measures

the differential pressure in ranges of 0.249 kPa (1 in w.c.) to 49.82 kPa (200 in w.c.). It has an accuracy of ± 0.5% at a temperature range of 15.6 to 25.6 ˚C and ± 1.5% for 25.6 to 40 ˚C. Its temperature limits are -17.8 ˚C to 60 ˚C.

3.3.6 Hot wire Anemometer

The Alnor thermal anemometer AVM440 was used to measure the air velocity coming from the centrifugal blower. This device measures velocity in the range of 0-20 m/s and has an accuracy of ± 5% over the mentioned range. Its temperature range is -18 to 93 ˚C.

3.3.7 Data Acquisition Unit

The flow meters and thermocouples were connected to an Agilent 34970A Data Acquisition & Switch unit, which collected data and made accessible through the Agilent BenchLink Data Logger 3 software. The Agilent data acquisition unit was utilized to record data from thermocouples and flow meters. The switching, conversion and reference junction errors of thermocouples were already taken into account by the unit.

3.3.8 Power Supply

Two power supplies were used to power the centrifugal blower and the heating element. Their descriptions are as follows.

3.3.8.1 Heating Element Power Supply

A TDK-LAMDA GEN 600-2.6 DC power supply was used to power the heating element. The DC power supply was selected to provide a variable heat input to the incoming air. It could operate on an 85-265 VAC continuous input voltage and the output

voltage ranged from 0 to 600 V. The allowable power was 1560 W and maximum current was 2.6 Amps. Fig. 37 shows the LAMDA power supply that was used in the experiments.

Figure 37. Heating Element Power Supply

3.3.8.2 Centrifugal blower Power Supply

An Extech DCP60 DC power supply was used to run the centrifugal blower. The DC power supply was selected to provide a variable air flow rate. It operated at an output voltage ranged from 1 to 60 V. The allowable power was 600 W and maximum current was 10 Amps.

3.3.10 Humidifier

For the condensation heat transfer tests, an ultrasonic humidifier, model LV600HH manufactured by Levoit, was used to direct the humid air to the shell side of the heat exchanger. It has a rated power of 280 W and delivers a maximum output of 300 ml/h of cool mist. Fig. 38 shows the humidifier that was used in the experiments.

Figure 38. LV600HH Ultrasonic Humidifier

3.3.11 Axial Fan

A DC axial fan model number CFM-A238-13-10 manufactured by CUI Devices was used to circulate the air in the duct work for condensation heat transfer tests. This DC brushless type fan operates at 4600 RPM and delivers maximum flow of 340 m^3/h (200.9 CFM) under maximum static pressure of 0.2 kPa (0.78 inH2O).

3.3.12 Heat Gun

A Wagner FURNO 500 heat gun was used to heat the incoming air coming from the axial fan. This heat gun has a maximum and minimum heat output 0f 648 ˚C (1200 ˚F)

and 65 ˚C (150 ˚F) respectively. Its maximum rated output voltage is 1500 W. Fig. 39 shows the heat gun that was used in the experiments.

Figure 39. Wagner FURNO 500 heat gun

3.3.12 Humidity Sensor

A humidity sensor model number CNiTH-i8DH was used to measure the inlet relative humidity of the air coming from the heat gun. The humidity sensor has an accuracy range of ±2% for 10 to 90% RH and ±3% for 0 to 10% RH and 90 to 100% RH. The humidity sensor used in the experiments is shown in Fig. 40.

Figure 40. Omega Humidity Sensor

3.3.12 Humidity Meter

A humidity meter model HH 314 manufactured by OMEGAETTE was also used to measure the humidity of the outlet air coming from the heat exchanger. The meter has a resolution of 0.1%R.H and an operating range of 0 to 100% R.H. It has an accuracy of ±2.5% at 25 ˚C. Its operating temperature range is 0 ˚C (32 ˚F) to 55 ˚C (132 ˚F). Fig. 41 shows the humidity meter that was used in the experiments.

Figure 41. Omegaette HH314 Humidity Meter

The temperature of the water and air were measured by four T-type thermocouples, which were installed at the inlet and outlet nozzle of the PHXs with a data measurement accuracy of ± 0.5 ^{o}C. The overall shell side pressure drop was recorded by a handheld digital manometer (Dwyer 475-FM Mark III), which were calibrated with an accuracy of ±0.5% at a range 0–1.0 MPa. The volume flow rate of water was measured using the electromagnetic flowmeter (Seametrics PE-202) with an accuracy of ±1% of rated range of 0.68 m^3/h (3 GPM). The shell side fluid velocity was measured by a hand held thermal anemometer (Alnor AVM410) with an accuracy of ± 5% over the mentioned range. The velocity readings were later converted to volume flow rate readings by taking into account the cross section of the measuring pipe.

All instruments including thermocouples and flow meter were connected to a data acquisition system (Agilent Data Logger Unit 34972A), which was used for data collection. The exchangers and other sensitive sections were insulated with polyurethane and fiber glass insulation to avoid heat losses.

Several experiments were carried out, and in each run, the flux and the inlet temperature of water in the tube side were fixed to 0.036 m^3/h and 25 $^{\circ}$C. The flux of the shell side oil varied from 7 m^3/h to 10 m^3/h and the inlet temperature was fixed to 70 $^{\circ}$C. All the data were measured after the system had achieved steady state conditions (generally within 20 minutes). Energy balance calculations between the shell side and the tube side were performed to estimate the heat losses, which were found to be less than 10%.

3.4 Data Reduction

During the experiments, temperatures for the inlet and outlet of the coil and shell side heat exchanger as well as flowrates were acquired. In order to obtain the required performance variable data, the data transformation processed are discussed below.

3.4.1 Single Phase Heat Transfer

In analyzing a heat exchanger, it is usually necessary to establish the rate of heat transfer for a set of flow rates and entering conditions. For heat exchanger design and analysis, the heat flow is typically determined using either the Log-mean-temperature difference or the effectiveness-NTU method.

The LMTD Method for Heat Exchanger Analysis

Heat flux is an important parameter in heat exchanger analysis. Q_w is defined as the heat transferred to the cold water, which can be calculated as follows,

$$\dot{Q}_w = \dot{m}_w c_{p,w} (T_{w,o} - T_{w,i}) \quad (1)$$

where $\dot{m}_w$ and $c_{p,w}$ are the mass flow rate and specific heat of water, respectively.

$\dot{Q}_a$ is the heat transferred by the hot air which can be calculated as follows,

$$\dot{Q}_a = \dot{m}_a c_{p,a} \left(T_{a,i} - T_{a,o}\right) \quad (2)$$

where $\dot{m}_a$and $c_{p,a}$ are the mass flow rate and specific heat of hot air, respectively.

The average heat exchange rate is defined as,

$$\dot{Q}_a = \frac{\dot{Q}_w + \dot{Q}_a}{2} \quad (3)$$

The heat balance deviation in percentage is,

$$\delta = \frac{|\dot{Q}_w + \dot{Q}_a|}{2} \times 100\% \quad (4)$$

In the present study, only the data satisfying the heat balance condition (δ is less than 10%) are used in the analysis.

Overall heat transfer coefficient:

The overall heat transfer coefficient is basically a reciprocal of the total thermal resistance. As the fluid moves inside the heat exchanger the heat transfer process involves several mechanisms. It involves convective heat transfer from the hot fluid to the wall, conductive heat transfer through the wall and further convective heat transfer from the wall to the cold fluid. The overall process involves heat transfer through the boundary

layer near the wall, might involve fouling. All these various effects can be expressed in terms of a thermal resistance as follows [26]:

$$\frac{1}{R_{th}} = \frac{1}{h_o} + \frac{l}{k_w} + \frac{1}{h_i} + \frac{1}{f_o} + \frac{1}{f_i} = U \tag{5}$$

where R_{th} is the total thermal resistance, h_o and h_i are the shell side and tube side heat transfer coefficient, f_o and f_i are the shell side and tube side fouling resistances and k_w is the thermal conductivity of the tube wall. The above method can be used if the value of all the resistances are known. However, there is alternative method to determine the overall heat transfer coefficient, which is defined as,

$$\dot{Q} = U A_o \Delta T_{LM} \tag{6}$$

where $A_o$is the heat exchanger area based on the number of tubes, outer diameter of the tube $d_o$and effective length l. The A_o area is given by

$$A_o = n\pi d_0 l \tag{7}$$

ΔT_L is the log mean temperature difference and is given by,

$$\Delta T_{LM} = \frac{(T_{h,i} - T_{c,i}) - (T_{h,o} - T_{c,o})}{\ln\left(\frac{T_{h,i} - T_{c,i}}{T_{h,o} - T_{c,o}}\right)} \tag{8}$$

The appropriate form of the log-mean temperature difference for shell and tube heat exchanger is more difficult to derive [27]. Although an analytical solution can be obtained for some specific configuration but the resulting expression is algebraically complicated and therefore inconvenient. An alternative approach can be used which recognizes that the ΔT_{LM} for these heat exchangers will always be less than the log-mean

temperature difference for the counter flow arrangement. Therefore ΔT_{LM} for any configuration can be expressed as

$$\Delta T_{LM} = F\ \Delta T_{LM,cf} \tag{9}$$

where $\Delta T_{LM,cf}$ is the log mean temperature difference for a counter flow arrangement and F is the correction factor that always has a value less than unity. For a given heat exchanger F depends on the capacitance rates and heat exchanger conductance. The effect of these numbers can be defined by two non-dimensional numbers which are defined as follows,

$$P = \frac{(T_{c,o} - T_{c,i})}{(T_{h,i} - T_{c,i})} \tag{10}$$

$$R = \frac{(T_{h,i} - T_{h,o})}{(T_{c,o} - T_{c,i})} \tag{11}$$

The quantity P and R are sometimes referred to as the LMTD effectiveness and LMTD capacitance ratio, respectively. In order to compute these variables, there are built in libraries that have been developed and integrated in software packages as Engineering Equation Solver (EES) to provide the value of F. These functions can be accessed from the function information window by selecting the category Heat Exchangers and sub category F for $LMTD$.

In the analysis if heat exchanger data, it is convenient to know the shell side Reynolds number, which is defined as follows,

$$Re_s = \frac{u_s \rho D_{equ}}{\mu} \tag{12}$$

where u_s is shell side velocity, ρ is the density of the air, μ is the dynamic viscosity and D_{equ} is the equivalent diameter, which is found as follows,

$$D_{equ} = \frac{4\ (free\ flow\ area)}{wetted\ perimeter} = \frac{4A_f}{P_w} \tag{13}$$

The free flow area and wetted perimeter are calculated as follows,

$$A_f = \frac{\pi}{4} {D_i}^2 - n\ \frac{\pi}{4} {d_0}^2 \tag{14}$$

$$W_p = \pi D_i + n\pi d_0 \tag{15}$$

where D_i is the internal diameter of the shell, d_0 is the external diameter of the tubes and n is the number of tubes. Hence,

$$D_{equ} = \frac{{D_i}^2 - n\ {d_0}^2}{D_i + n d_0} \tag{16}$$

For obtaining the mean shell side velocity u_s, the following formula is used,

$$u_s = \frac{\dot{m}_a}{\rho A_{cross}} \tag{17}$$

where $\dot{m}_a$ is the mass flow rate of air on the shell side and A_{cross} shows the cross-flow area at the shell centerline, ρ is the density of the air. The cross-flow area can be defined as follows,

$$A_{cross} = L(D_i - n_c d_0) \tag{18}$$

where D_i is the internal diameter of the shell, d_0 is the external diameter of the tubes, L is the baffle spacing and n_c is the number of tubes in the central row and is given by,

$$n_c = \frac{D_i}{P_t} \tag{19}$$

where P_t is the pitch of the tube.

The ε-NTU Method for Heat Exchanger Analysis

In the ε-NTU method the heat transfer rate from the hot fluid to the cold fluid in the exchanger is expressed as,

Heat Exchanger Effectiveness

$$\dot{Q} = \varepsilon C_{min}\left(T_{h,i} - T_{c,i}\right) = \varepsilon C_{min}\Delta T_{max} \tag{20}$$

where ε is the heat exchanger effectiveness and is given by,

$$\varepsilon = \frac{\dot{Q}}{\dot{Q}_{max}} \tag{21}$$

which is the ratio of actual heat transfer rate in a heat exchanger to the thermodynamically limited maximum possible heat transfer rate if an infinite heat transfer surface area were available in a heat exchanger.

The actual heat transfer is obtained by either the energy given off by the hot fluid or the energy received by the cold fluid, from the following equations,

$$\dot{Q} = \dot{m}_h c_h \left(T_{h,i} - T_{h,o}\right) = \dot{m}_c c_c \left(T_{c,o} - T_{c,i}\right) \tag{22}$$

The fluid that might undergo the maximum temperature difference is the fluid with the minimum heat capacity rate C_{min}. Therefore, the maximum possible heat transfer is expressed as,

$$\dot{Q}_{max} = (\dot{m}c_p)_c \left(T_{h,i} - T_{c,i}\right) \; if \; C_c \; < C_h \tag{23}$$

or

$$\dot{Q}_{max} = (\dot{m}c_p)_h \left(T_{h,i} - T_{c,i}\right) \; if \; C_h \; < C_c \tag{24}$$

Heat exchanger effectiveness, ε, is therefore written as,

$$\varepsilon = \frac{C_h\left(T_{h,i} - T_{h,o}\right)}{C_{min}\left(T_{h,i} - T_{c,i}\right)} = \frac{C_c\left(T_{c,o} - T_{c,i}\right)}{C_{min}\left(T_{h,i} - T_{c,i}\right)} \quad (25)$$

The first definition is for $C_h = C_{min}$ and the second is for $C_c = C_{min}$.

The heat exchanger effectiveness ε is nondimensional, and is dependent on the number of transfer units NTU, the heat capacity rate ratio $C^*$and the flow arrangement for a direct transfer type heat exchanger[6]:

$$\varepsilon = \varphi\ (NTU, C^*, flow\ arrangement) \quad (26)$$

Heat Capacity Rate Ratio

The heat capacity rate of each flow is the product of the mass flow rate and specific heat. It is convenient to identify the streams which have minimum or maximum value of the heat capacity rate. The heat capacity rate ratio of heat exchanger is given by,

$$C^* = \frac{C_{min}}{C_{max}} \quad (27)$$

where C_{min} and C_{max} are the smaller and larger of the two magnitudes of heat capacity rates, respectively. The C_{max} fluid experiences a smaller temperature change than the temperature change for the C_{min} fluid. However, for a condensing or an evaporating fluid at ideally constant temperature, ΔT range is zero and hence the heat capacity rate C approaches to infinity. Since $C = \dot{m}c_p$ The effective specific heat of condensing or evaporating fluid is hence infinity.

Number of Transfer Units

The number of transfer units is a combination of overall heat transfer coefficients, transfer area, fluid flow rate and heat capacity. It is defined as the ratio of the overall thermal conductance to the smaller heat capacity rate:

$$NTU = \frac{UA}{C_{min}} = \frac{1}{C_{min}} \int UdA \tag{28}$$

It summarizes these dimensional parameters into one dimensionless parameter. NTU designates the non-dimensional heat transfer size or thermal size of the heat exchanger, and therefore is a design parameter. It is a nondimensional expression of the "heat transfer size" of the exchanger. Hence when NTU is small, the exchanger effectiveness is low; and when the NTU is large, the effectiveness approaches asymptotically the limit imposed by the flow arrangement and thermodynamic limits[28].

3.4.2 Condensation Heat Transfer

When the heat exchanger surface temperature is below the dew point temperature of the incoming moist air, the surface is subjected to condensation by the moisture contained in the air. A heat exchanger that causes moisture removal in addition to removing the sensible heat is said to undergo a cooling and dehumidification process. Condensation through the dropwise mode, filmwise mode or a combined condensation mode will take place on the surface depending on its wettability. Dropwise condensation forms on a surface having poor wettability, whereas filmwise condensation occurs on a surface having good wettability [29] mainly.

In most air conditioning applications, air is considered to be a mixture of water vapor and air, both of which enter the air conditioning coil at the same dry bulb temperature. As the air-water mixture travels through the coil, it losses sensible heat when it comes into contact with the first part of the cooling coil, in the same way as in dry cooling coils. The moisture removal process occurs only in those portions of the coil where the temperature of the coil is below the dew point temperature of the air mixture [31].

Mixture condensation differs from the pure vapor condensation in two ways. Firstly, the temperature at which the condensation occurs changes throughout the condenser as the relative humidity of air decreases. Secondly, in air-water mixtures there are two mass transfer and heat transfer resistances whereas in pure condensation there is only one heat and mass transfer resistances on the surface of the coil. The key point to note here is that as the vapor mixture flows through the condenser, its dew point falls and thus causing the condensing equilibrium temperature of vapor in the air to fall [30].

Surface condition of the cooling coil

For a given cooling coil there are three possible operating conditions that determined the amount of moisture removal. The approaches used for determining the heat transfer for each of these situations are as follows [29]:

1) The tube surface on the air side is completely dry. In this situation the temperature of the tube surface on the air side is above the dew point temperature of the entering air and condensation does not occur anywhere in the coil. For this condition, the cooling process only includes the sensible cooling process, and the humidity ratio is always constant. It can be indicated by a horizontal line toward the saturation curve on the psychrometric chart, shown in Fig.41. In this case, the conventional sensible heat transfer analysis can be performed using the ε-NTU method.
2) The tube surface on the air side is completely wet. In this situation the temperature of the tube surface on the air side is below the dew point temperature of the entering air and condensation occurs immediately as the air enters the coil. To

determine the coil performance for this situation, wet coil analysis should be performed.

3) The coil surface area on the air side is partially dry and partially wet. In this situation the temperature of the tube surface on the air side is below the dew point temperature of the entering air at some position inside the coil. Hence, there is some dry section where the air enters which is followed by a wet section, where the air leaves. Therefore, there would be sensible heat transfer in the entering section of the coil, which is followed by heat and mass transfer, where condensation occurs. In this case, both the dry and wet coil analysis will be used to determine the coil performance.

In most of the cooling processes in the cooling coil, the dew point of the entering air is higher than the cooling coil surface temperature, because of this, the coil is usually under wet or partially wet conditions. Under these conditions the water vapor in the entering air will be condensed and then the condensate will be drained out. The cooling coil not only cools the air but also dehumidifies the air. The cooling and dehumidification process is shown on the psychrometric chart as shown in Fig. 42.

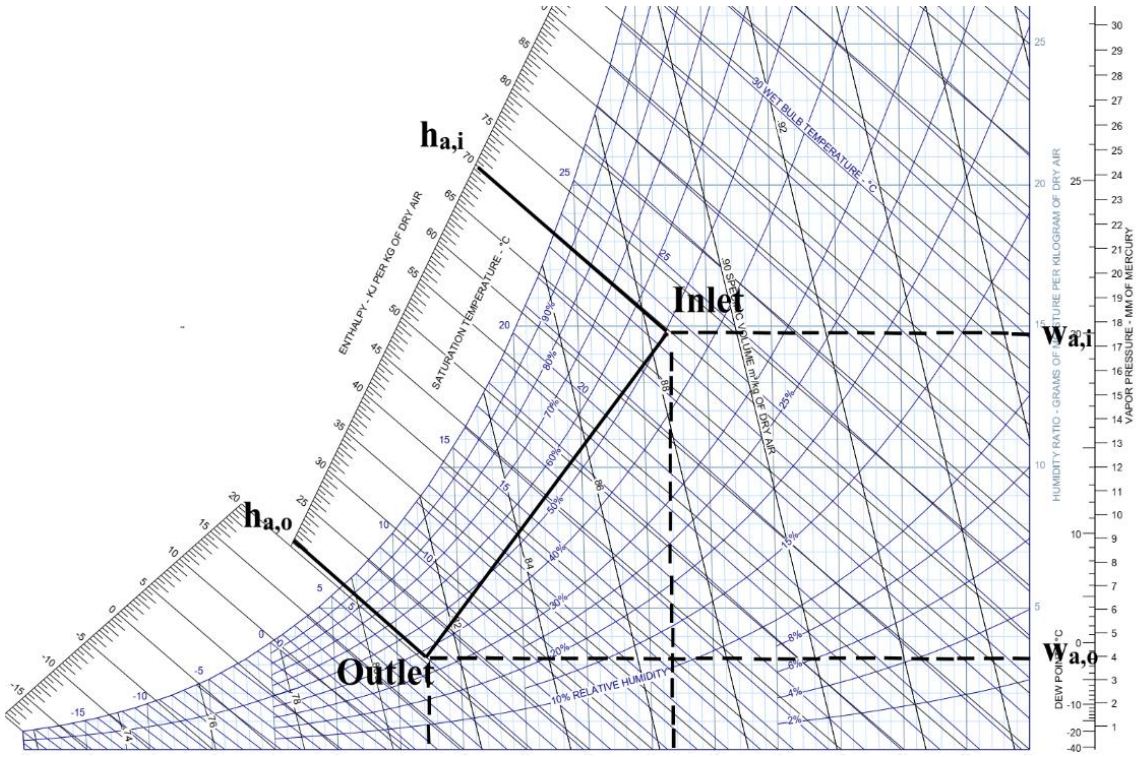

Figure 42. Psychrometric chart of cooling and dehumidifying process

During the condensation heat transfer experiments, the water inlet temperature was around 15˚C less than the dew point temperature of the entering air. Hence in this research we have assumed that the tubes were completely wet and have determined the heat and mass transfer using wet coil analysis.

The LMTD Method for Heat Exchanger Analysis for Condensation

The air side heat transfer coefficient of shell and tube heat exchanger is much more difficult to determine under wet conditions than as compared to dry conditions. This is because in the case of wet condition, the sensible and latent heat transfer processes occur

simultaneously. Hence, the difference in temperatures cannot give a true representation of the heat transfer rate [31].

Therefore, the enthalpy potential equation is used to calculate the air side heat transfer coefficient under wet conditions. The equation is given by,

$$\dot{Q}_{avg} = U_0 A_o \Delta h_m \tag{29}$$

where U_0 is the overall heat transfer coefficient, A_o is the total heat transfer area, $\dot{Q}_{avg}$ is the mathematical average of $\dot{Q}_a$ and $\dot{Q}_w$ and is given by,

$$\dot{Q}_{avg} = \frac{\dot{Q}_a + \dot{Q}_w}{2} \tag{30}$$

$$\dot{Q}_a = \dot{m}_a \left(h_{a,i} - h_{a,o}\right) \tag{31}$$

$$\dot{Q}_w = \dot{m}_w c_{pw} \left(T_{w,o} - T_{w,i}\right) \tag{32}$$

Δh_m is the log mean enthalpy difference and is given by Eq. 30 [32],[33].

$$\Delta h_m = \frac{(h_{a,i} - h_{w,o}) - (h_{a,o} - h_{w,i})}{\ln\left(\frac{h_{a,i} - h_{w,o}}{h_{a,o} - h_{w,i}}\right)} \tag{33}$$

where $h_{a,i}$ and $h_{a,o}$ are the inlet and outlet enthalpies of the air that have been computed from the psychrometric chart against the inlet and outlet air temperature and relative humidity. $h_{w,i}$ and $h_{w,o}$ are the saturated air enthalpy at the inlet and outlet water temperature.

Here the term $\dot{Q}_a$ accounts for both the sensible and latent heat transfer from the air to the coolant flowing in the tubes.

The $\boldsymbol{\varepsilon}$-NTU Method for Heat Exchanger Analysis for Condensation

The energy transfer for a cooling coil is written in a form analogous to that for a sensible heat exchanger. Using an effectiveness for the heat and mass transfer ε_h, the inlet enthalpy of the air stream, and the enthalpy of saturated air at the water inlet temperature, the energy transfer to the water stream is,

$$\dot{Q} = \varepsilon_h \dot{m}_a (h_{a,i} - h_{w,sat,i}) \tag{34}$$

The heat and mass transfer effectiveness are based on the air side enthalpies and is the ratio of the actual enthalpy change of the air to the maximum possible change. The maximum change would occur if the air stream exited the coil in equilibrium with the water at the inlet, and the enthalpy would then be the saturation value at the water inlet temperature [34].

In order to evaluate the thermal performance of the dehumidifier, Braun *et al.* [35] proposed the effectiveness-NTU method for modeling cooling towers and cooling coils. Braun *et al.* [35] developed the effectiveness relationships through the introduction of an air saturation specific heat. These relationships can be used to set up heat transfer models for cooling coils under dry, wet, and partially wet conditions. Moreover, for the partially wet conditions, Braun *et al.* [35] assumed the cooling coils were initially completely dry or wet to get two distinct results; then they chose the larger value as the result of partially wet conditions. They proved that the error of this method when used to estimate the heat transfer of cooling coils under partially wet conditions is less than 5%.

The two dimensionless parameters proposed by Braun *et al.* [35] are the enthalpy effectiveness and humidity effectiveness. The enthalpy effectiveness is used to evaluate

the performance of coil in terms of removing the total cooling-load and is defined as follows,

$$\varepsilon_h = \frac{h_{a,i} - h_{a,o}}{h_{a,i} - h_{w,sat\ i}} \tag{35}$$

where $h_{a,i}$ and $h_{a,o}$ are the inlet and the outlet enthalpy values of the air determined from the measured inlet and outlet relative humidity ratio values and temperature values, respectively. $h_{w,sat\ in}$ is the enthalpy of the saturated air at the water inlet temperature. Secondly, the humidity effectiveness is used to evaluate the latent load removal performance of the coil.

$$\varepsilon_w = \frac{w_{a,i} - w_{a,o}}{w_{a,i} - w_{w,sat\ i}} \tag{36}$$

where $w_{a,i}$ and $w_{a,o}$ are the inlet and the outlet humidity ratio of the air determined from the inlet and outlet relative humidity ratio and temperatures values, respectively. $w_{w,sat\ in}$ is the humidity ratio of the saturated air at the water inlet temperature.

In dehumidification, the air stream enthalpy $h_a$is analogous to the temperature of the minimum capacitance fluid at T_{min}, and the saturated air enthalpy at the fluid temperature, $h_{w,sat}$ is analogous to the temperature of the maximum capacitance fluid at T_{max}. There is also a correspondence between the capacitance rate ratios for the sensible-only and sensible-latent cooling. Similarly $m^*$is analogous to the capacitance rate ratio C_{min}/C_{max} used in sensible cooling only (single phase cooling), as follows

$$m^* = \frac{\dot{m}_a c_s}{\dot{m}_w c_{p,w}} \tag{37}$$

where $\dot{m}_a$is the mass flow rate, c_s an effective specific heat, $\dot{m}_w$ the mass flow rate, and $c_{p,w}$the water specific heat. The effective specific heat, c_s, is the change in enthalpy with respect to the temperature along the saturation line and is evaluated numerically using the water inlet and outlet states as follows:

$$c_s = \left(\frac{h_{w,sat,in} - h_{w,sat,out}}{T_{w,i} - T_{w,o}} \right) \tag{38}$$

Braun *et al.* [35] proposed the following model to compute the $\epsilon_{a,\,wet}$,

$$\varepsilon_{a,\,wet} = \frac{1 - \exp\left(-Ntu_{wet}(1 - m^*)\right)}{1 - m^* \exp\left(-Ntu_{wet}(1 - m^*)\right)} \tag{39}$$

It is convenient to define a mass transfer number of units, NTU^*that is analogous to the heat transfer, NTU as follows:

$$NTU^* = \frac{U^* A_o}{C_{min}} \tag{40}$$

Where C_{min} is the same as that used in Equation 28 because the amount of water in air-water mixture is relatively insignificant. Hence by replacing the sensible heat exchanger variables of the effectiveness-NTU equations with the corresponding variables for the heat and mass transfer processes, the heat exchanger effectiveness-NTU relations can be used to evaluate dehumidification performance on a standard basis.

CHAPTER IV

RESULTS AND DISCUSSION

4.1 Single phase heat transfer in Plastic Heat Exchanger (PHXs)

Several single phase heat transfer experiments were conducted to evaluate the performance of the four PHXs with different baffle configurations. Each prototype was tested at five different volume flowrates of the air. In each test, the air inlet temperature and the water inlet temperature were kept approximately constant. Also, the flow rate of the water side was fixed around 11cm^3/s. As a result, flow inside the tubes was laminar (Re_{tube} = 50). The effectiveness, overall heat transfer coefficient and number of transfer units (NTU) were determine using experimental data. All the values of the process and performance parameters for the different baffle configuration are shown in the Tables 2-9.

Table 2. Flowrates and temperature data for segmental baffle heat exchanger

Trial No.	$\dot{V}_a$ (m^3/hr)	$\dot{V}_w$ (cm^3/s)	$T_{w,i}$ (°C)	$T_{a,i}$ (°C)	$T_{w,o}$ (°C)	$T_{a,o}$ (°C)
1	7.18	11.1	23.5	72.7	25.1	34.5
2	7.48	11.1	24.1	72.6	25.8	35.4
3	8.06	11.1	24.2	72.0	26.0	35.8
4	8.24	11.1	23.7	70.8	25.6	36.2
5	8.79	11.1	23.3	69.8	25.3	36.6

Table 3. Performance parameters of segmental baffle heat exchanger

Trial No.	ΔP (Pa)	$\dot{Q}$ (W)	U (W/m^2.$^\circ$C)	ε	Re_s	NTU
1	180	65.6	6.87	0.65	683	1.408
2	196	71.9	7.55	0.70	711	1.485
3	218	80.2	8.43	0.73	769	1.536
4	235	77.8	8.41	0.70	792	1.493
5	260	83.5	8.49	0.71	848	1.408

Table 4. Flowrates and temperature data for continuous helical baffle heat exchanger

Trial No.	$\dot{V}_a$ (m^3/hr)	$\dot{V}_w$ (cm^3/s)	$T_{w,i}$ ($^\circ$C)	$T_{a,i}$ ($^\circ$C)	$T_{w,o}$ ($^\circ$C)	$T_{a,o}$($^\circ$C)
1	8.83	11.1	21.9	68.6	23.6	36.9
2	9.31	11.1	24.3	70.0	26.3	36.8
3	9.64	11.1	24.3	68.6	26.3	35.8
4	10.04	11.1	25.2	69.2	27.5	34.5
5	10.63	11.1	24.5	69.2	27.2	35.0

Table 5. Performance parameters for continuous helical baffle heat exchanger

Trial No.	ΔP (Pa)	$\dot{Q}$ (W)	U (W/m^2.$^\circ$C)	ε	Re	NTU
1	152	66.9	6.98	0.56	623	1.15
2	171	76.6	8.68	0.63	651	1.36
3	185	85.6	9.85	0.69	679	1.49
4	206	92.9	12.10	0.73	706	1.76
5	228	104.2	12.46	0.76	747	1.71

Table 6. Flowrates and temperature data for trisection helical baffle heat exchanger

Trial No.	$\dot{V}_a$ (m^3/hr)	$\dot{V}_w$ (cm^3/s)	$T_{w,i}$ (˚C)	$T_{a,i}$ (˚C)	$T_{w,o}$ (˚C)	$T_{a,o}$(˚C)
1	9.34	11.1	25.3	70.3	27.1	36.8
2	9.82	11.1	25.5	69.5	27.4	38.4
3	10.08	11.1	24.1	70.2	26.2	38.1
4	10.33	11.1	24.5	69.6	26.7	39.4
5	11.18	11.1	25.3	70.0	27.8	39.7

Table 7. Performance parameters for trisection baffle heat exchanger

Trial No.	ΔP (Pa)	$\dot{Q}$ (W)	U (W/m^2.˚C)	ε	Re	NTU
1	151	74.4	8.61	0.61	307	1.46
2	164	79	8.61	0.63	333	1.34
3	180	85.8	8.72	0.64	344	1.32
4	193	87.5	8.58	0.65	360	1.24
5	210	96.2	9.67	0.67	385	1.31

Table 8. Flowrates and temperature data for quadrant helical baffle heat exchanger

Trial No.	$\dot{V}_a$ (m^3/hr)	$\dot{V}_w$ (cm^3/s)	$T_{w,i}$ (ºC)	$T_{a,i}$ (˚C)	$T_{w,o}$ (˚C)	$T_{a,o}$(˚C)
1	8.46	11.1	25.0	70.3	26.8	37.2
2	9.34	11.1	25.8	70.1	27.7	38.1
3	9.75	11.1	26.0	69.2	28.0	38.1
4	10.32	11.1	25.4	69.5	27.5	37.7
5	10.85	11.1	24.3	69.3	26.7	37.8

Table 9. Performance parameters for the quadrant baffle heat exchanger

Trial No.	ΔP (Pa)	$\dot{Q}$ (W)	U ($W/m^2.^{\circ}C$)	ε	Re	NTU
1	148	77.7	8.48	0.703	302	1.43
2	160	84.3	9.16	0.707	332	1.43
3	170	86.6	9.60	0.712	349	1.47
4	188	93.9	10.23	0.714	368	1.45
5	203	106.4	10.29	0.754	388	1.38

It can be seen from Tables 2 through 9 that, the flow on the shell side of the heat exchangers was primarily laminar in nature. However, baffle design and configuration did promote adequate convective heat transfer as seen and discussed in the next section.

4.1.1 Heat Transfer Rate in PHXs

Heat transfer rate is a significant parameter to determine the performance of heat exchangers. Fig. 43 presents the variation of the heat transfer rate as a function of the shell side volume flow rate. It can be seen from both the figures that heat transfer rate increases with the shell side volume flow rate for all baffle configurations. It can be seen from Fig. 43 that for the same volume flow rate of air (9 m^3/h), the heat transfer rate of the segmental baffle configuration was on average 18% higher than the rate for the continuous and trisection helical baffle configurations. Furthermore, the segmental baffle configuration was around 6% higher for the quadrant baffle heat exchanger. One of the main difference between the segmental baffle HX and the other HX configurations is the baffle inclination angle (helix angle), which is zero for the segmental HX. For HX with low or zero

inclination angle, less cross sectional flow area is available, which in turn leads to higher fluid velocities and greater momentum transfer.

Moreover, it can be seen that the heat transfer rate of the circumferential overlap quadrant baffle is relatively higher than the trisection baffle heat exchanger configuration. This is because some of the flow bypasses through the triangular section present in that type of configuration.

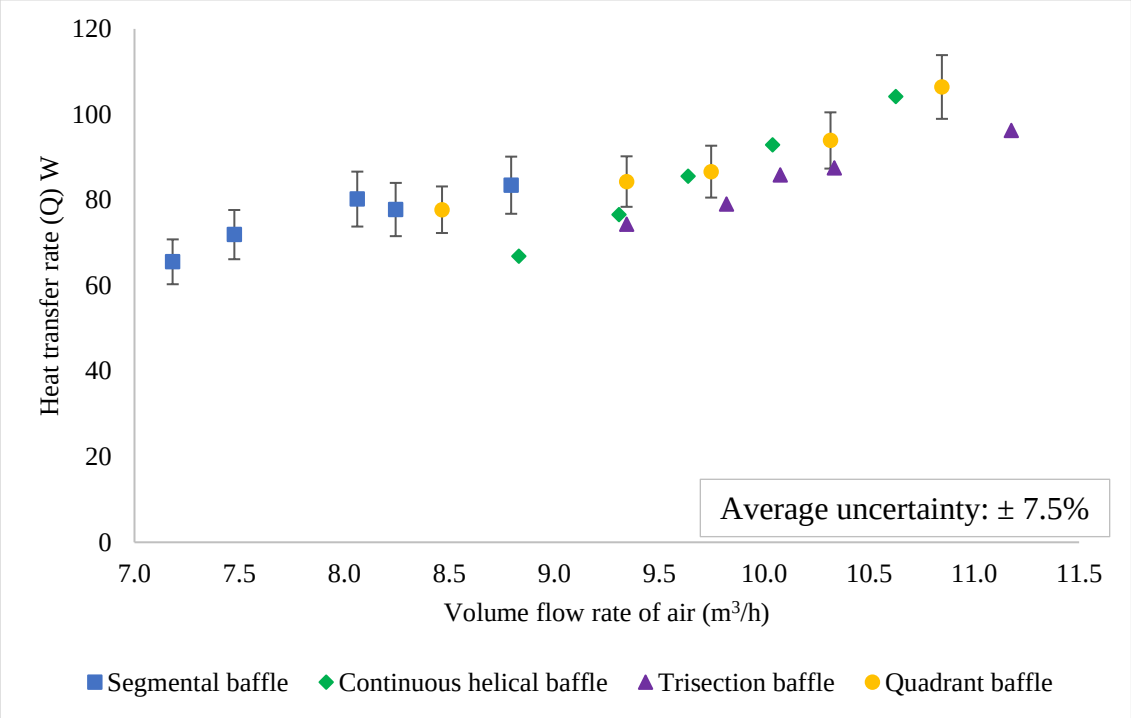

Figure 43. Heat transfer rate of plastic heat exchangers as a function of shell side volume flowrate

4.1.2 Overall Heat Transfer Coefficient in PHXs

The overall heat transfer coefficient was determined by using the average rate of heat transfer and the log mean temperature difference. As it can be seen from Fig. 44, the overall heat transfer coefficient increases with the shell side volume flow rate. It can be

seen from the figure that at the same volume flow rate of air (9 m^3/h), the overall heat transfer coefficient of the segmental baffle was on average 18%, 20% and 7% higher than the continuous helical, trisection and quadrant baffle heat exchangers respectively.

On comparing the helical baffles, the overall heat transfer coefficient of the circumferential overlap quadrant baffle is higher than the continuous helical and trisection one. This result suggests that in the case of quadrant helical baffle, the corresponding triangular leakage area is less due to the circumferential baffle overlap, which prevents a considerable amount of fluid to leak from the upstream to the downstream chamber. Hence, the fluid flows around the tube bundle in a helical flow pattern [9]. This result is in accordance with previous studies wherein the heat transfer enhancement increases gradually as the baffle helix angle increases from 25^o to 40^o [36]. Hence this effect was not considerable in the case of continuous helical baffle which has a baffle inclination angle of 20^o .

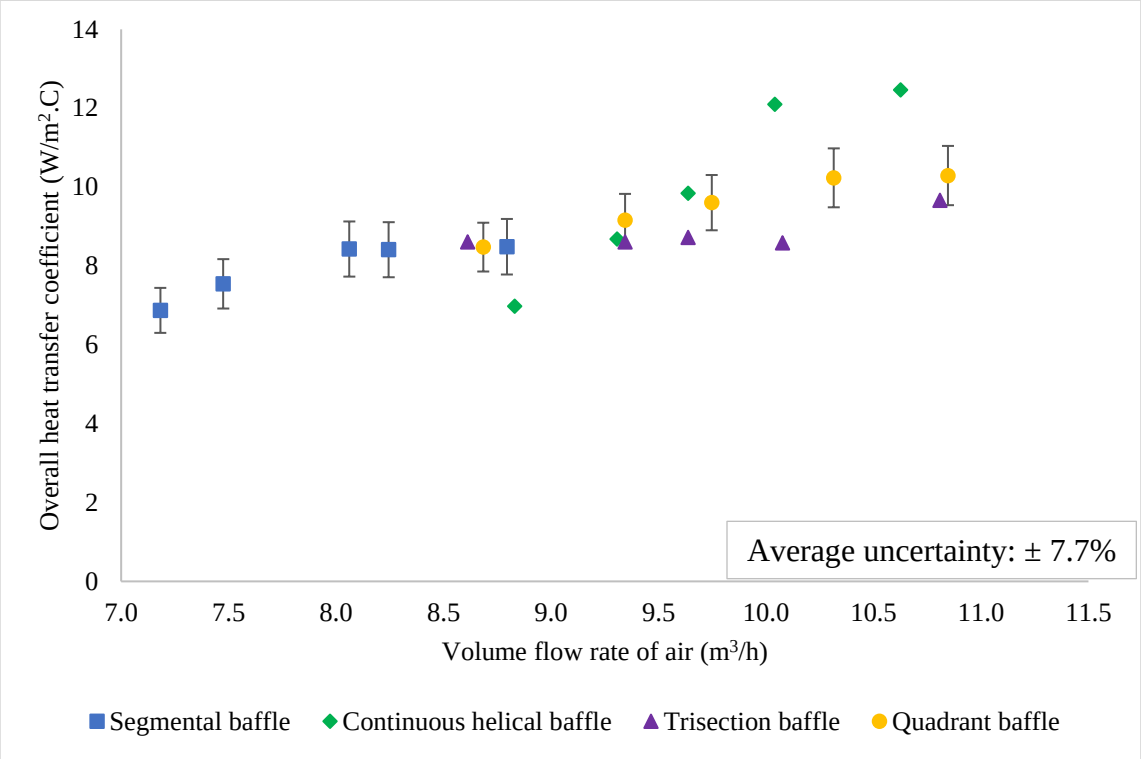

Figure 44. Overall heat transfer coefficient of plastic heat exchanger as a function of shell side volume flowrate

4.1.3 Pressure Drop in PHXs

The pressure drop is an important parameter in the design of STHXs. Pumping costs are dependent on the pressure drop of an exchanger; therefore, lower pressure drop leads to lower operating cost.

Fig. 45 depicts the variation of shell side pressure drop versus the shell side volume flow rate for the four PHXs with different baffle configuration. As it can be seen from the figure, the pressure drop increases proportionally with volume flowrate of the shell side fluid. Moreover, the pressure drop of all the PHXs increases with the decrease of baffle inclination angle. In contrast, the pressure drop of all helical baffle heat

exchangers are lower than that of segmental heat exchanger. This is because in segmental baffle heat exchanger, the flow on the shell side does follow zigzag pattern, which could lead to flow separation on the edges of baffles. Moreover, the baffle cut in the case of the segmental baffle heat exchanger is about 10% of shell diameter. Such a small opening in the HX led to higher pressure drop even though it also led to better heat transfer performance [30]. In most STHX, the segmental baffle cut varies from 20 to 49% with the most common being 20-25%. The 20% baffle cut produces highest level of heat transfer for a given pressure drop [37]. Baffle cut smaller than 20% can enhance heat transfer performance but results in high pressure drop. Similarly, as the baffle cut increases beyond 20%, the flow pattern deviates from crossflow pattern, which leads to the formation of stagnant regions with low fluid velocities.

For the current study, the tube layout pitch of all the prototypes was fixed at 7.62 mm. This tube layout pitch determines the net cross-flow area. As per TEMA standard [37], the minimum tube pitch value should be 6.3 mm. These factors could have contributed to the enhanced heat transfer performance of the PHXs.

In the design of STHX, there is a small acceptable baffle spacing required for good flow distribution. This minimum baffle spacing ensures a good flow pattern through the shell side of the heat exchanger. As per TEMA standard [37], the minimum baffle spacing should be close to 20% of the shell diameter but it should not be less than approximately 50 mm. The shell diameter of all prototypes was 76.2 mm with a baffle spacing of approximately 15 mm. In the case of the segmental baffle and continuous helical baffle heat exchangers, the baffle pitch was fixed at 51mm and 76.2 mm, respectively. In the

case of quadrant and trisection baffle the baffle distance was set at 140 mm, which was fixed based on the 40° baffle inclination angle. As the results show, the PHX dimensions played a role both in terms of heat transfer performance and pressure drop.

Also, it can be noted from the figure that at the same volume flow rate of air (9 m^3/h) the overall pressure drop of the continuous helical was 40% less than the segmental one. Also, the pressure drop of trisection and quadrant baffle was around 45% less than the segmental baffle heat exchanger. This is because as the inclination angle increases then the flow is expected to be more axial in nature while experiencing less flow resistance.

Also, in the case of trisection baffle, the pressure drop is less because it has an end-to-end baffle arrangement, which causes the fluid to leak through the triangular zones directly to the next flow channel instead of flowing around the tube bundle. In summary, the HX with helical baffles do show lower pressure drop than the segmental one.

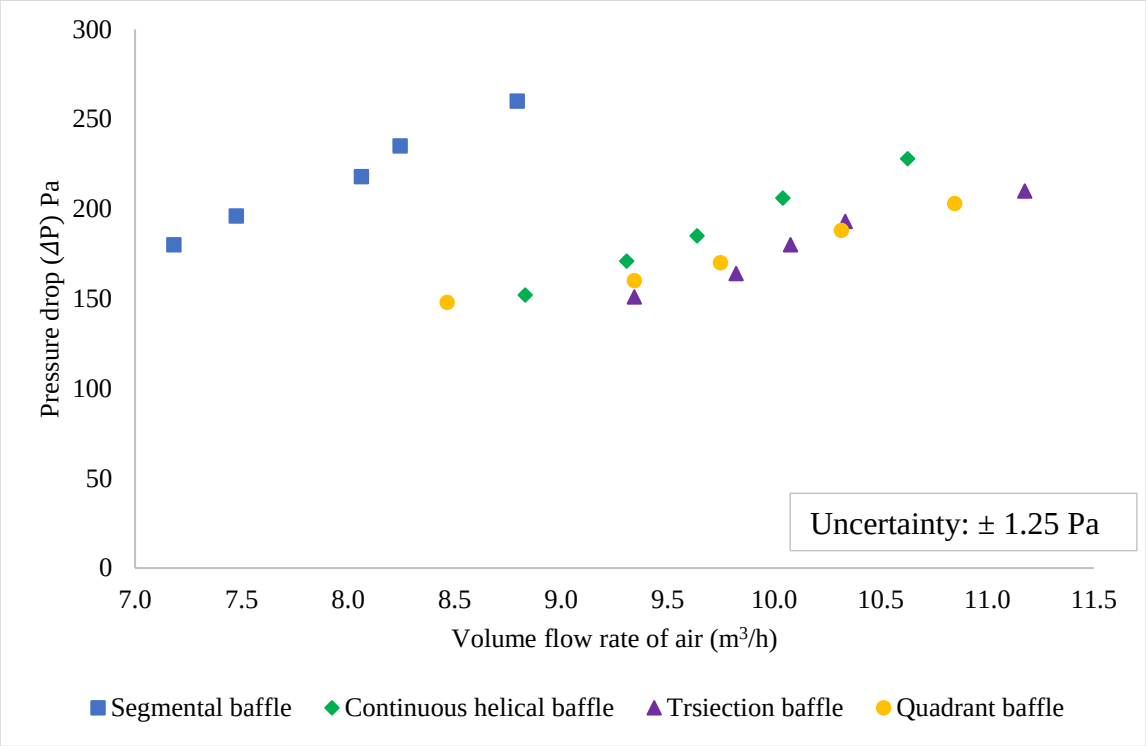

Figure 45. Pressure drop of plastic heat exchanger as a function of shell side volume flowrate

4.1.4 Heat Exchanger Effectiveness of PHXs

Fig. 46 shows that the effectiveness of PHXs as a function of the shell side volume flow rate. As it can be seen from the figure, the effectiveness increases with the shell side volume flow rate. Also, it can be noted from the figure, for a volume flow rate of air (9 m^3/h), the effectiveness of the segmental baffle was on average 19%, 17% and 4% higher for continuous helical, trisection and quadrant baffle heat exchangers, respectively. The results are consistent with the heat transfer results shown above.

Moreover, it can be seen that the effectiveness of the circumferential overlap quadrant baffle heat exchanger is much higher than the trisection and continuous helical one. These results suggest that the circumferential overlap quadrant baffles reduces the

leakage flow in the triangular zones of adjacent baffles. Thus, the circumferential overlapping is assumed to produce helical flow in the shell.

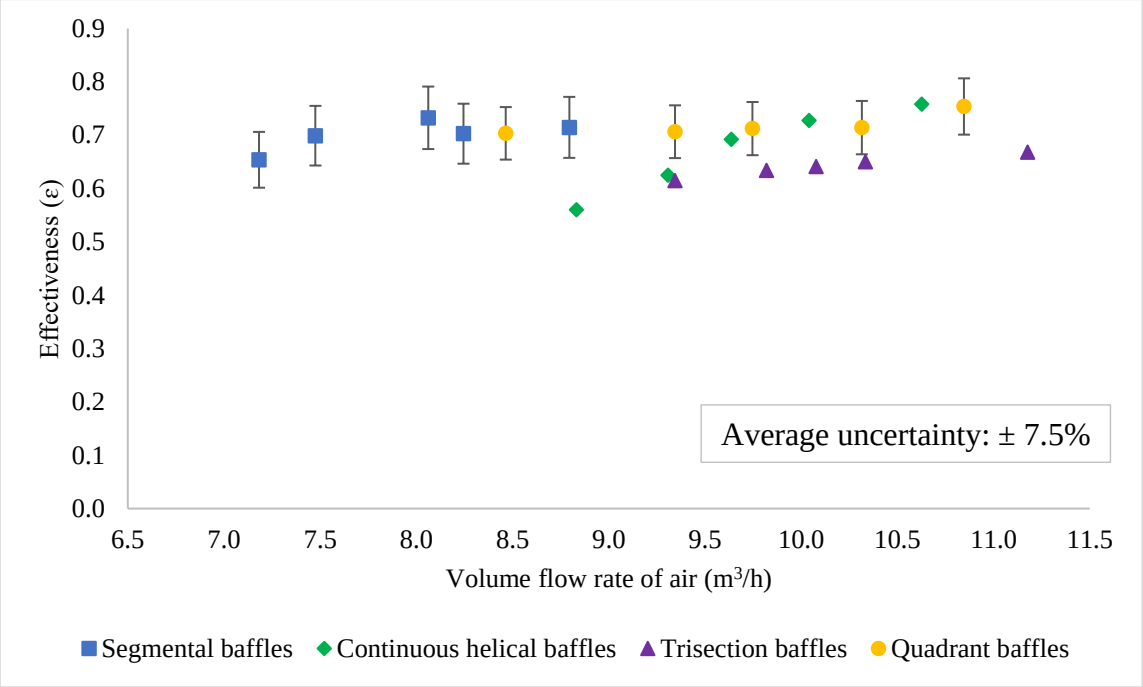

Figure 46. Effectiveness of plastic heat exchanger as a function of shell side volume flowrate

4.1.5 Number of Transfer Units of PHXs

Number of transfer units is often referred to as a heat exchanger size factor. Since all the prototypes have the same heat transfer area, NTU effectively depends on the ratio of $\frac{U}{C_{min}}$. It can be seen from Fig. 47, effectiveness increases with NTU. Moreover, at the same value of NTU (1.5), the effectiveness of segmental baffle heat exchanger was on average 6% higher than that of the continuous helical baffle heat exchanger.

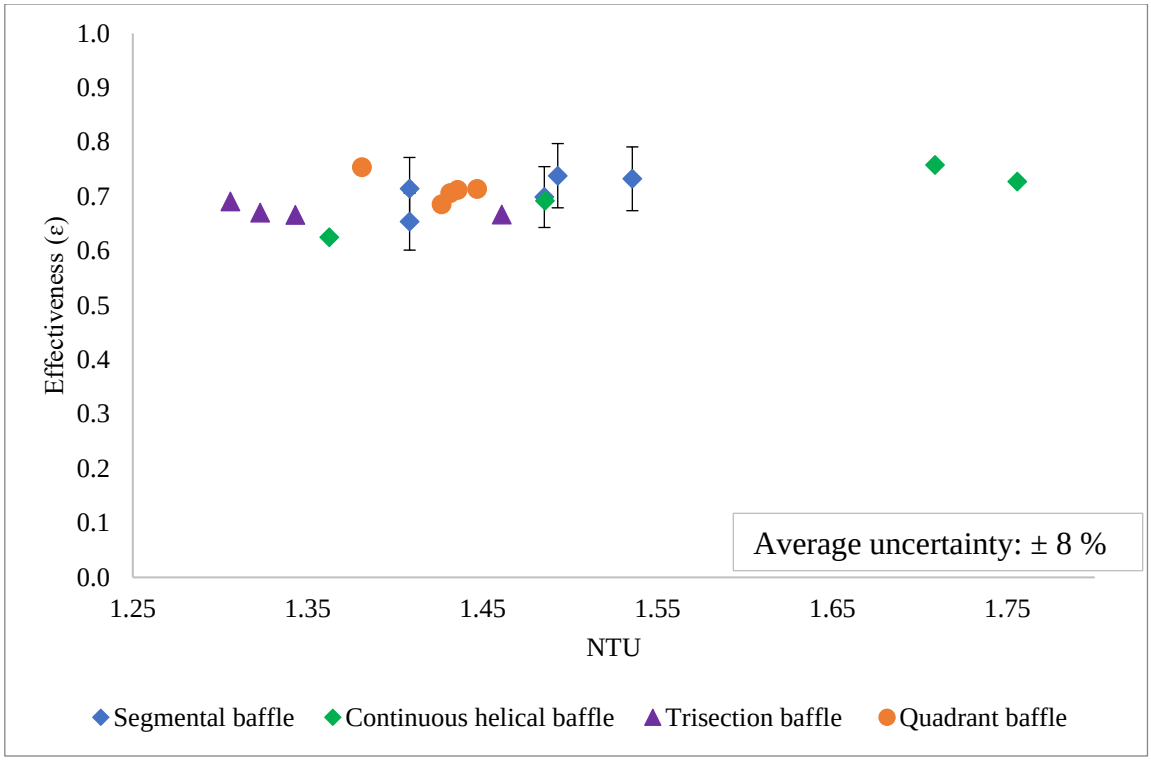

Figure 47. Effectiveness as a function of air side transfer units (NTU)

Fig. 48 shows the effectiveness of PHX as a function of NTU. In the same figure, the NTU values of cross flow and parallel flow arrangement have been plotted in order to compare the results with the four PHXs. From the figure, it can be seen that all the PHXs resembles a cross flow heat exchanger and a parallel flow type at low capacitance ratio and relatively low NTU values. This is because all of the PHXs have a 30^{o} triangular tube layout with tube pitch-to-tube diameter of 1.6, which is relatively high for STHX. In such a configuration, a high tube density results in high surface area per unit volume.

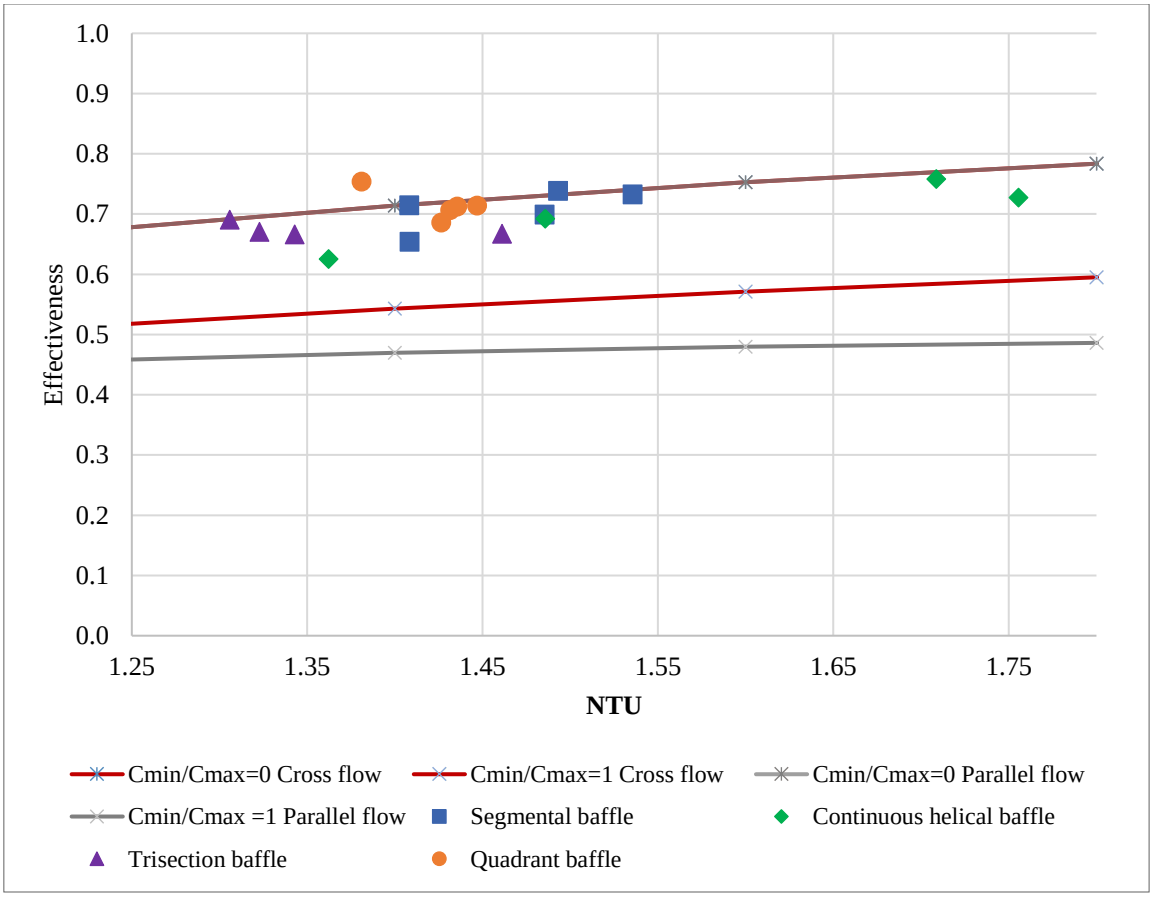

Figure 48. Comparison of Effectiveness as a function of NTU between the prototypes and standard cross flow model

4.1.7 Comprehensive performance index of PHXs

In the design of STHX, a proper trade-off between heat transfer rate and effective pumping power should be found. Hence, in order to better evaluate the efficiency of STHXs with different kinds of baffle configurations, it is advisable to compute the heat transfer rate per unit of pumping power.

Fig. 49 shows the comparisons of the ratio of heat transfer rate to the effective pumping power for four PHXs with different baffle configurations. From the figure, it can be seen that the comprehensive performance index Q_a/P_p decreases with the increase in

the shell side volume flow rate. It can be noted from the figure that at the same volume flow rate of air (9 m^3/h), the overall performance coefficient for continuous helical, quadrant and trisection baffle heat exchangers was on average 76%, 82% and 77% (respectively), greater than for the segmental PHX.

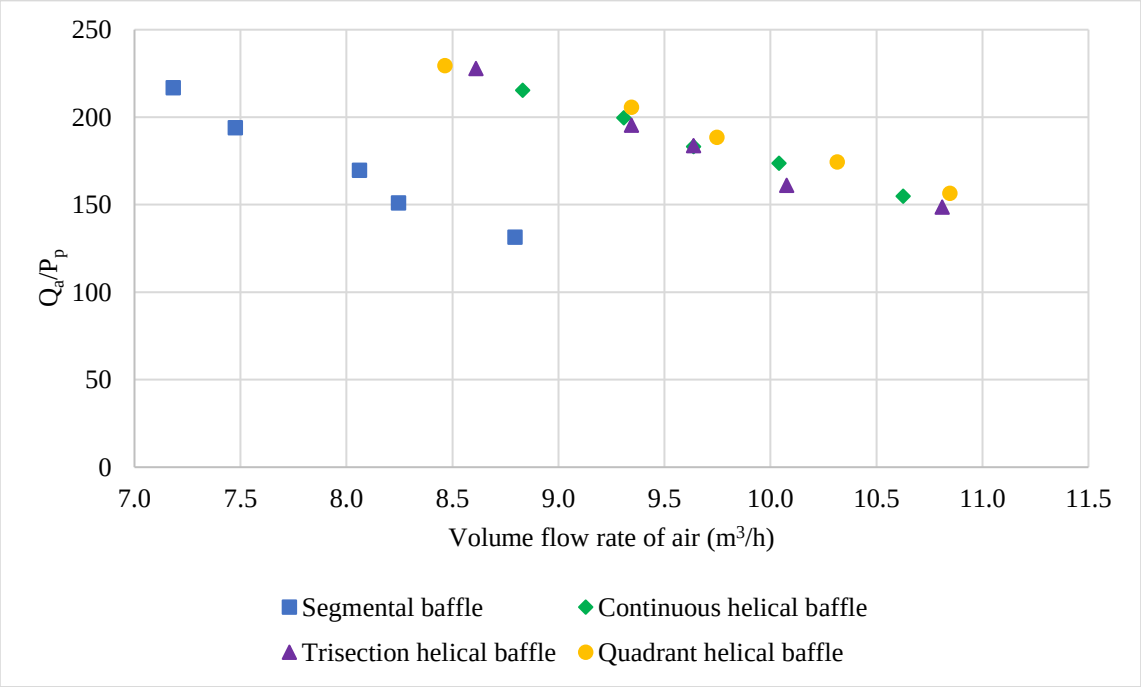

Figure 49. Performance evaluation index as a function of shell-side volume flow rate

In summary, PHX with helical baffles do perform better than PHX with segmental baffles. Also, the low helical baffles in PHX can result in capital cost saving in pumping equipment, operation and maintenance. In the case of discontinuous helical baffle, by selecting an optimum helix angle and overlap portion the helical baffle can be used to maintain the desired flow velocities of the fluid in the shell side of the shell and tube heat exchanger.

4.2 Condensation heat transfer in PHXs

After conducting single phase experiments with the PHX, only the segmental baffle and continuous helical baffle heat exchangers were used during the condensation (dehumidification) experiments. For the condensation experiments, the air flow rate was varied. In each test, both the air and water inlet temperature were kept approximately constant. The relative humidity of air was also kept the same for each test. The flow rate of the water side was fixed around 11000 mm^3/s, which produced laminar flow inside the tubes of all of the prototypes. Effectiveness, overall heat transfer coefficient and number of transfer units (NTU) were determined using experimental data. All the values of the process and performance parameters for the different baffle configuration are shown in Table 10-13.

Table 10. Inlet condition of moist air and water for segmental baffle heat exchanger

Trial No.	Ta_1 (°C)	φ_1 (%)	w_1 (kg_w/kg_a)	T_{DP} (°C)	Tw_1 (°C)	Ta_2 (°C)	φ_2 (%)	w_2 (kg_w/kg_a)	Tw_2 (°C)	$\dot{V}_a$ (m^3/hr)
1	33.3	40.4	0.0129	18.7	1.3	11.8	56	0.0055	2.1	2.32
2	34.1	41	0.0137	19	1.4	12.8	49.8	0.0053	2.3	2.66
3	34.0	42.4	0.0140	19.4	1.5	13.5	39.7	0.0051	2.5	3.10
4	31.8	48.5	0.0142	19.6	1.4	12.8	35.9	0.0047	2.6	4.09

Table 11. Performance parameters for segmental baffle heat exchanger

Trial No.	ΔP (Pa)	$\dot{Q}_w$ (W)	$\dot{Q}_a$ (W)	$\dot{Q}_s$ (W)	$\dot{Q}_l$ (W)	C (ml)	U (W/m^2.$^\circ$C)	ε_h	ε_w	NTU
1	42	28.4	31.6	16.9	14.7	6	1.46	0.77	0.83	1.52
2	68	37.4	38.1	18.9	19.3	9	1.79	0.78	0.87	1.56
3	77	42.0	46.4	21.2	25.3	13	1.92	0.81	0.89	1.72
4	85	58.0	61.9	26.3	35.6	19	2.66	0.84	0.93	1.86

Table 12. Inlet condition of moist air and water for continuous helical baffle heat exchanger

Trial No.	Ta_1 ($^\circ$C)	φ_1 (%)	w_1 (kg$_w$/kg$_a$)	T_{DP} ($^\circ$C)	Tw_1 ($^\circ$C)	Ta_2 ($^\circ$C)	φ_2 (%)	w_2 (kg$_w$/kg$_a$)	Tw_2 ($^\circ$C)	$\dot{V}_a$ (m^3/hr)
1	34.4	41.5	0.0138	19.4	1.4	8.9	52.5	0.0052	2.4	2.80
2	34.0	39.3	0.0132	18.2	1.5	8.7	49.8	0.0048	2.6	3.86
3	33.3	41.8	0.0132	18.3	1.3	8.9	46.4	0.0045	2.4	4.32
4	33.0	47.7	0.0149	20.2	1.5	9.1	30.9	0.0042	2.6	4.70

Table 13. Performance parameters for continuous helical baffle heat exchanger

Trial No.	ΔP (Pa)	$\dot{Q}_w$ (W)	$\dot{Q}_a$ (W)	$\dot{Q}_s$ (W)	$\dot{Q}_l$ (W)	C (ml)	U (W/m^2.$^\circ$C)	ε_h	ε_w	NTU
1	30	37.0	47.1	24.2	22.9	10	1.48	0.89	0.83	2.28
2	46	54.4	65.9	28.2	37.7	14	2.16	0.91	0.87	2.43
3	65	57.0	75.4	32.7	42.7	18	2.22	0.91	0.89	2.47
4	73	59.1	85.4	38.8	46.6	24	2.26	0.95	0.93	3.23

4.2.1 Heat transfer rate of PHXs under condensation conditions

As it can be seen from Fig. 50, the heat transfer rate increases with the shell side volume flow rate. It can be seen from the figure that at the same volume flow rate of air (3.5 m^3/h), the heat transfer rate of the segmental baffle was on average 8% higher than the continuous helical baffle heat exchanger. This result is consistent with the single-phase heat transfer results shown above.

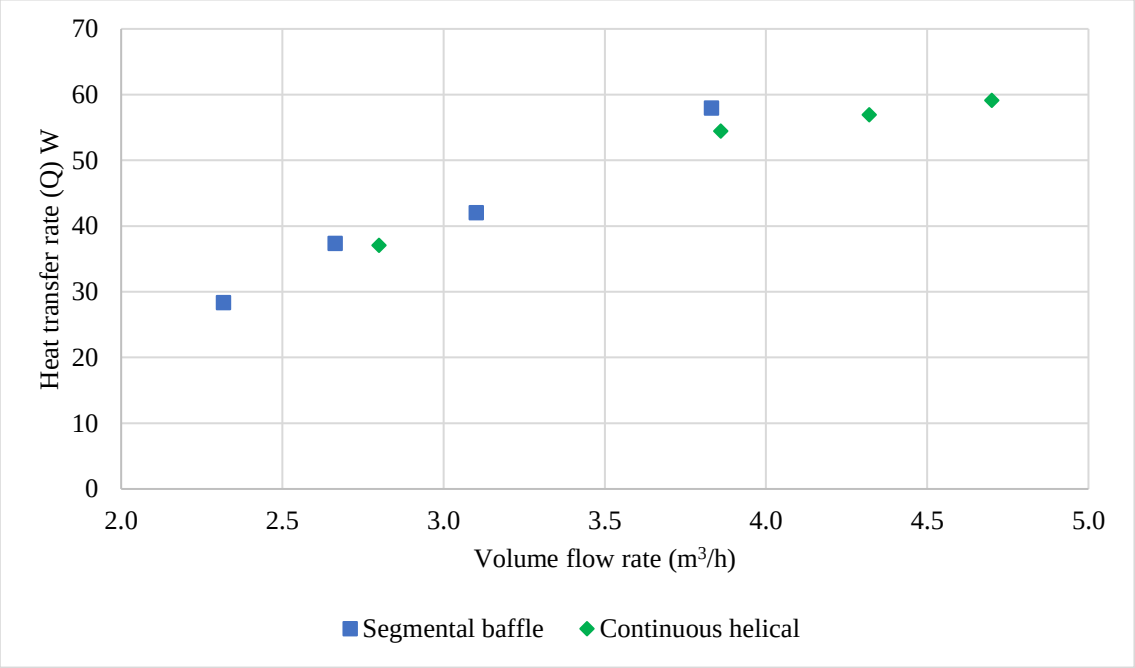

Figure 50. Heat transfer rate of plastic heat exchangers as a function of shell side volume flow rate

Fig. 51 shows sensible and latent heat transfer for the continuous and helical baffle plastic heat exchanger. The figure shows that the sensible heat transfer decreases as compared to the latent heat transfer as the volume flow rate on the shell side is increased. This may be attributed to the high condensation rate on the coil surface, which covers the coil with a

thick layer of condensate film. This film is assumed to increase the thermal resistance, which reduces sensible heat transfer.

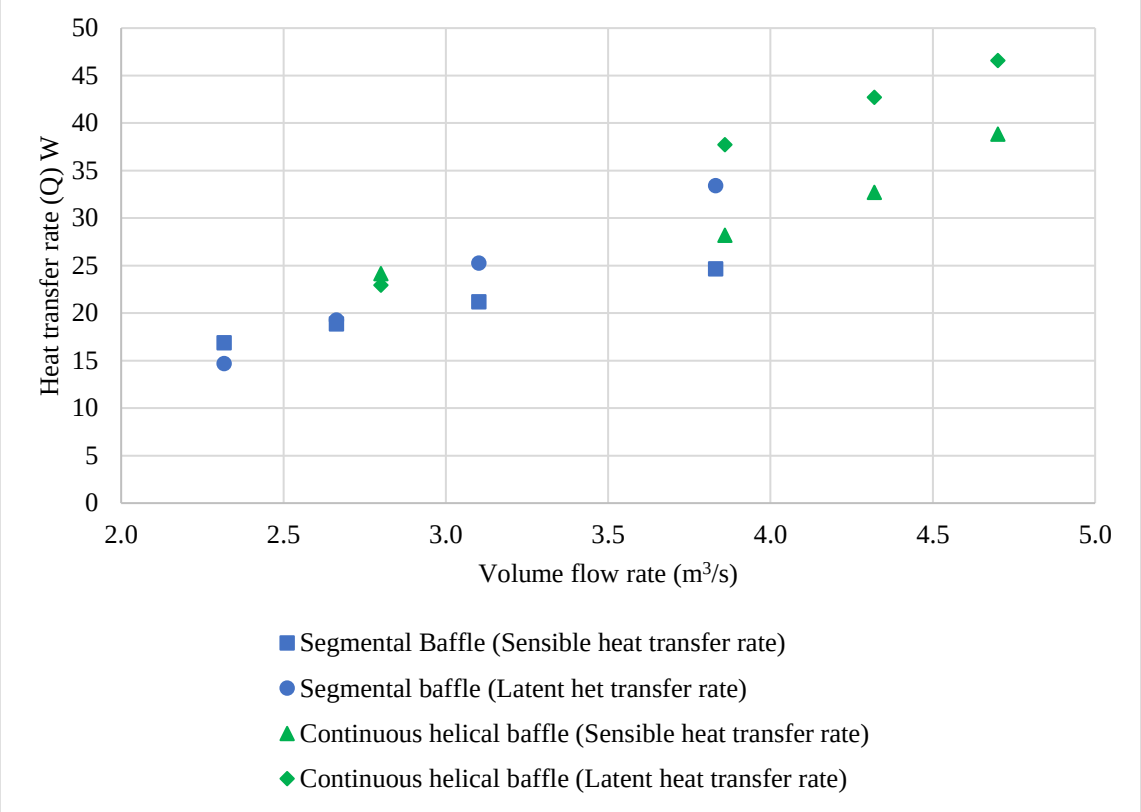

Figure 51. Comparison between sensible and latent heat transfer for segmental and continuous helical baffle as function of shell side volume flow rate

4.2.2 Overall heat transfer coefficient of PHXs under condensation conditions

As can be seen from Fig. 52, the overall heat transfer coefficient increases with the shell side volume flow rate. The increase of the overall heat transfer coefficient can be attributed to the increase of the heat transfer rates at higher shell side volume flow rates. It can be seen from the figure that at the same volume flow rate of air (3.5 m^3/h), the

overall heat transfer coefficient of the segmental baffle was on average 16% higher than the continuous helical baffle heat exchanger. This result is consistent with the single phase flow experiments described and explained above.

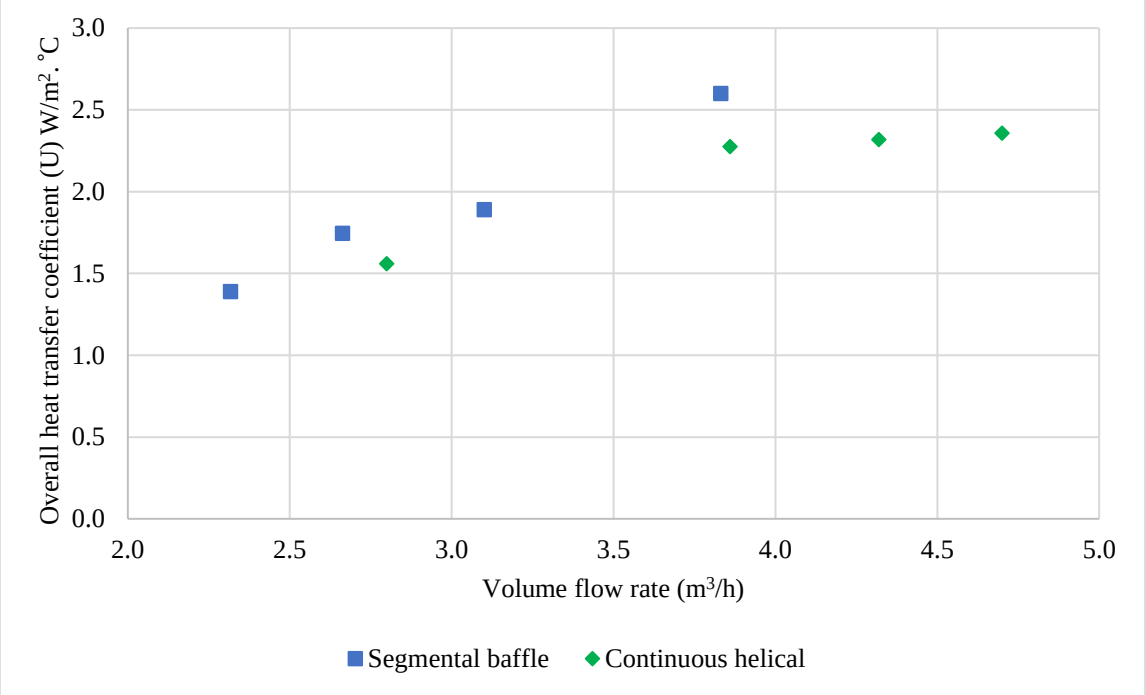

Figure 52. Overall heat transfer coefficient of plastic heat exchangers as a function of shell side volume flow rate

4.2.5 Pressure drop in PHXs under condensation conditions

Fig. 53 compares the pressure drop of the segmental baffle plastic heat exchanger with the continuous baffle one. From the figure, it can be seen that the pressure increases with the shell side volume flow rate. It can be seen from the figure that at the same volume flow rate of air (3.5 m^3/h) the pressure drop of segmental baffle heat exchanger was on average 50 % than the continuous helical baffle heat exchanger. Again, in the segmental baffle heat exchanger, the flow pattern on the shell side is essentially zigzag in nature.

Moreover, there could be flow separation at the edge of the baffles which causes abrupt momentum change and severe pressure loss. This result is consistent with the single-phase flow experiments explained above; however, the pressure drop values shown Fig. 52 are lower than for the single phase experiments because lower flow rates were considered for the condensation experiments.

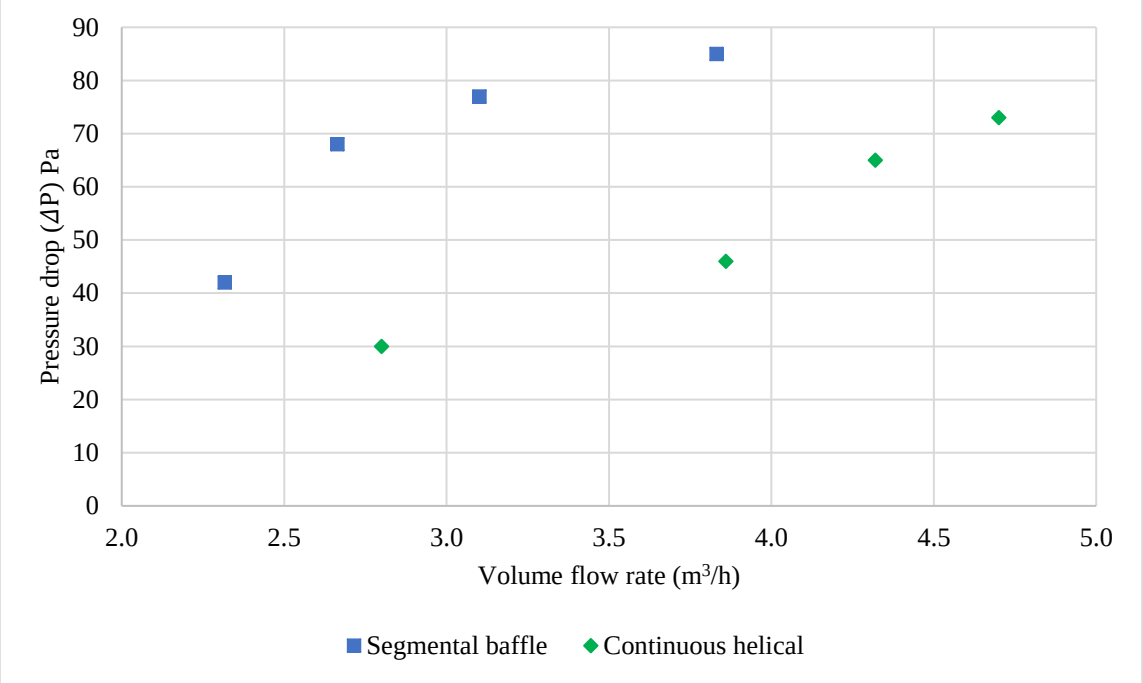

Figure 53. Pressure drop of plastic heat exchangers as a function of shell side volume flow rate

4.2.3 Enthalpy Effectiveness of PHXs under condensation conditions

Fig. 54 compares the enthalpy effectiveness of the segmental baffle plastic heat exchanger with the continuous baffle one. From the figure, it can be seen that the enthalpy effectiveness increases with the shell side volume flow rate. It can be seen from the figure that at the same volume flow rate of air (3.5 m^3/h), the enthalpy effectiveness of the

continuous helical baffle heat exchanger was around the same as that of the segmental baffle heat exchanger. In summary, enthalpy effectiveness is used to evaluate the performance of a HX in terms of total cooling load removal.

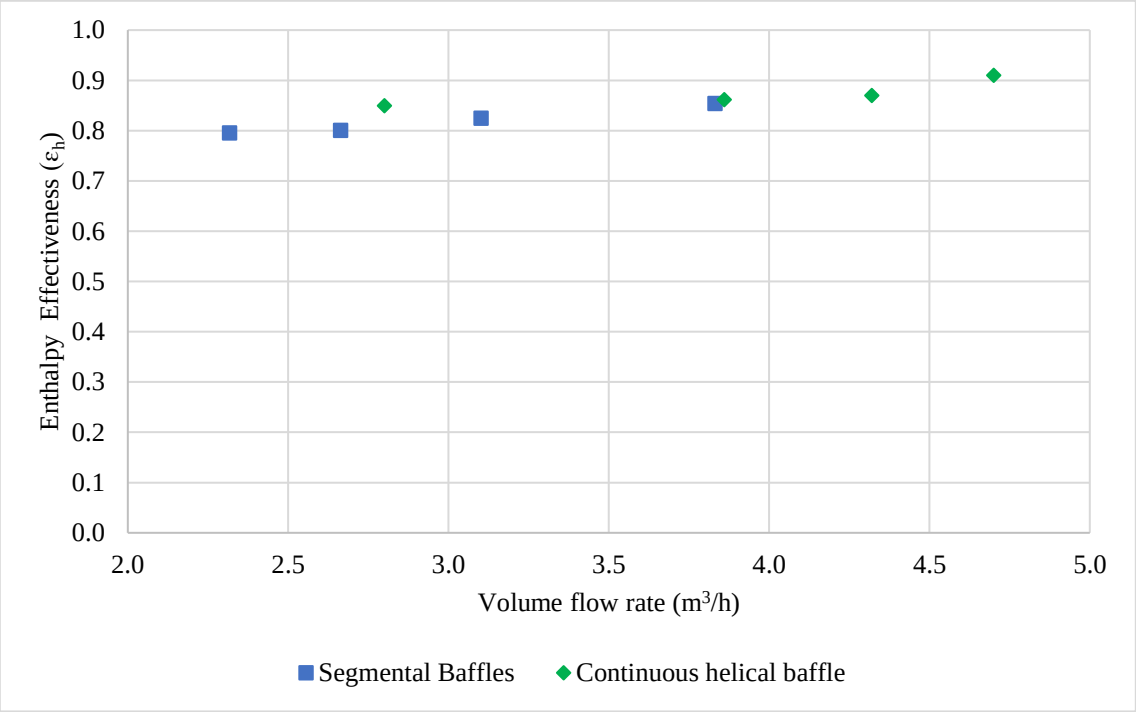

Figure 54. Enthalpy effectiveness of plastic heat exchangers as a function of shell side volume flow rate

4.2.4 Humidity Effectiveness of PHXs under condensation conditions

Fig. 55 compares the humidity effectiveness of the segmental baffle plastic heat exchanger with the continuous baffle one. From the figure, it can be seen that the humidity effectiveness increases with the shell side volume flow rate. It can be seen from the figure that at the same volume flow rate of air (3.5 m^3/h), the humidity effectiveness of the segmental baffle heat exchanger was 2% higher than the continuous helical baffle heat

exchanger. The results also show that PHX can achieve have effectiveness values as dehumidifying units, which demonstrate their potential.

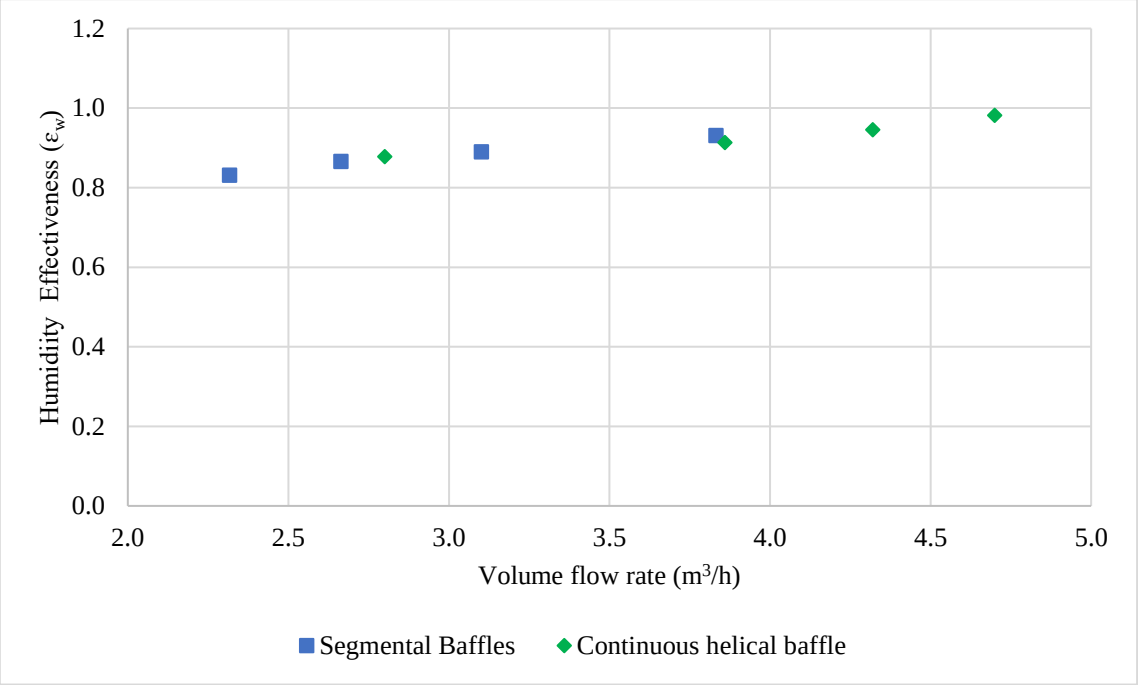

Figure 55. Enthalpy effectiveness of plastic heat exchangers as a function of shell side volume flow rate

4.2.5 Dehumidification rate in PHXs under condensation conditions

Fig. 56 shows the water condensation rate as a function of the shell side volume flow rate. It can be seen from the figure that the water condensation rate increases with the increasing flow on the shell side. This is because as the flow rate of the humid air is increased, more vapor comes into contact with the tube surface, which leads to greater condensation rate.

It can be seen from the figure that at the same volume flow rate of air (3.5 m^3/h) the dehumidifying capacity of the segmental baffle heat exchanger was on average 16% higher than compared to that of continuous helical baffle heat exchanger.

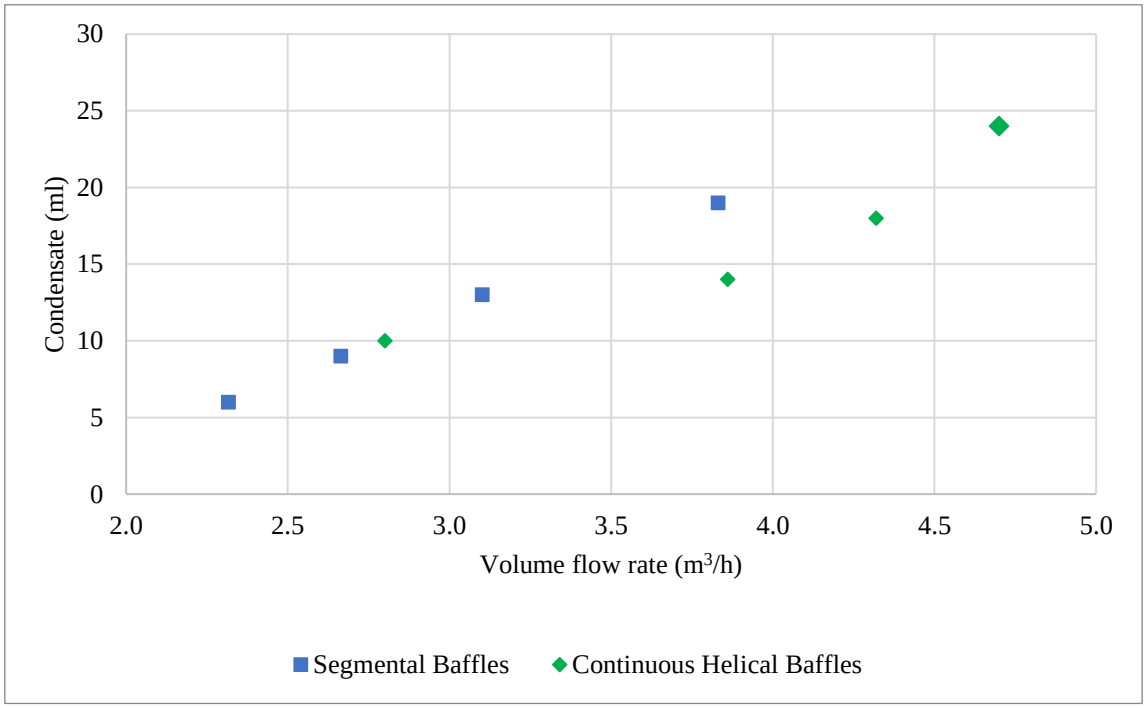

Figure 56. Dehumidifying capacity of plastic heat exchangers as a function of shell side of volume flow rate ($\Delta T = T_{dp} - T_{surface} \sim 17\ ^oC$)

4.2.6 Comprehensive performance index in PHXs under condensation conditions

Fig. 56 shows the comprehensive performance index as a function of the shell side volume flow rate. It can be seen from the figure that the comprehensive performance index decreases with the increase of flow on the shell side. It can be seen from the figure that under the same volume flow rate of air (3.5 m^3/h) the comprehensive performance index of continuous helical baffle heat exchanger was on average 46% higher than the segmental baffle heat exchanger.

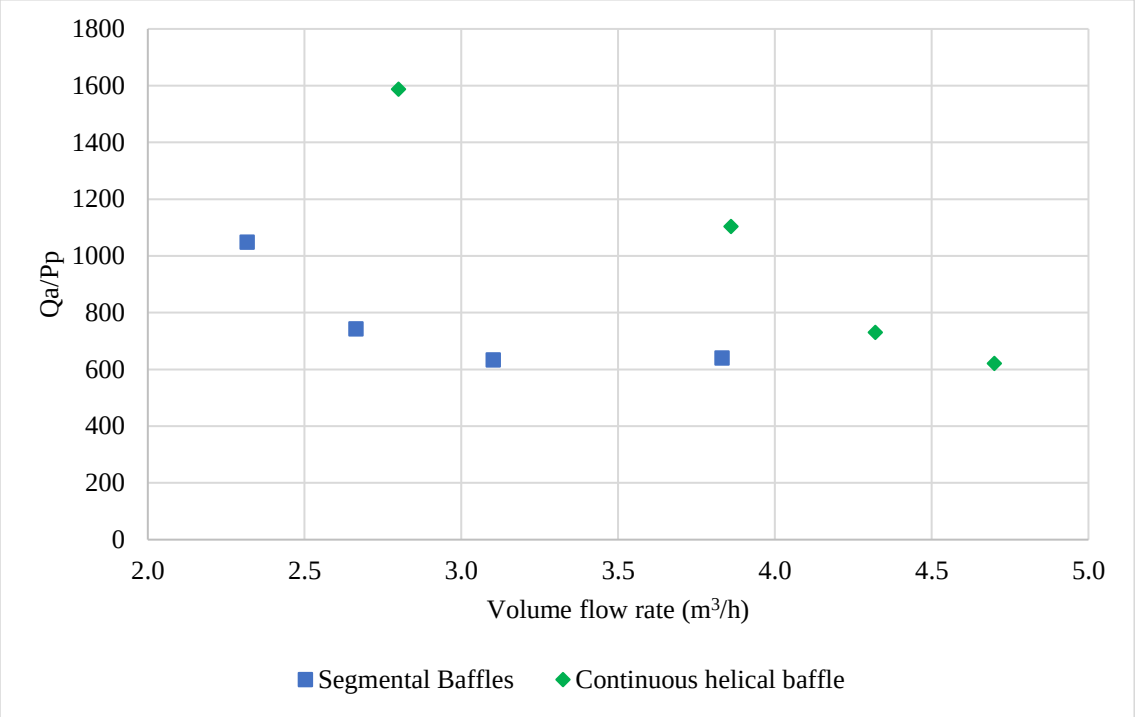

Figure 57. Comprehensive performance index of plastic heat exchangers as a function of the shell side volume flowrate

4.2.6 Number of transfer units (NTU) under condensation conditions

Fig. 58 shows the effectiveness as a function of NTU for segmental and continuous helical baffle heat exchanger. It can be seen from the figure that at low NTU value, the effectiveness of segmental baffle was approximately the same as that of the continuous helical one. Moreover Fig. 59 shows the comparison of the two PHXs with the Braun dehumidifying cooling coil model [35]. As the figure shows, the PHXs performed quite well as dehumidification units. Moreover, it fits well the Braun model [35] under complete condensation. Therefore, the results clearly indicate that both plastic HX can perform as well as conventional condensers.

In summary, plastic heat exchangers have the potential as condensing and dehumidification units. Moreover, the type of baffle clearly can also lead to enhanced thermal performance.

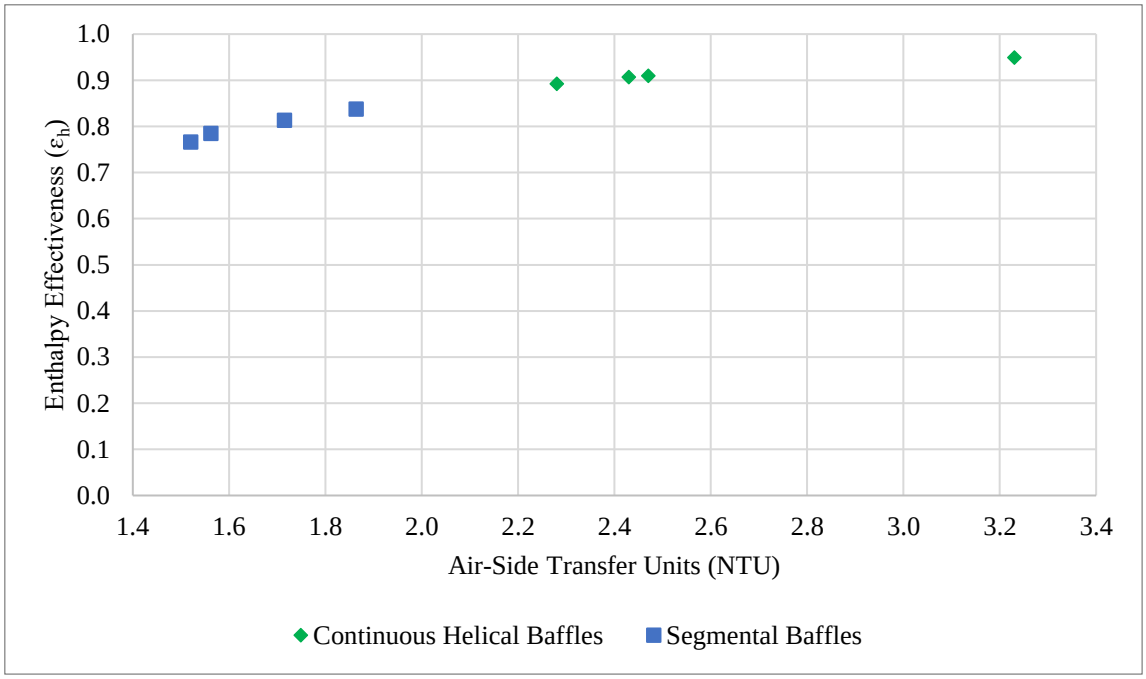

Figure 58. Effectiveness of plastic heat exchangers as a function of number of transfer units (NTU)

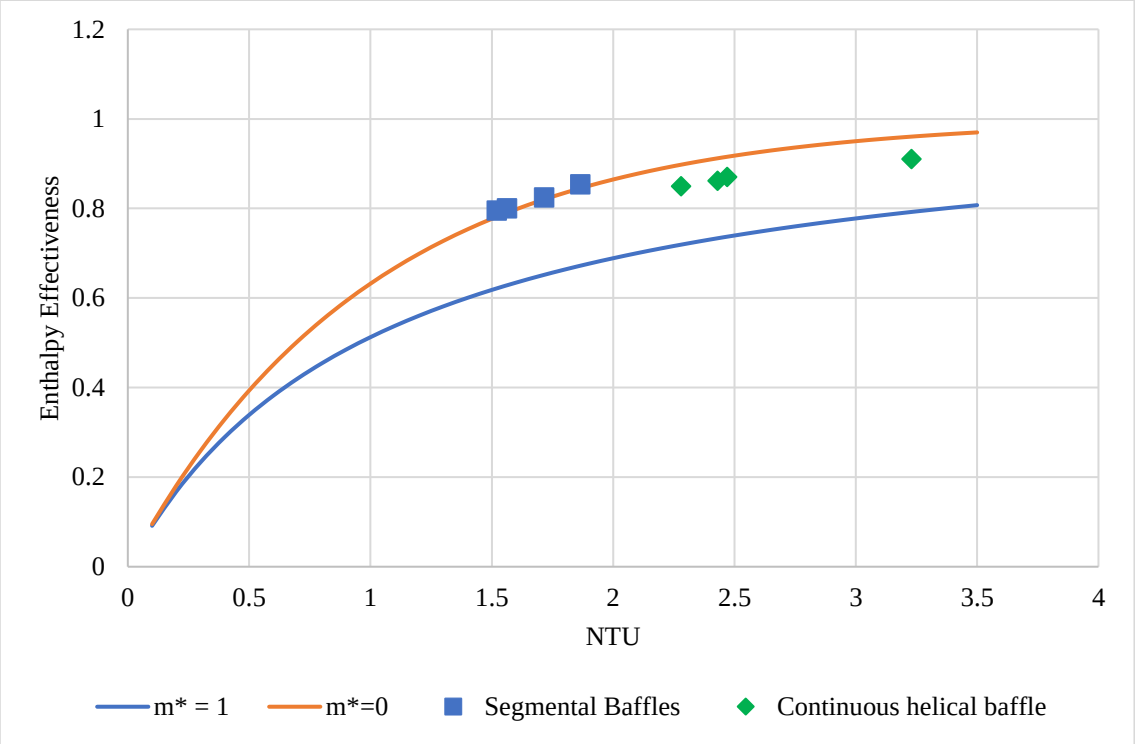

Figure 59. Effectiveness as a function of number of transfer units (NTU) compared with standard Braun model [35]

4.2.7 Comparison between plastic and metallic STHXs

A comparison has been performed between a conventional metallic and plastic STHXs assuming an identical shell side volume of 1.22 m^3. Table 14. shows the result of the comparison analysis based on thermal conductance through the tubes. The tube dimensions selected for the metallic STHXs are the minimum recommended as per TEMA standard. Moreover, the number of tubes for the metallic STHXs was determined considering the same heat exchanger volume as that of the plastic STHX. From the table it can be seen that for the same given volume, the plastic STHXs are more compact and have a heat transfer area of about 2 and 4 times greater than that of the copper and steel

STHXs, respectively. Hence, though the thermal conductivity value of plastics is relatively lower than that of metals, this can be overcome by using thin and low diameter tubes, which can offset the low thermal conductivity values. Table 14 also shows that the $UA_{conduction}$ value for the plastic STHX is about the same order of magnitude as the stainless steel STHX. Future studies should consider the convective process on the air or vapor side of STHX when calculating and comparing UA values.

Table 14. Comparison between a metallic and plastic STHX

Material	**NPS**	**Tube Dimensions (mm)**		**k (W/ m.K)**	**R . 10^4 value (m^2. K/W)**	**$U_{conduction}$ ($W/m^2.K$)**	**No. of tubes**	**Total Heat Transfer Area (m^2)**	**$UA_{conduction}$ (W/K)**
Plastic (LLDPE)	3/16"	O.D	4.76	0.33	10.28	973.1	61	0.417	406.10
		I.D	4.41						
Copper (70% Cu, 30% Ni)	3/4"	O.D	22.2	29	1.05	9528.3	9	0.287	2737.86
		I.D	18.9						
Steel (Stainless Steel type 316)	1"	O.D	25.4	16	1.92	5199.1	4	0.146	758.82
		I.D	22.1						

CHAPTER V

CONCLUSION

The present experimental study has shown that the helical baffles results in an increase in the heat transfer performance per unit of pumping power. Single phase and condensation heat transfer tests were performed on different plastic shell and tube heat exchangers having different baffle configuration. The results indicate that continuous helical baffle and circumferential overlap quadrant baffles led to lower shell side pressure drop and higher heat transfer performance.

The overall heat transfer coefficient, number of transfer units, enthalpy and humidity effectiveness and dehumidification capacity were computed. The main conclusions of both of the studies are summarized below,

1) For all the single shell-pass helical baffles (discontinuous and continuous helical baffle) the ratios of heat transfer coefficient to pressure drop are higher than those of a conventional segmental baffle heat exchanger under laminar conditions. However, for the same volume flow rate, the segmental baffle PHX have a higher heat transfer rate and much higher pressure drop.

2) The single shell-pass PHX with quadrant baffle has superior thermal and flow characteristics than the PHX with trisection and continuous baffle. Moreover, quadrant baffle as compared to continuous helical baffle are much easier to manufacture and assemble in STHX.

3) The condensation results show that PHX are highly effective dehumidifying units. Despite consisting of plastic components, the PHX were able to perform well as condensing units.

CHAPTER VI

PROPOSED SCOPE OF FUTURE WORK

The following recommendation should be considered in future studies,

- Investigation of a proper baffle inclination angle that can provide an optimal performance of the heat exchangers in the case of helical baffles
- Investigation of an optimal baffle spacing in the case of helical baffle to produce a plug flow pattern
- Investigation of varying other design parameters that may have an effect on shell side thermo-hydraulic performances
- Used of a different polymer material for the tubing of the PHX
- Numerical simulation for the different helical baffle configurations to completely understand the transport mechanism responsible for the observed enhancement in heat transfer and reduction in pressure drop.

REFERENCES

1. Bashir I. Master, K.S.C., Venkateswaran Pushpanathan. *Fouling Mitigation Using Helixchanger*

Heat Exchangers. in *Engineering Conferences International*. 2003. Santa Fe, US.

2. Liu, J., et al., *Heat-transfer characteristics of polymer hollow fiber heat exchanger for vaporization application.* AIChE Journal, 2018. **64**(5): p. 1783-1792.
3. Ozden, E. and I. Tari, *Shell side CFD analysis of a small shell-and-tube heat exchanger.* Energy Conversion and Management, 2010. **51**(5): p. 1004-1014.
4. Wen, J., et al., *Experimental investigation on performance comparison for shell-and-tube heat exchangers with different baffles.* 2015. **84**: p. 990-997.
5. Stehlík, P., et al., *Comparison of Correction Factors for Shell-and-Tube Heat Exchangers with Segmental or Helical Baffles.* Heat Transfer Engineering, 1994. **15**(1): p. 55-65.
6. Wang, Q., et al., *Review of Improvements on Shell-and-Tube Heat Exchangers With Helical Baffles.* 2010. **31**(10): p. 836-853.
7. Dong, C., Y.-P. Chen, and J.-F. Wu, *Performance Comparison of Trisection Helical Baffle Heat Exchangers with Different Circumferential Overlap Sizes.* Chemical Engineering & Technology, 2015. **38**(7): p. 1277-1284.
8. Lutcha, J.a.N., J, *Performance improvement of tubular heat exchangers by helical baffles.* Chem. Eng. Res. Des.Chemical Engineering Research and Design, Rugby, 1990. **68**(A3): p. 263-270.
9. Kral, D., et al., *Helical Baffles in Shell-and-Tube Heat Exchangers, Part I: Experimental Verification.* 1996. **17**(1): p. 93-101.
10. Zhang, J.-F., et al., *Experimental performance comparison of shell-side heat transfer for shell-and-tube heat exchangers with middle-overlapped helical baffles and segmental baffles.* Chemical Engineering Science, 2009. **64**(8): p. 1643-1653.
11. Xiao, X., et al., *Numerical investigation of helical baffles heat exchanger with different Prandtl number fluids.* International Journal of Heat and Mass Transfer, 2013. **63**: p. 434-444.
12. Lei, Y.-G., et al., *Design and optimization of heat exchangers with helical baffles.* Chemical Engineering Science, 2008. **63**(17): p. 4386-4395.
13. Dong, C., Y.-P. Chen, and J.-F. Wu, *Influence of baffle configurations on flow and heat transfer characteristics of trisection helical baffle heat exchangers.* Energy Conversion and Management, 2014. **88**: p. 251-258.
14. Chen, Y., et al., *Experimental Study on Shell Side Heat Transfer Performance of Circumferential Overlap Trisection Helical Baffle Heat Exchangers*. 2011. p. 27-33.
15. Dong, C., Y.P. Chen, and J.F. Wu, *Performance Comparison of Trisection Helical Baffle Heat Exchangers with Different Circumferential Overlap Sizes.* Chemical Engineering & Technology, 2015. **38**(7): p. 1277-1284.

16. Peng, B., et al., *An Experimental Study of Shell-and-Tube Heat Exchangers With Continuous Helical Baffles.* Journal of Heat Transfer, 2007. **129**(10): p. 1425-1431.
17. Lei, Y.-G., et al., *Effects of baffle inclination angle on flow and heat transfer of a heat exchanger with helical baffles.* Chemical Engineering and Processing: Process Intensification, 2008. **47**(12): p. 2336-2345.
18. Browne, M.W. and P.K. Bansal, *An overview of condensation heat transfer on horizontal tube bundles.* Applied Thermal Engineering, 1999. **19**(6): p. 565-594.
19. Grant, I.D.R. and D. Chisholm, *Two-Phase Flow on the Shell-Side of a Segmentally Baffled Shell-and-Tube Heat Exchanger.* Journal of Heat Transfer, 1979. **101**(1): p. 38-42.
20. Morcos, V.H. and H.M. Shafey, *Performance Analysis of a Plastic Shell-and-Tube Heat Exchanger.* Journal of Elastomers & Plastics, 1995. **27**(2): p. 200-213.
21. Dincer, I., Y. Haseli, and G.F. Naterer, *Thermal Effectiveness Correlation for a Shell and Tube Condenser with Noncondensing Gas.* Journal of Thermophysics and Heat Transfer, 2008. **22**(3): p. 501-507.
22. Allen, B. and L. Gosselin, *Optimal geometry and flow arrangement for minimizing the cost of shell-and-tube condensers.* International Journal of Energy Research, 2008. **32**(10): p. 958-969.
23. Hu, H., et al., *Heat transfer characteristics of mixed hydrocarbon refrigerant flow condensation in shell side of helically baffled shell-and-tube heat exchanger.* Applied Thermal Engineering, 2018. **133**: p. 785-796.
24. Lin, L., et al., *Performance of flow and heat transfer in vertical helical baffle condensers.* International Communications in Heat and Mass Transfer, 2016. **72**: p. 64-70.
25. Amer, M., et al., *Experiments for suitability of plastic heat exchangers for dehumidification applications.* Applied Thermal Engineering, 2019. **158**: p. 113827.
26. Taborek, J., *Industrial Heat Exchangers: A Basic Guide By G. Walker, Hemisphere Pub L. Corp. Washington Dc, 1982, $41.50, 408 Pg.* AIChE Journal, 1983. **29**(2): p. 349-350.
27. Nellis, G. and S.A. Klein, *Heat transfer*. First paperback edition. ed. 2012, Cambridge: Cambridge University Press.
28. Kays, W.M., *Compact Heat Exchangers*. McGraw-Hill series in mechanical engineering. 1998.
29. Irvine, T.F., et al., *Advances in heat transfer. Volume 37*. 2003, Academic Press: Amsterdam.
30. Hewitt, G.F., *Handbook of heat exchanger design*. 1992, New York, NY ;: Begell House.
31. Yun, R., Y. Kim, and Y. Kim, *Air side heat transfer characteristics of plate finned tube heat exchangers with slit fin configuration under wet conditions.* Applied Thermal Engineering, 2009. **29**(14): p. 3014-3020.

32. Wang, C.-C., Y.-C. Hsieh, and Y.-T. Lin, *Performance of Plate Finned Tube Heat Exchangers Under Dehumidifying Conditions.* Journal of Heat Transfer, 1997. **119**(1): p. 109-117.
33. Myers, R.J., *The effect of dehumidification on the air side heat transfer coefficient for a finned-tube coil*. 1967.
34. Mitchell, J.W. and J.E. Braun, *Principles of heating, ventilation, and air conditioning in buildings*. 2013, Hoboken, NJ: Wiley.
35. Braun, J.E., S.A. Klein, and J.W. Mitchell, *Effectiveness model for cooling towers and cooling coils*. Vol. 95. 1989.
36. Gao, B., et al., *Experimental study of effects of baffle helix angle on shell-side performance of shell-and-tube heat exchangers with discontinuous helical baffles.* Experimental Thermal and Fluid Science, 2015. **68**: p. 48-57.
37. Tubular Exchanger Manufacturers, A., *Standards of Tubular Exchanger Manufacturers Association*. 4th ed. ed. 1959, New York.

APPENDIX A

The following figures show linear regressions for each PHX considered in the study. The linear regressions were used to estimate the enhancement levels among the units under identical flow rates.

SINGLE PHASE HEAT TRANSFER (LINEAR REGRESSIONS)

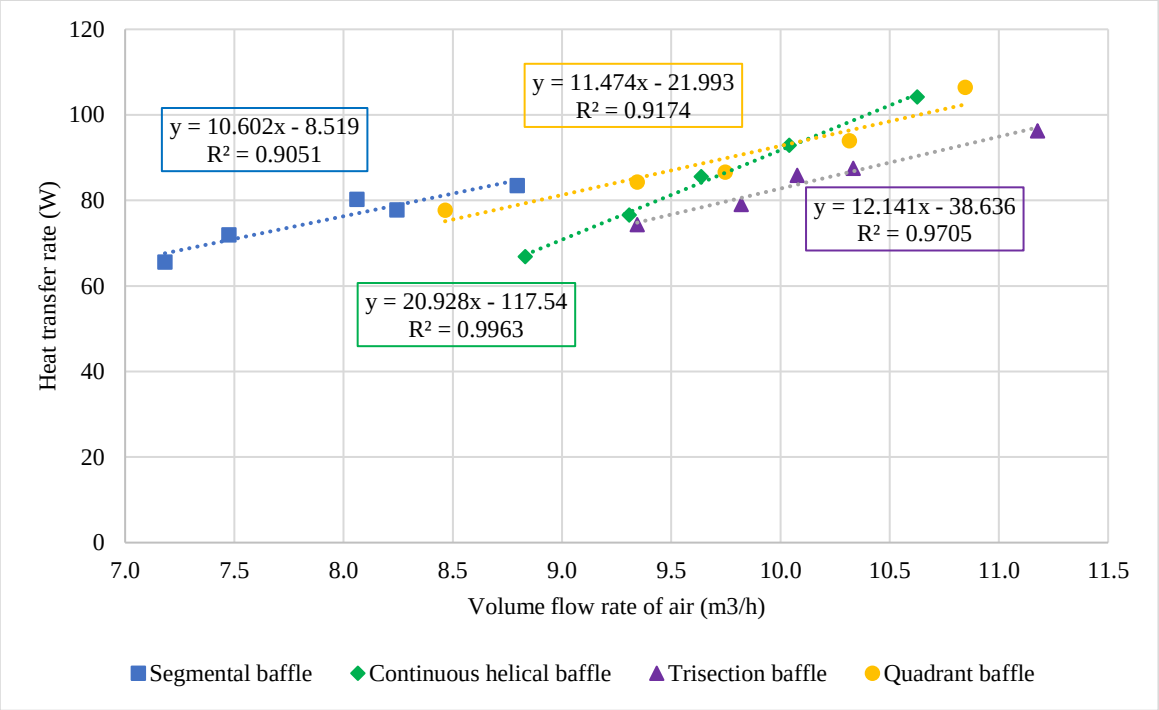

Figure A1. Heat transfer rate of plastic heat exchangers as a function of shell side volume flowrate

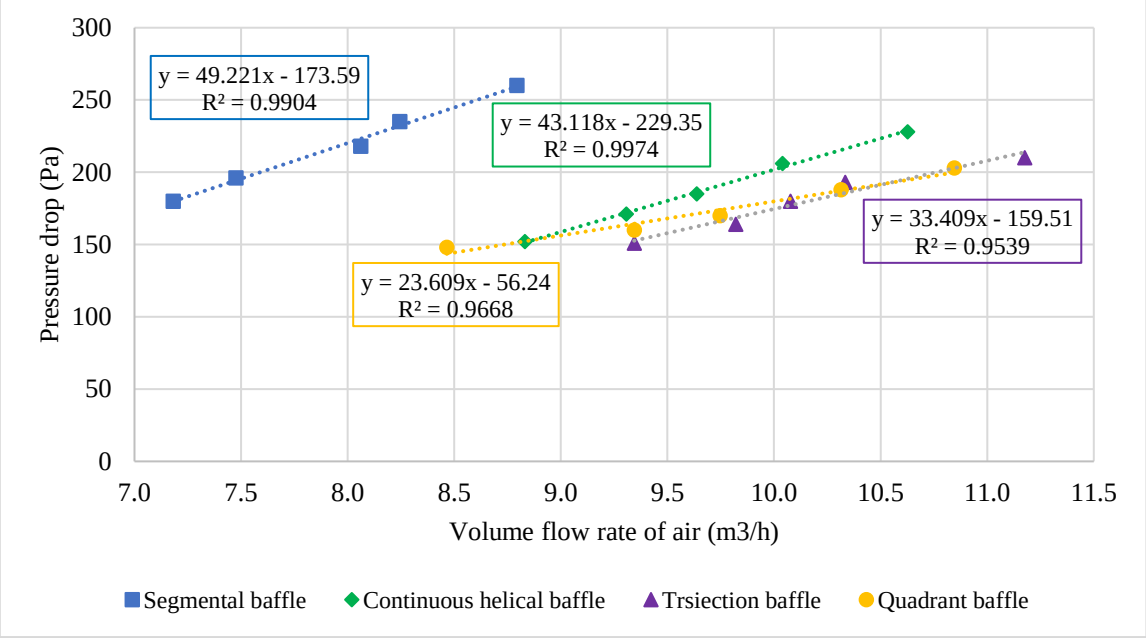

Figure A2. Pressure drop of plastic heat exchangers as a function of shell side volume flowrate

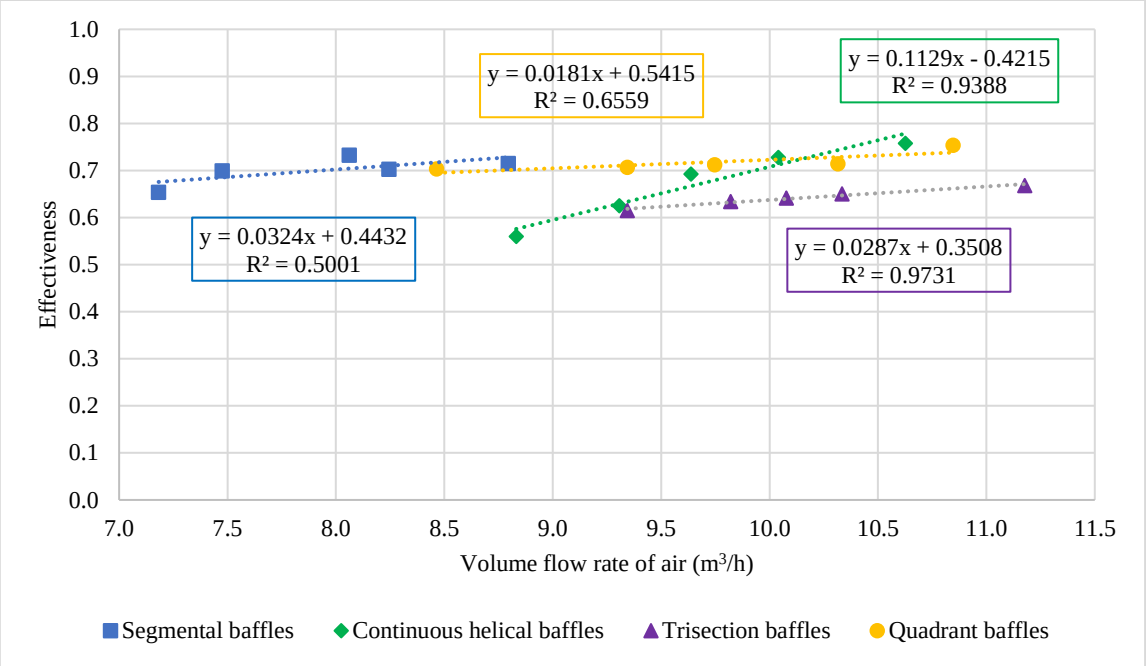

Figure A3. Effectiveness of plastic heat exchangers as a function of shell side volume flowrate

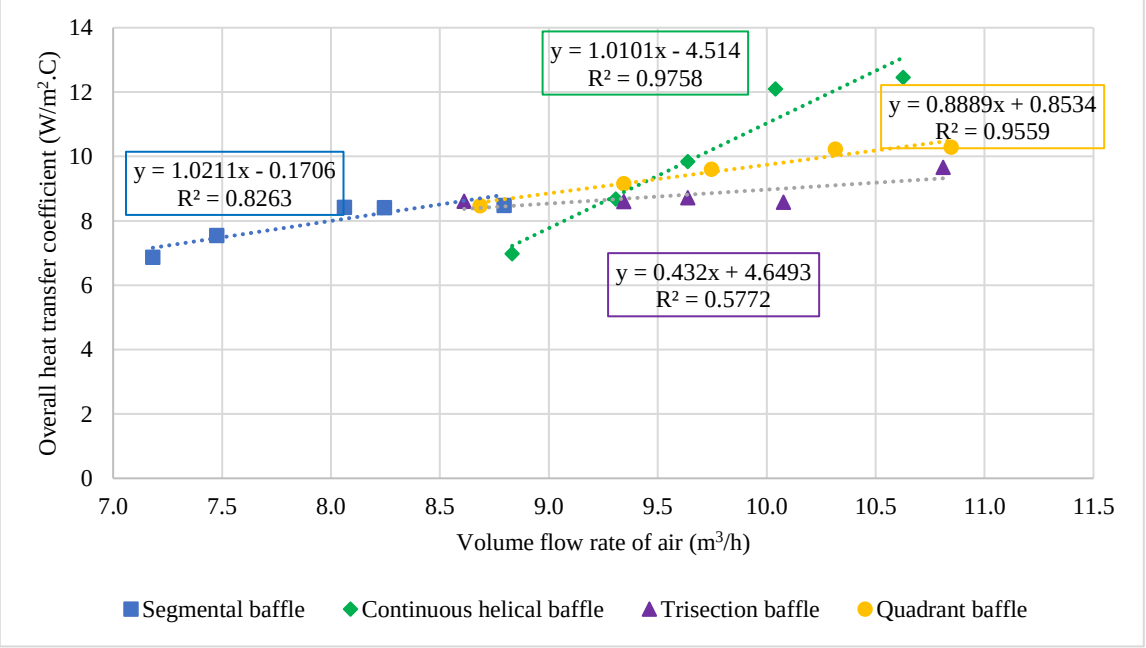

Figure A4. Overall heat transfer coefficient of plastic heat exchangers as a function of shell side volume flowrate

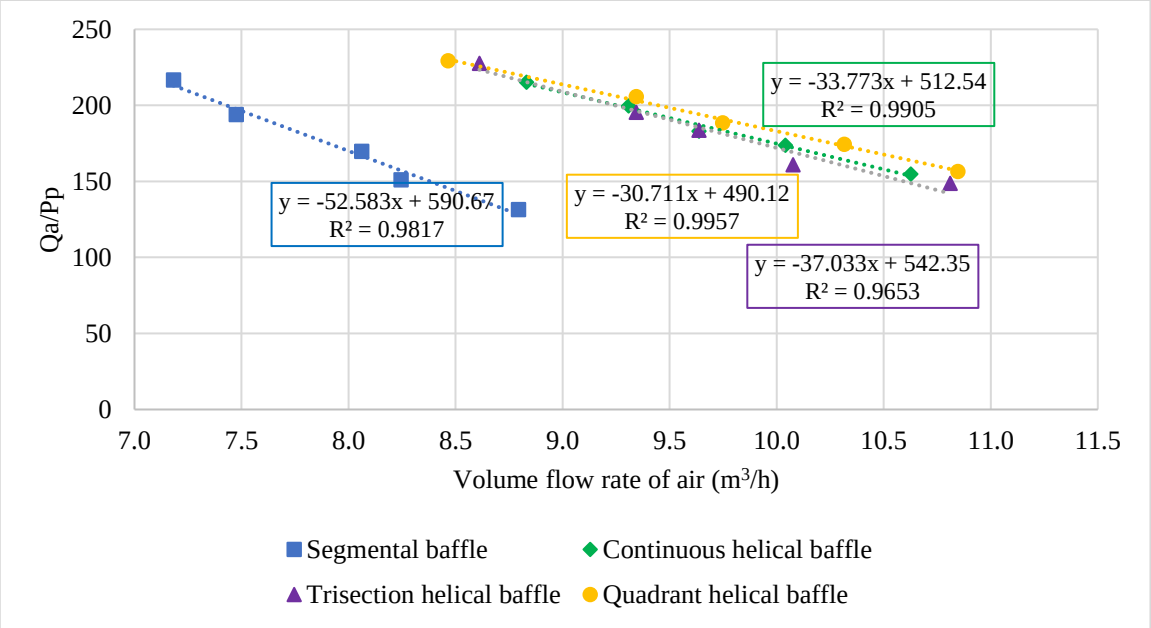

Figure A5. Comprehensive performance index of plastic heat exchangers as a function of shell side volume flowrate

CONDENSATION PHASE HEAT TRANSFER

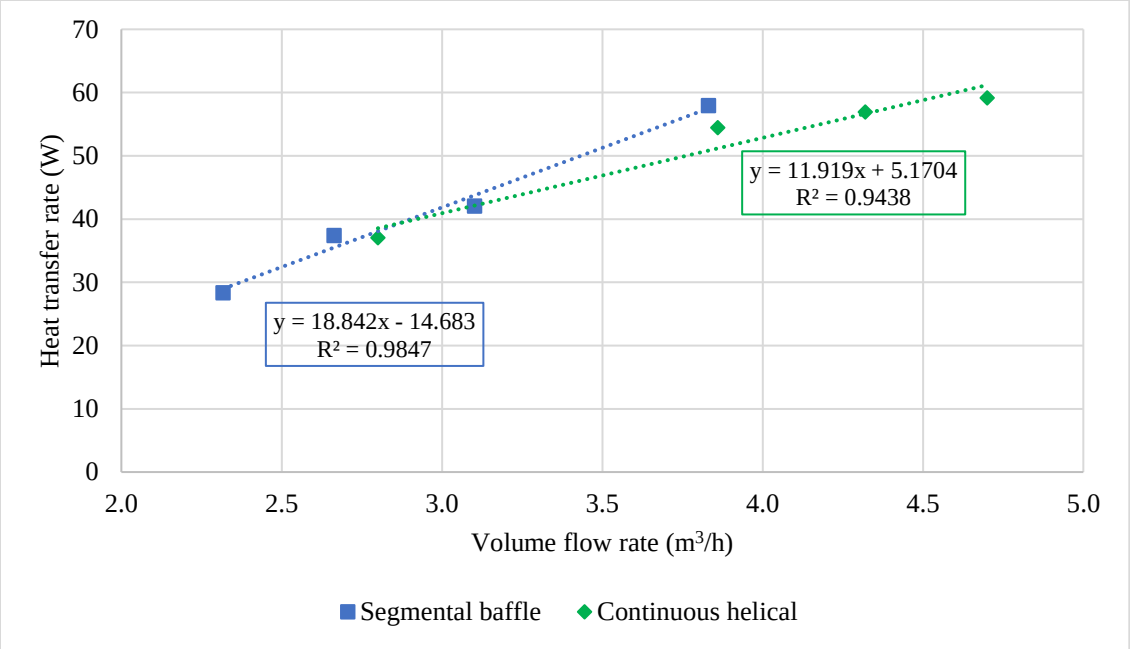

Figure A6. Heat transfer rate of plastic heat exchangers as a function of shell side volume flow rate

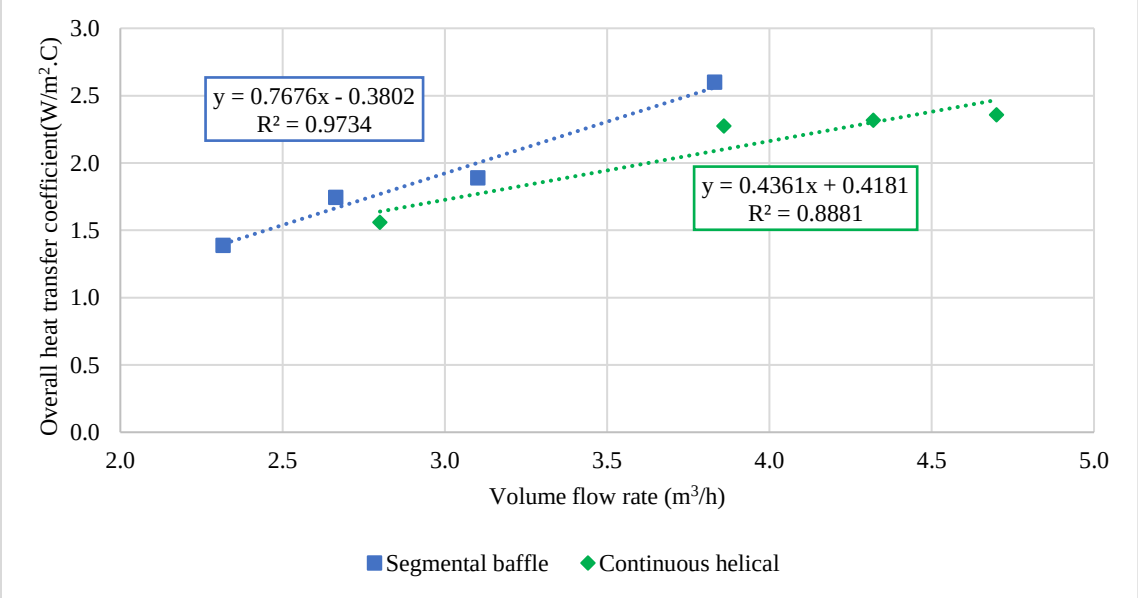

Figure A7. Overall heat transfer of plastic heat exchangers coefficient as function of shell side volume flow rate

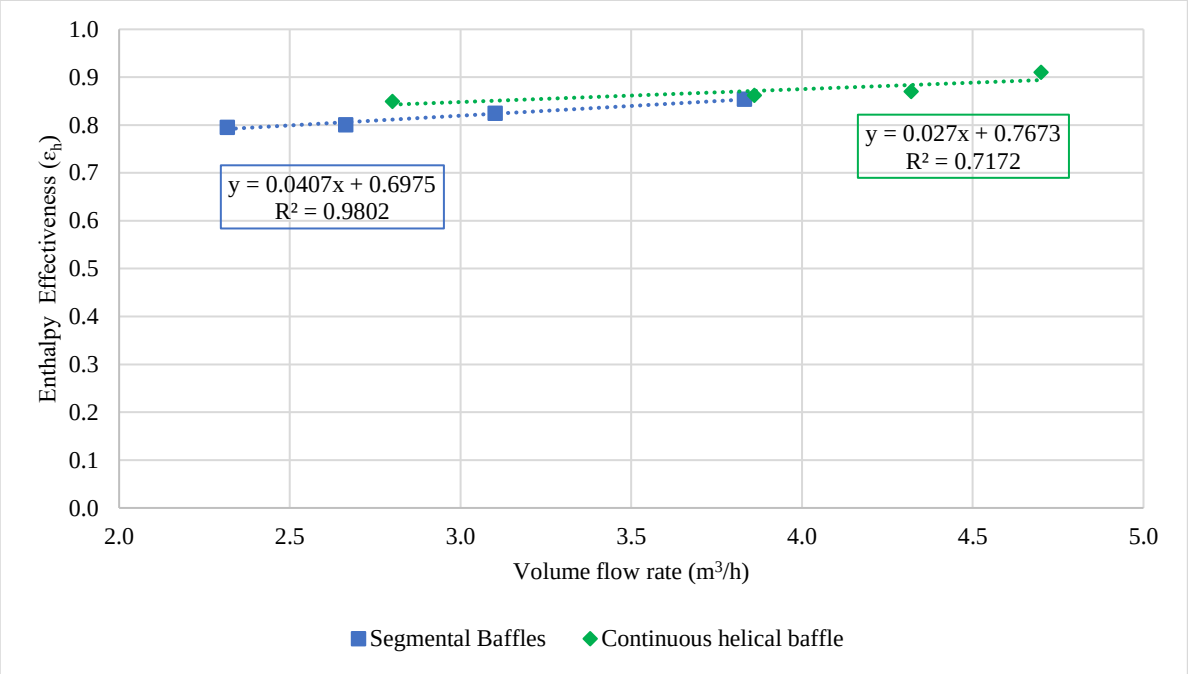

Figure A8. Enthalpy effectiveness of plastic heat exchangers as function of the volume flow rate

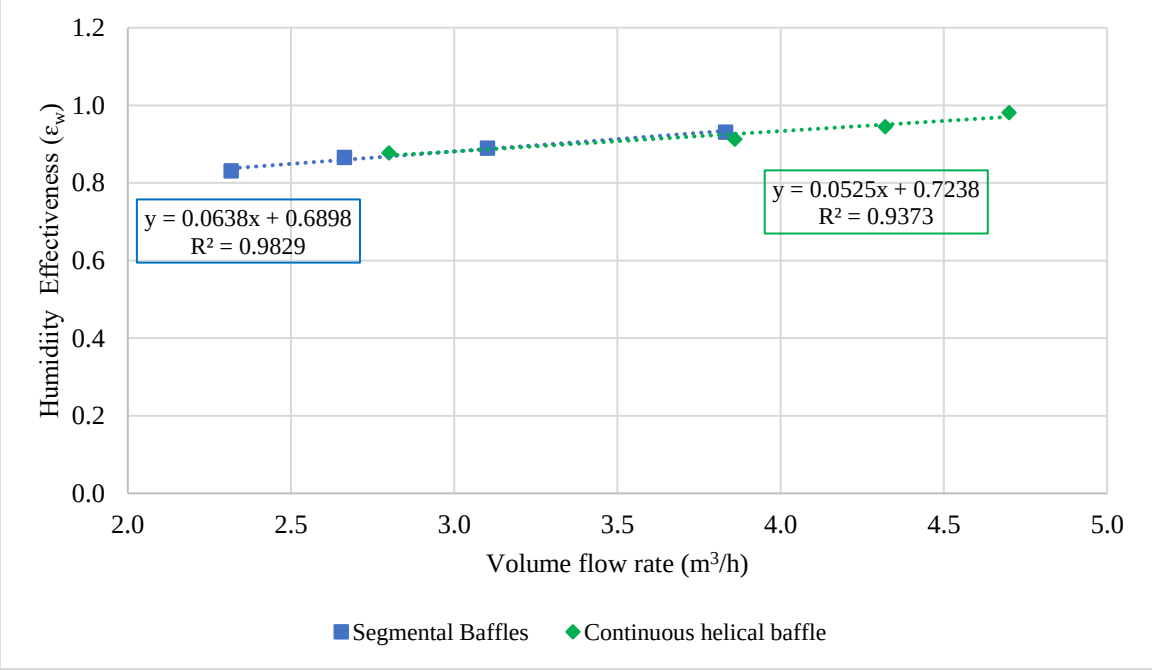

Figure A9. Humidity effectiveness of plastic heat exchangers as function of the volume flow rate

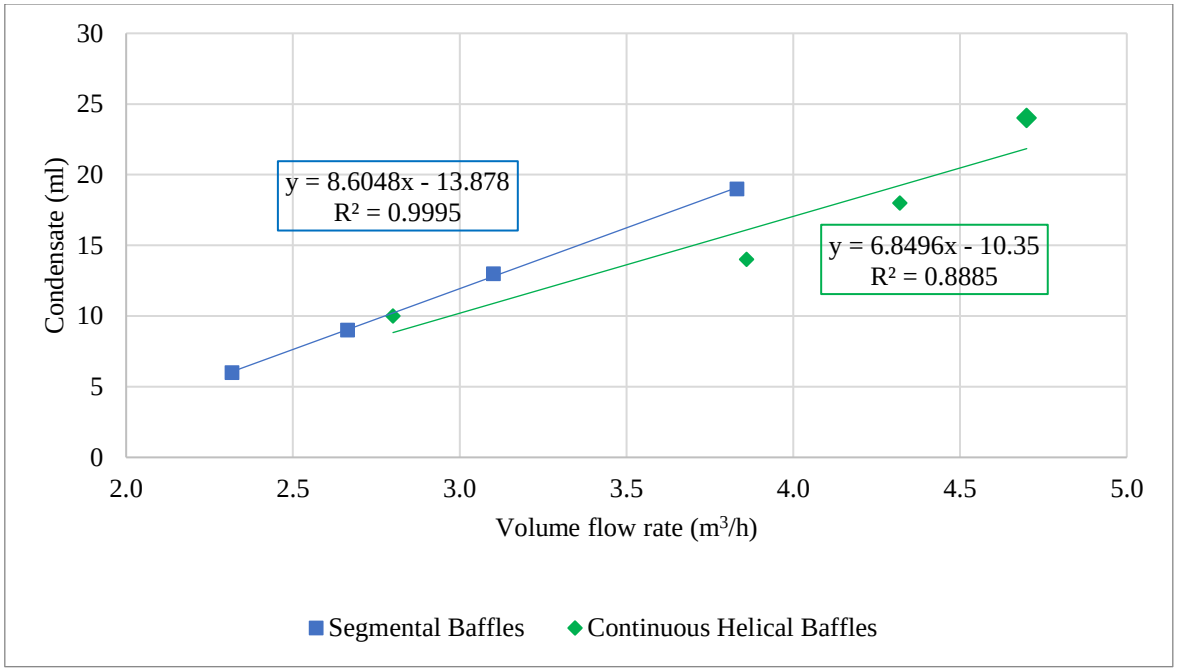

Figure A10. Dehumidifying capacity of plastic heat exchangers as function of the volume flow rate

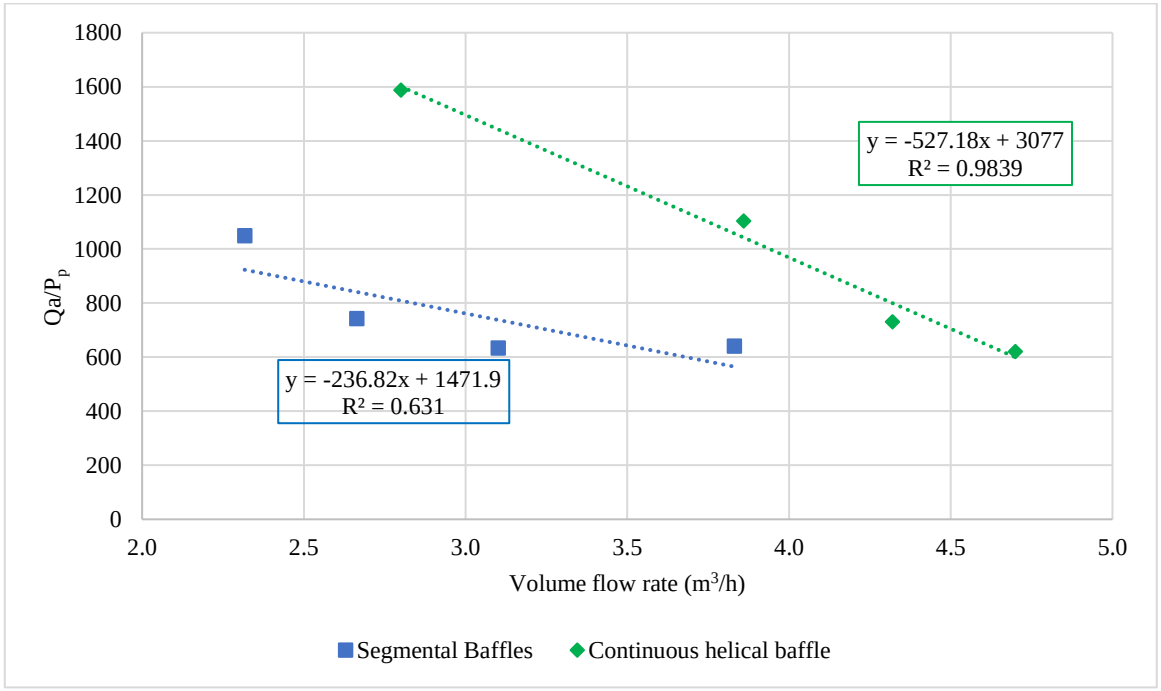

Figure A11. Comprehensive performance index of plastic heat exchangers as function of the volume flow rate

APPENDIX B

CALIBARTION OF THERMOCOUPLES

This section presents the procedures and the results for the thermocouple calibrations. Four fluid temperature thermocouples were used and calibrated before heat transfer experiments. The thermocouple calibration was conducted with pure water and air under isothermal conditions. All the temperatures were measured using an Agilent data logger at steady state conditions. The calibration process is as follows:

Experimental measurements were taken for all the thermocouples under equilibrium isothermal conditions for a period of 30 minutes with a scanning interval of 2 secs which resulted in getting 900 readings. To get the average temperature value for each thermocouple, an arithmetic mean was taken and defined as,

$$T_{avg,i} = \frac{\sum_{n=1}^{900} T_{measured,i}}{900}$$

where i is the number of each thermocouple, which is from 1 to 4.

A total average was calculated using the average temperature values of the thermocouple, as follows:

$$T_{avg,total} = \frac{\sum_{n=1}^{4} T_{avg,i}}{4}$$

Finally, correction factor (CF_i) was found for each of the corresponding thermocouple based on the deviation from the total average temperature value, as follows:

$$CF_i = T_{avg,total} - T_{avg,i}$$

The correction factors for all the thermocouples used in the experiments are shown in Table A.1 and were incorporated directly in the data acquisition system software

Thermocouples	**Average Temperature ($T_{avg,i}$)**	**Correction Factor (CF_i)**
$T_{a,i}$	33.59	0.01
$T_{a,o}$	33.56	-0.01
$T_{w,i}$	17.89	0.17
$T_{w,o}$	17.54	-0.17

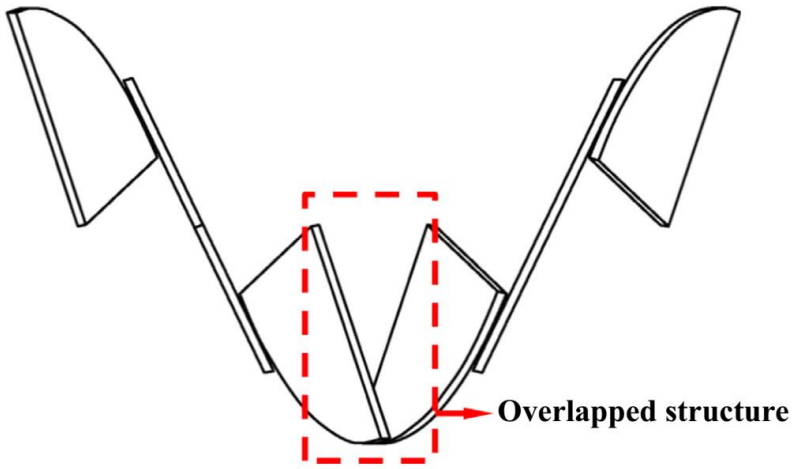

Figure A12. Schematic of helical baffle circumferential overlap scheme

APPENDIX C

ERROR PROPORGATION ANALYSIS

Uncertainty analysis of the experimental results was undertaken using the Engineering Equation Solver (EES) software. The EES software follows the multivariate propagation of error approach, which is based on the following equation,

$$\sigma_U = \sqrt{\left(\frac{\partial U}{\partial X_1}\right)^2 {\sigma_{X_1}}^2 + \left(\frac{\partial U}{\partial X_2}\right)^2 {\sigma_{X_2}}^2 + \cdots + \left(\frac{\partial U}{\partial X_n}\right)^2 {\sigma_{X_n}}^2}$$

where:

U: given function of independent variables, $U = U(X_1, X_2, \ldots\ldots, X_n)$

X_n: independent variable

σ_{X_n}: uncertainty associated with corresponding independent variable, X_n

σ_U: uncertainty associated with dependent variable U

The uncertainty values of the measurements or input variables are shown in Table C1.

Table C1. Measured variables and uncertainties

Parameter	Uncertainty
ΔP	± 0.25 kPa
T	± 0.1 °C
Velocity of air	± 0.01 m/s
$\dot{V}_w$	± 6.8 L/h

Heat transfer rate, overall heat transfer coefficient, effectiveness, and NTU uncertainties were calculated following the approach shown above. The code used in the EES program can be seen in APPENDIX D. The calculated data and their uncertainties can be seen in Table C2.

Table C2. Calculated data uncertainties during single phase heat transfer test

	S. No	Q water (W)	U(W/m2.K)	Effectiveness	NTU
Segmental Baffle	1	67.2±6.062	6.692±0.6169	0.5433±0.04832	1.112±0.1026
	2	69.72±6.071	6.95±0.6186	0.5427±0.04655	1.095±0.09759
	3	76.44±6.097	7.63±0.623	0.5833±0.04576	1.161±0.09494
	4	78.54±6.106	7.682±0.6105	0.5842±0.04464	1.122±0.08928
	5	84.84±6.133	8.197±0.6058	0.6043±0.04287	1.131±0.08371
Continuous Helical	1	72.66±6.082	6.548±0.5565	0.6193±0.05102	1.088±0.09255
	2	81.48±6.118	8.154±0.6264	0.674±0.0497	1.285±0.09886
	3	85.26±6.135	9.052±0.6692	0.7022±0.04955	1.378±0.102
	4	98.7±6.2	11.78±0.7732	0.7855±0.04827	1.721±0.1131
	5	116.3±6.298	13.22±0.7491	0.86±0.04543	1.825±0.1036
Trisection	1	76.86±6.099	8.026±0.6523	0.6808±0.05308	1.333±0.1085
	2	79.8±6.111	8.045±0.6293	0.6854±0.05152	1.268±0.09931
	3	87.36±6.144	8.307±0.5968	0.6914±0.04771	1.264±0.09097
	4	90.3±6.158	8.44±0.5871	0.701±0.04685	1.233±0.08589
	5	103.7±6.226	10.03±0.6171	0.7677±0.04505	1.385±0.08532
Quadrant	1	77.7±6.102	7.841±0.6296	0.6826±0.05268	1.302±0.1047
	2	80.64±6.114	8.268±0.6415	0.6876±0.05118	1.303±0.1012
	3	83.58±6.127	8.798±0.661	0.7062±0.05076	1.339±0.1007
	4	90.3±6.158	9.346±0.6543	0.7161±0.04784	1.365±0.09573
	5	102.5±6.22	9.914±0.6168	0.7537±0.04473	1.369±0.08527

APPENDIX D

EES Uncertainty Analysis Code

```
"Constants"
ID_shell = 0.0762 [m]
OD_tube = 0.0047625 [m]
ID_tube = 0.0044069 [m]
Number_of_tubes = 61
Length_of _tube= 0.4572 [m]
ID_air_inlet_duct= 0.040386 [m]
c_p_water= 4.2[kJ/kg·K]
c_p_air= 1[kJ/kg·K]
rho_air=1.025[kg/m3]


"Calculated constants"
Heat_transfer_area = pi*OD_tube*Length_of_tube*Number_of_tubes
Area_air_inlet__duct=(pi/4)*ID_air_inlet_duct

"Measured variables"
Q = m_dot*c_p_water*(T_2-T_1)*1000
U=Q/(Heat_transfer_area*LMTD)
LMTD = ((T_3-T_1)-(T_4-T_2))/ ln((T_3-T_1)/(T_4-T_2))
Effectiveness = Q/(vel_air*rho_air*Area_air_inlet_duct*1000*c_p_air*(T_3-T_1))
NTU=(U*heat_transfer_area)/(vel_air*rho_air*Area_air_inlet_duct*c_p_air*1000)
uncertainity_T=0.1[K]
uncertainity _m_dot=0.00018[kg/s]
uncertainity _vel_air=0.01[m/s]
```